FZA-450-1
15 SEPTEMBER 1970

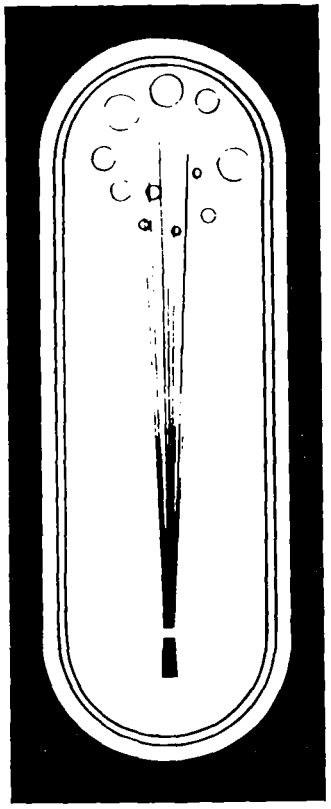

STUDY OF CRYOGENIC FLUID MIXING TECHNIQUES

Final Report

(JULY 1969-JULY 1970)

Volume I - Large-Scale Experimental Mixing Investigations and Liquid-Oxygen Mixer Design

GENERAL DYNAMICS
Fort Worth Division

GENERAL DYNAMICS
Fort Worth Division

FZA-450-1
15 September 1970

STUDY OF CRYOGENIC FLUID MIXING TECHNIQUES

FINAL REPORT

(July 1969 - June 1970)

Volume I: Large-Scale Experimental Mixing Investigations and Liquid-Oxygen Mixer Design

J. R. Van Hook
L. J. Poth

Prepared for the
George C. Marshall Space Flight Center
National Aeronautics and Space Administration
Huntsville, Alabama

Under

Contract No. NAS8-24882

Approved by:

J. R. Van Hook
Project Manager

Approved by:

R. A. Stevens
Aerothermodynamics Group Engineer

F O R E W O R D

This document is Volume I of the final report on NASA Contract NAS8-24882, "Study of Cryogenic Propellant Stratification Reduction Techniques." The study was performed by the Fort Worth Division of General Dynamics Corporation for the George C. Marshall Space Flight Center of the National Aeronautics and Space Administration. The program was conducted under the technical direction of Mr. T. W. Winstead of the MSFC Astronautics Laboratory. His assistance in the performance of this study is gratefully acknowledged.

The final report consists of three volumes:

Volume I.	Large-Scale Experimental Mixing Investigations and Liquid-Oxygen Mixer Design
Volume II.	Large-Scale Mixing Data
Volume III.	Computer Procedure for the Prediction of Stratification in Supercritical Oxygen Tanks

Volume I contains a presentation of the large-scale experimental investigation and liquid-oxygen mixer design study together with a summary of the important findings of the study. Volume II contains a presentation of the experimental data utilized in this study. Volume III describes the computer procedure developed during the study for the prediction of stratification development in supercritical oxygen tanks.

TABLE OF CONTENTS

TABLE OF CONTENTS (Cont'd)

T A B L E O F C O N T E N T S (Cont'd)

L I S T O F F I G U R E S

L I S T O F F I G U R E S (Cont'd)

L I S T O F F I G U R E S (Cont'd)

L I S T O F T A B L E S

N O T A T I O N

Symbol		Units
A	Liquid surface area	ft^2
a	Acceleration	ft/sec^2
b	Constant, 0.25	--
C_2	Constant, $C_2=Rh_vC/C_vV_v$	$lbf^{1/2}/hr\ ft$
C*	Constant, $C^* = 0.456\ V_oD_o/D_t^2$	1/sec
C_v	Constant volume specific heat	$Btu/lbm\ ^oR$
D_o	Nozzle exit diameter	ft
D_t	Tank diameter	ft
G_o	Nozzle flow rate	gpm
g	Acceleration of gravity	ft/sec^2
h_v	Vapor enthalpy	Btu/lbm
I_m	Energy integral, $I_m=1-\frac{(T_s-T_m)}{(T_s-T_b)}$	--
I_{m_i}	Initial energy integral	--
m	Mass	lbm
$\dot{m}_o$	Nozzle exit mass flow rate	lbm/hr
N	Mixing parameter, $N = \frac{4b^2N_i^*(I_{m_i}-I_{m_i}^2)}{1+2\ I_{m_i}}$	--
N_i^*	Ratio of modified Grashof number to the Reynolds number squared, $N_i^* = \frac{g\beta\Delta T_i Z_b^3}{(V_oD_o)^2}$	--

Symbol		Units
N_{Re}	Reynolds number	--
P	Tank pressure	psia
P_b	Saturation pressure of bulk fluid	psia
P_i	Initial tank pressure	psia
Q_v	Ullage heating rate	Btu/hr
R	Gas constant	ft-lbm/lbf-^oR
T_b	Bulk or nozzle exit temperature	^oF
T_m	Mean fluid temperature	^oF
T_s	Average surface temperature	^oF
T_{s_1}	Centerline surface temperature	^oF
V	Volume	ft^3
V_o	Nozzle exit velocity	ft/sec
V_v	Ullage volume	ft^3
Z	Axial distance from bottom of dye interface to nozzle top	ft
Z_b	Axial distance from nozzle to liquid/vapor interface	ft
Z_d	Axial distance from bottom of dye interface to nozzle top	ft
Z_s	Stratification thickness	ft
β	Coefficient of thermal expansion	$1/^oR$
$\Delta\theta_j$	Jet transit time	sec
ΔT_i	Initial temperature stratification	^oF

Symbol		Units
θ	Time or time after pump turned on	sec
θ_m	Mixing time	sec
θ_1	Time after mixing begins	sec
ρ	Fluid density	lbm/ft^3
σ	Surface tension	lbf/ft

Subscripts

i	Initial

S U M M A R Y

The design of present and future spacecraft utilizing cryogenic fluids requires that adequate prediction and control of thermal stratification be accomplished. In previous studies (References 1 and 2) methods were selected for mixing the thermally stratified fluid layer with the remaining colder bulk fluid in the tank and a mixer design procedure was developed. The results of the mixer design procedure were applied to liquid-hydrogen storage systems and estimates made of the mixer requirements.

The previously developed mixer design procedure was partially based on small-scale mixing tests in which water was used as the test fluid. In the present study, the validity of scaling small-scale test data for use in designing mixer systems for full-scale tanks has been verified through use of a test tank intermediate in size between the previous small-scale tank and the full-scale tanks of spacecraft.

The experimental mixing investigation involved mixing in a large-scale (10-foot-diameter, 20-foot-long) stratified tank with non-pressurized water used as the test fluid.

Tests were conducted to duplicate the range of the previous small-scale test parameters. The data obtained consist of temperature histories in the tank during mixing and a limited amount of jet motion data. The bulk of this data is presented in Volume II.

The temperature mixing data were reduced to a dimensionless form of temperature stratification. These data were used to make correlations of mixing time and the effect of buoyancy on mixing. The jet motion data were used to check the time required for the jet to move from the nozzle exit to the liquid surface.

The correlation of buoyancy effects showed that the delay in the initial surface temperature decay (due to mixing being retarded by the buoyancy of the stratified layer) decreased with decreasing values of the parameter N. This parameter is a function of the energy distribution in the tank and the ratio of the modified Grashof number divided by the square of the Reynolds number. Since the modified Grashof number is a function of acceleration, N is also a function of acceleration. The large-scale data correlation of the buoyancy effects indicates that the delay in mixing time due to buoyancy is relatively small for conditions simulating low-g environments. The data indicate that this condition can be ignored in designing mixers for low-g conditions.

The correlation of the mixing time required to reduce an initial stratification to some fraction of its value was initially accomplished by the use of dimensionless time versus the parameter N_i^*, which is the ratio of the modified Grashof number divided by the square of the Reynolds number. This correlation resulted in the data being grouped according to the thickness of the initial stratification. A correlation of N versus the mixing time resulted in good data grouping.

Comparison of large- and small-scale data correlations revealed excellent agreement between the two sets of data. The previous conclusion that buoyancy effects in the small-scale tests were small for conditions simulating low-g environments was upheld. Mixing time correlations indicated that the dimensionless mixing times required to mix the fluid in large- and small-scale tanks are approximately the same for the similar test conditions. Previous jet motion predictions based on the small-scale data were also verified.

Since the large-scale data correlations did not differ greatly from previous small-scale correlations, the mixer design parameters are not changed. Consequently, no changes are required in the previous liquid-hydrogen mixer system estimates.

The previously defined methods of predicting thermal stratification and mixer performance were applied to the de-

sign of mixers for oxygen storage. Two tanks were considered: (1) an S-IIB/TK orbital LOX tanker and (2) a small supercritical storage tank. The previously developed methods of predicting stratification were found to be adequate for the S-IIB/TK tank. The prediction of stratification in a supercritical tank required the development of an entirely new computer procedure. This procedure is presented in Volume III.

The design of the mixer system for the S-IIB/TK tank was complicated by the large ullage, which results in ullage heating being the dominant cause of the tank pressure rise. Also, if the liquid oxygen consisted of globules distributed throughout the tank, fluid control would be difficult. Therefore, a mixer system was devised that does not disrupt the interface. The mixer design considers only conventional pumps.

The prediction of stratification in the supercritical oxygen was complicated by the continuous withdrawal of mass from the tank and by the heating of the tank during withdrawal in order to maintain tank pressure. The stratification due to the heaters is controlled partially by termination of heating when the desired tank operating pressure is exceeded. Therefore, the major concern was that a sudden mixing of the tank might cause a pressure collapse to some pressure below the tank operating range. Equilibrium mixing of the stratified

tank considered did not result in significant pressure decay. It is expected, however, that if mixers are not employed the extent of the pressure collapse will increase with time as the stratification increases (Ref. 11). Also, the severity of pressure collapse is determined by the location and severity of the energy added to the tank. The mixer requirements are consistent with conventional (existing) mixer designs although the recent Apollo 13 failure may cause changes in the electric motor design to eliminate combustible electrical insulation.

It was found that there is a lack of consistent close-spaced property data over the operating range considered. Since in the supercritical region small temperature changes can result in large pressure variations, interpolation between data points could induce property value errors.

SECTION 1

INTRODUCTION

The prediction and control of the thermodynamic state of stored cryogens is required in order to design both present and future spacecraft. The technology required to predict the development of thermal stratification and the methods of obtaining thermal equilibrium (mixing) were developed during a previous study (Reference 1). These methods are based on analytical results which are supported and verified by mixing tests conducted in small-scale tanks. In this study, the use of the small-scale test data to develop mixing parameters for use in the design of mixing systems in full-size tanks is verified by testing in an intermediate-size tank. In addition, the previously developed techniques (which were intended for use in liquid-hydrogen mixer designs) are applied to liquid-oxygen systems.

The principal effort in this study has been expended in the experimental evaluation of axial jet mixing in a large-scale tank (intermediate in size between small tank used in earlier study and full-sized spacecraft tank) and the establishment of correlations with existing small-scale data. This includes the assessment of the effect of nozzle diameter, jet

flow rate, and buoyancy on mixing parameters and the comparison of small-scale-tank test parameters with large-scale-tank test parameters. Also considered is the effect of the large-scale test results on prior estimates of low-g liquid-hydrogen mixer systems.

The analysis of the oxygen systems considers an S-IIB LOX tanker concept and a small supercritical storage system. Techniques developed in the previous study are applied to the S-II system to predict stratification development and to size the required mixer system. A new stratification prediction procedure was developed for predicting stratification in a supercritical storage tank. The results of the supercritical oxygen stratification study reveal no evidence that mixing the stratification buildup will result in the collapse of tank pressure. The stratification developed in the tank (due to heating to maintain pressure during withdrawal) is controlled by maintaining pressure limit switches on the heaters. Therefore a mixer system is not strictly necessary.

1.1 STUDY OBJECTIVES

The objectives of this study were (1) to verify the validity of utilizing small-scale-tank mixing parameters in the design of full-scale-tank mixers, and (2) to apply previously developed

mixing techniques to the design of liquid-oxygen mixer systems.

In order to verify the validity of using small-scale tank data correlations to develop mixer parameters for the design of full-scale-tank mixers, the small-scale data correlations were confirmed in a large-scale tank. The large-scale tank was an order-of-magnitude larger than the previous small-scale tank. The range of dimensionless mixing conditions considered in the small-scale tests were duplicated as far as possible in the large-scale tests. The large-scale test data were used to obtain correlations for comparison with similar small-scale data correlations. These correlations considered the effect of nozzle diameter, liquid depth, flow rate, and stratification. Any variation between the large- and small-scale correlations were evaluated to determine their effect on the previously developed liquid-hydrogen mixer estimates.

The mixer design techniques used in developing the liquid-hydrogen mixer estimates were evaluated to determine if they could be applied to liquid-oxygen systems. Necessary modifications were made and new techniques developed as required. The techniques were then applied to an S-II LOX tanker and a supercritical tank.

1.2 BACKGROUND

The study of methods of maintaining thermodynamic equilibrium of stored cryogens has been pursued in previous studies (References 1 and 2). These studies consisted of both analytical and experimental investigations into methods of predicting thermal stratification development and subsequent stratification reduction. The results of these studies include (1) stratification prediction techniques, (2) selection of mixing methods, (3) prediction of mixing histories, (4) development of mixer-system design methods, and (5) application of the design methods to low-g liquid-hydrogen systems. The analytical investigation resulted in the selection of jet mixing as the most suitable method of mixing a tank in a low-g environment.

The earlier analytical investigations were supplemented and verified by extensive mixing tests conducted in small-scale cylindrical tanks. The tests used water as the test fluid and included both pressurized and non-pressurized cases. Test variables included nozzle diameter, liquid depth, flow rate, and stratification. Various tank bottoms were also investigated. Three mixer types were studied: an axial jet, a radial jet, and a 60-degree jet. The test results indicated

that the axial jet provides the most efficient means of jet mixing a tank.

The small-scale test results included data on the jet motion, bulk fluid motion, and temperature and pressure histories in the tank during mixing. Mixing time and the effects of buoyancy were evaluated from these data. Also, these data were correlated and used to develop design parameters for use in the design of mixer systems for full-scale cryogenic hydrogen tanks.

The resulting correlations from the experimental testing and analytical investigations were used to size mixer systems for various liquid-hydrogen tanks. These sizing analyses resulted in mixer designs. Also, penalties associated with the mixer systems were assessed.

Verification of the analytical results based on these small-scale tests and the associated development of mixer parameters based on these results would not be sufficient if the correlations could not be applied to full-scale tanks. The small-scale tanks were approximately 1 foot in diameter, and the full-scale tanks could be 20 or 30 times larger; therefore, the scaling up of small-scale data correlations to predict mixing in a large tank could possibly induce serious errors in mixer design. This possibility warranted additional

testing to be accomplished with a tank intermediate in size between the small test tanks and full-size tanks. The tank selected is approximately an order-of-magnitude larger than the small test tank. The experimental investigation conducted with this tank is discussed in Section 2. The large-scale-tank test data correlations are discussed in Section 3 and compared with the earlier small-scale-tank correlations in Section 4.

The results of the mixing investigations could be applied to any non-viscous fluid. In particular, the study results are applied to another cryogen, oxygen, that is commonly stored in low-g environments. The results of the application of the stratification prediction and mixing techniques to an S-IIB LOX tanker and a supercritical tank are given in Section 5.

SECTION 2

EXPERIMENTAL INVESTIGATIONS

The experimental phase of the program has provided data on the mixing of a thermally stratified layer in a large-scale tank. These investigations considered axial jet mixing in a non-pressurized, upright cylindrical tank in which water was used as the test fluid. The tests conducted were designed to duplicate, where possible, the range of parameters considered in previous small-scale tests. The experimental data have been used to validate the use of the previous small-scale data to develop mixing predictions and mixer design parameters for use in the design of axial jet mixer systems for a large-scale tank.

2.1 EXPERIMENTAL TEST OBJECTIVES

The objective of the experimental tests, performed in a large-scale water tank, was to validate the use in large-tank mixer design of parameters based on small-scale-mixing test data.

2.1.1 Test Data Requirements

The test data required were those data that pertained only to mixing. The test parameters were required to duplicate

where possible the range of the parameters used in the small-scale tests.

The tests were designed to yield data on temperature decay in the tank during mixing. The temperature histories were analyzed to yield mixing times and transient temperature effects. Some data on the jet motion were obtained. No data on the bulk fluid motion were obtained.

2.1.2 Large and Small-Scale Test Data Comparison

Comparison of large- and small-scale data is primarily concerned with a comparison of mixing times and the effect of buoyancy on mixing for the same test parameters. This comparison requires that the large-scale data be first reduced to a dimensionless form of temperature stratification versus a dimensionless time. The comparison of tests under the same conditions was then accomplished. Also, a general expression for the temperature decay developed from small-scale bulk-fluid-motion data can be compared with the transient temperature decay from individual tests. Interpretation of the data is often a matter of judgement. This is especially true in selection of mixing times from the test data.

2.1.3 Experimental/Analytical Data Comparison

The comparison of experimental data and analytical

predictions was reported in Reference 2 for the small-scale data. The presence of a major variation of large-scale-tank data from the small-scale data was the criterion which determined if new comparisons needed to be made.

2.2 TEST FACILITY DESIGN CONSIDERATIONS

The comparison of the results from the large-scale tests performed during this study and the small-scale tests performed in earlier studies required that careful consideration be given to geometrical similarity. The first criterion used was to maintain the configuration of the tanks in as similar a shape as possible. The original small-scale test tanks consisted of a cylinder with concave or convex bottoms. The non-pressurized small-scale tanks had no top, while the pressurized small-scale tanks had a hemispherical top. The large-scale tank was selected to be a cylinder. It was not possible to retain the curved bottom bulkheads in the large-scale tank and still maintain a simple test setup. However, the previous small-scale test results indicated that there was very little fluid motion below the nozzle, so the use of a flat-bottomed tank did not detract from the results.

The tank diameter of 10 feet was established as a basic test guideline. This dimension was approximately an order of

magnitude larger than those used in the small-scale tests. The tank length was determined from the maximum previous L/D ratio of approximately 2. The nozzle diameters were then selected by scaling up the small-scale nozzle diameters, using the ratio of the small-scale water depth to the small-scale nozzle diameter, and multiplying by the large-scale water depth. The values of the dimensionless geometry parameters Z_b/D_t and Z_b/D_o were thus maintained approximately the same.

Axial jet flow rates in the large-scale tank were selected from values of the dimensionless parameter N_i^* found in the small-scale tests. Substituting into the expression for N_i^* values of the ranges of temperature stratification, liquid depth, and nozzle diameter enabled values of the axial jet flow rate to be selected which would reproduce the same values of N_i^* in the large-scale tank as were used in the small-scale tank.

Maintaining the same geometry ratios and N_i^* range in the large-scale tank as were used in the small-scale tank resulted in an increase in the jet Reynolds number. The parameter N_i^* had been previously found to be a more important parameter in predicting mixing than the jet Reynolds number; therefore the value of the Reynolds number was allowed to vary as required to maintain the previous range of N_i^*. The values of all

large-scale jet Reynolds numbers were in the turbulent region, as were the Reynolds numbers of the small-scale tests except for one test.

Table 1 shows the range of the various dimensionless parameters considered in this study. Values are shown for both large- and small-scale tanks. Although equipment availability and capacity were limited, almost the entire range of the small-scale parameters Z_b/D_t and Z_b/D_o were reproduced in the large-scale tests. As an example, the minimum value of the parameter Z_b/D_t was not reproduced since there were no readily available nozzles that were compatible with the system. Lowering the water level to obtain this value would have resulted either in requiring flow rates (to reproduce the N_i^* values) that were too small for the system or in producing unrealistic stratification levels. Because of these problems and the fact that the extreme values of these parameters often represented isolated data points that were of doubtful use in correlations, the range of Z_b/D_t was limited. The same situation existed for the parameter Z_b/D_o. Consequently, the system was designed to reproduce the range of the bulk of the small-scale parameters.

Table 1

RANGE OF TEST PARAMETERS

Parameter	Small-Scale Tank		Large-Scale Tank	
	Minimum	Maximum	Minimum	Maximum
$\frac{Z_b}{D_t}$	0.572	2.03	0.87	1.85
$\frac{Z_b}{D_o}$	70.8	744	122.06	349.44
N_{Re}	2,005	51,156	49,000	603,000
N_i^*	3.6	760	0.57	1,993.64

2.3 EXPERIMENTAL FACILITY

The experimental facility in which the large-scale tests were conducted consisted of a tank, associated flow systems, instrumentation for recording temperatures and measuring flow rates, and equipment for inducing stratification. These components were set up on an outside test site. A photograph of the test site and major components is shown in Figure 1.

2.3.1 Test Tank

The test tank was a vertical steel cylinder having a 10-foot diameter and a 20-foot length (L/D = 2). The tank had a flat bottom and an open top. The sidewall of the tank was penetrated by 3-inch-diameter portholes covered by plexiglass. The purpose of these portholes, arranged vertically at 2-foot intervals, was to allow observation of dye movements in the tank if feasible and necessary.

The tank was fitted with permanent internal and external ladders to allow access to the instrumentation and piping within the tank. The ladders were mounted over the portholes to enable personnel to use the portholes for observation purposes. The internal ladder, of open construction, extended 4 inches from the wall and did not present a significant flow

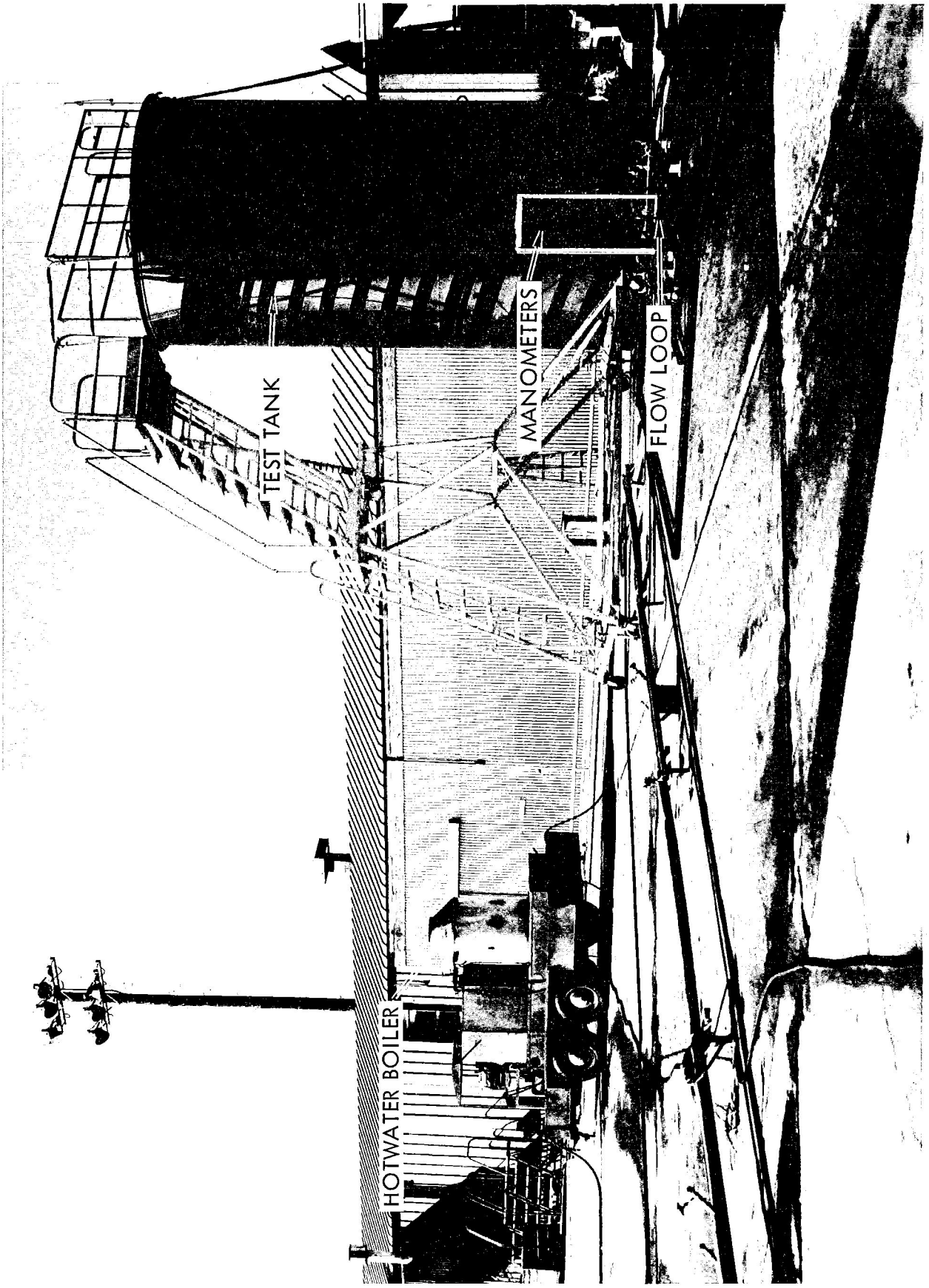

Figure 1 LARGE SCALE TEST FACILITY

restriction. In any case, the thermocouples were located 180° from the internal ladder.

The tank had a catwalk mounted across the open top. This was intended for use in mounting instrumentation, as a work platform for inducing stratification prior to tests, and as an observation platform during tests. Figure 2 shows a plan of the test tank and associated instrumentation.

2.3.2 Flow System

The flow system consisted of the axial jet flow loop and the hot water supply for stratification development prior to mixing. The hot water supply was a portable system that was removed prior to mixing. The axial jet flow loop was a fixed system.

The axial jet flow loop consisted of the pump, nozzle, associated piping and valves, and flow measurement devices. The axial jet nozzle was mounted on the center of the tank bottom and directed flow up the tank centerline toward the liquid surface. Two interchangeable nozzles were used, with diameters of 0.875 and 0.625 inches, respectively. These were commercial fountain nozzles designed to produce a vertical jet of water. The nozzle was supplied with water drawn into an intake located on the center of the tank bottom just below the

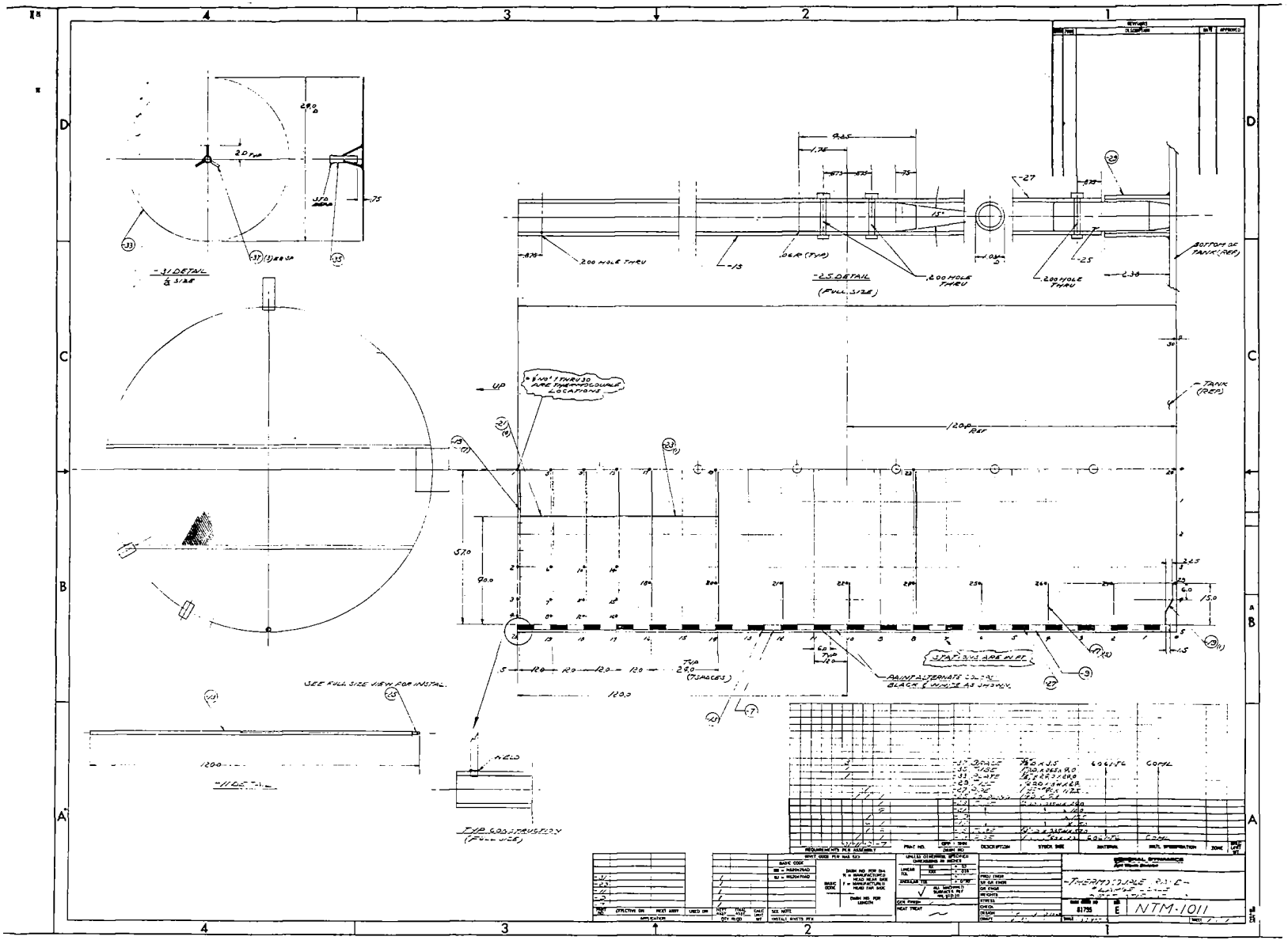

Figure 2 Test Tank and Instrumentation Rake

nozzle. This water was obtained by recirculating water drawn from the tank bottom and flowed out through a pump. After leaving the pump, the flow rate of the fluid was obtained by measuring the pressure drop of the fluid flowing through one of two calibrated orifice plates. The flow was then returned to the tank and passed through the nozzle. That part of the flow loop outside the tank is shown in the photograph presented in Figure 3.

The direction of flow and the flow rate were regulated by valves mounted in the flow loop. The valve arrangement allowed a quick selection to be made of the orifice plate required to measure a given flow range. The pump used in the loop was a centrifugal pump and the flow rate was varied by changing the pressure drop in the loop and by recirculating some of the fluid through the pump. Both of these tasks were accomplished by modulating globe valves in the line.

The hot water supply system consisted of a flexible rubber hose carrying hot water from a portable boiler (Figure 1). The hot water line delivered hot water to the top of the tank where it was used to produce a stratified layer of hot fluid in the tank. The stratified layer was produced either by flowing the water unto the surface of the colder fluid, producing an approximately uniform temperature layer of water on top of the colder

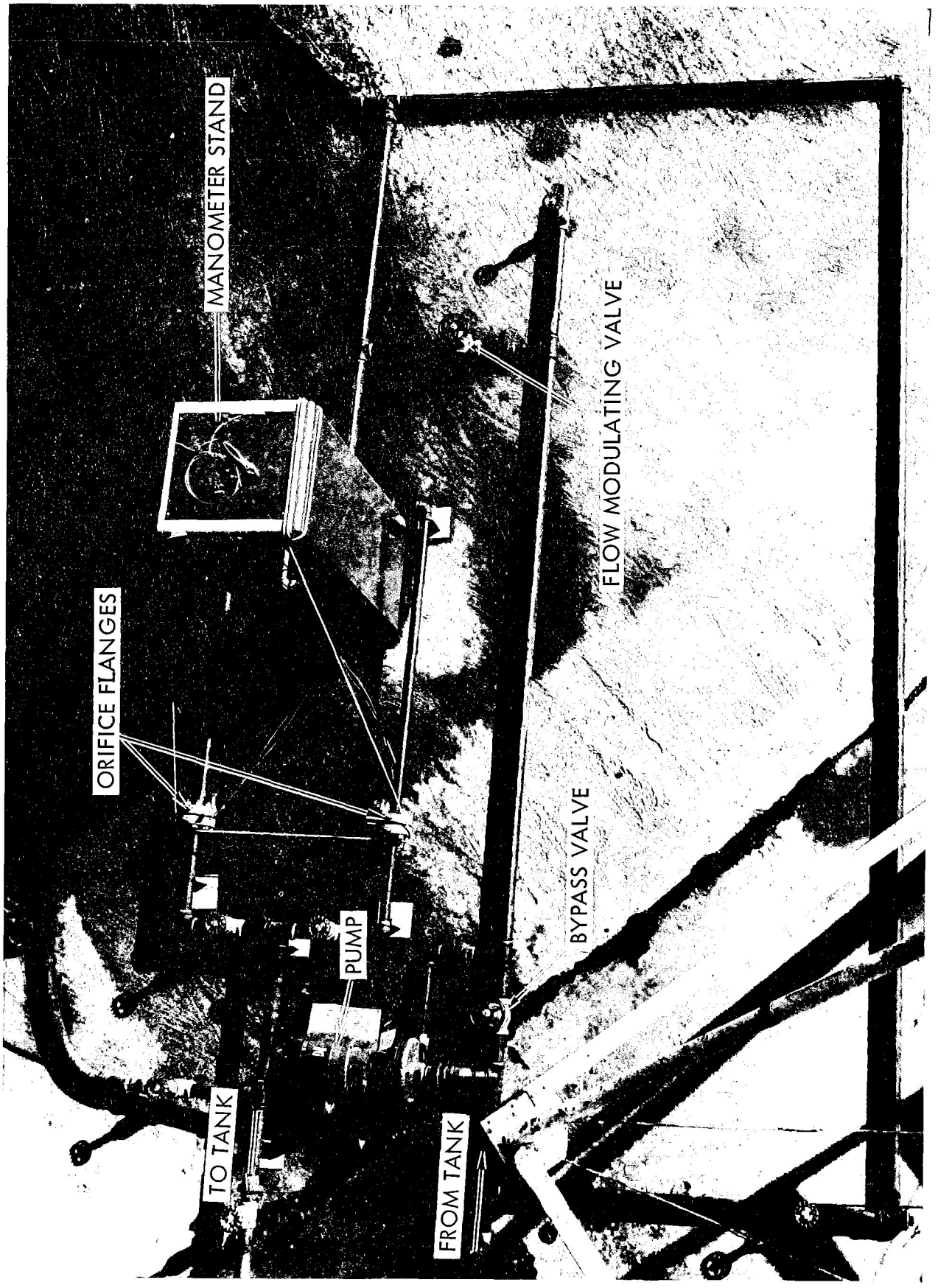

Figure 3 EXTERNAL FLUID FLOW LOOP

fluid, or by mixing the hot water with the colder fluid. The latter method produced a stratified layer that was thicker and had a definite temperature gradient in it. Thickness of the stratified layer was controlled by the depth at which the hot water entered the test tank. Uniformity of the temperature at any depth was obtained by swirling the hot water line around the tank at that depth.

2.3.3 Instrumentation System

Two types of data were obtained: water temperatures during mixing and nozzle flow rates. The temperature data were obtained from thermocouples mounted in the tank and recorded on strip chart recorders. The flow rate was obtained from orifice plate pressure drop measurements made with mercury manometers.

The thermocouples were mounted on a vertical rake in the tank and with its arms arranged radially across one half of the tank. Only one-half of the tank cross-section was used since the flow and temperature conditions in the tank were considered to be symmetrical. The thermocouples at a given depth in the tank were arranged radially such that equal-volume annular sections were formed when the boundaries of the sections were considered to be at one-half the distance between

thermocouples. This is illustrated in the following sketch of a top view of the tank.

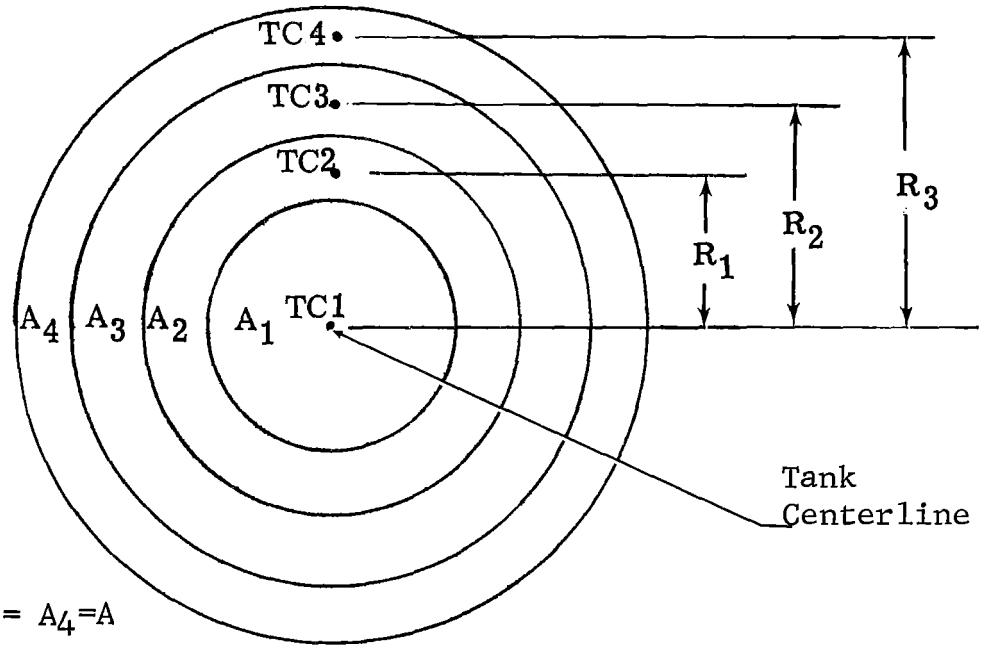

$A_1 = A_2 = A_3 = A_4 = A$

Assuming a uniform depth, h, the volume of a section is

$$V_1 = hA$$

and

$$V_1 = V_2 = V_3 = V_4 = V$$

If the density is approximately the same, then

$$m_1 = m_2 = m_3 = m_4 = m$$

and a numerical average of the thermocouples reflects a mass weighted average temperature.

Figure 2 shows the design of the rake used to support the thermocouples in the tank. This rake was designed and fabricated in two sections so that it could be used with both 20- and 10-foot water levels in the tank. The low-water-level rake

consisted of the upper half of the 20-foot rake which was disconnected and lowered into position for use. The distribution of the thermocouples was denser in the top four feet of the fluid since major mixing effects occur in this region. Below this level, the number of thermocouples at any given level decreases. The use of thermocouples at different levels in the tank provides a means of determining the stratification thickness and also indicates the extent of mixing. The rake support pole was painted with alternate black and white stripes for use in determining liquid depth in the tank.

A total of 28 thermocouples were used in the tank for the 20-foot depth and 22 for the 10-foot depth. These thermocouples were fabricated from 26-gauge copper-constantan wire. The thermocouple lead wires were covered with water-tight shrink tubing and connected above the water with lead wires which carried the signals to the recorders.

The temperature recording devices were two Brown multipoint strip chart recorders which converted the thermocouple signals into temperature readings. Since T_s and T_b were the primary temperatures of interest, the thermocouples giving these values were recorded on one recorder. As a check, measurements of the surface and bottom water temperatures were also made with mercury thermometers at the start and end of a mixing test.

The measurement of the axial jet flow rate was accomplished by measuring the pressure drop across an orifice plate in the flow loop. Two orifice plates were used, depending on the flow rate. Selection of the proper plate was made by setting valves in the flow loop to divert the flow through the plate. The plates were calibrated by physically measuring the volume of water flowing during a given time period, calculating the flow rate, and comparing it with the pressure drop. The pressure drop across an orifice plate was measured by a cistern-type 30-inch mercury manometer. These manometers were calibrated prior to use.

2.4 TEST PROCEDURE

The tests conducted during this study were performed to study axial jet mixing in a large-scale tank. Since the correlations made from the data taken in these tests were to be compared with correlations made in previous small-scale tests, the large and small-scale test procedures were similar.

The data taken during the tests consisted of temperature measurements as a function of time for various locations in the fluid. The test variables consisted of flow rate, nozzle size, stratification temperature, liquid height above the nozzle, and thickness of the stratified layer.

Two water levels were used in the tests: 10 feet and 20 feet above the tank bottom. The water level above the nozzle exit varied somewhat owing to the different heights of the two nozzles and to the different plumbing arrangements that were used. These differences were minor and did not compromise comparisons.

Temperature differences in the fluid were varied as required to produce the desired values of N_i^*. Prior to mixing, the temperature differences between the average surface temperature and the bulk or bottom temperatures varied between approximately 2 and 90°F.

The thickness of the stratified layer varied from about 0.5 to 19.5 feet. This variable could not be precisely controlled except for the thinner layers with maximum thicknesses of about 2 to 3 feet. Inducing a stratified layer thicker than this value required rather crude methods of operation. This involved suspending the hot water line into the tank and slowly swirling it around in the tank fluid at a depth of about 18 inches above the point at which stratification was desired to begin. If the boiler inadvertently produced wet or dry steam rather than water at any time during this operation, the stratified depth would drastically increase because the steam penetrated deeper into the bulk fluid than did the

water. This could not always be determined immediately and corrected. Consequently, the stratification thickness often varied considerably from the intended value.

The axial jet flow rates were set prior to each test run. The flow rates were based on the previous small-tank parameters and the new tank and nozzle dimensions. The range of these flow rates was from 11.7 to 136.5 gpm.

After a set of test conditions were selected within the range of available variables, the mixing test procedure was performed as follows:

1. Fill the tank to the desired water level after installing the desired nozzle. Position the flow loop valves to produce desired flow loop circuit.

2. Set the desired axial jet flow rate by use of the modulating valves and thoroughly pre-mix the tank fluid until no measurable temperature difference is observed. Then stop mixing and allow fluid movement to subside in the tank.

3. Induce a stratified layer into the tank fluid by flowing hot water onto or into the top layer of water. Drain water from the tank if necessary to correct an increase in the water level. Remove hot water line from the tank.

4. Mix tank fluid and record temperature at the various tank positions by use of multipoint strip-chart recorders.

5. Terminate test when temperature difference between the surface and the bottom fluid becomes negligible and appears to have reached a steady-state condition.

These steps were followed in all the jet mixing tests except

that, in actual practice, the tank was seldom drained between tests.

The movement of the jet at the beginning of mixing was observed by noting the time required for motion to appear on the liquid surface. This enabled the time for the jet to travel the length of the tank and penetrate the stratified layer to be determined.

The desired large-scale tank operating conditions are summarized in Figure 4. A flow diagram of the general test procedure for these tests is presented in Figure 5. The actual operating conditions are given in Table 1 of Volume II.

2.5 EXPERIMENTAL DATA

The experimental data obtained in the large-tank tests during this study consist of fluid temperatures as a function of time for various positions in the tank and a limited amount of jet transit time data. The temperature data are concerned entirely with mixing and do not include any stratification development data. The results of 52 tests are reported. The temperature data are shown separately in Volume II since the large amount of data is unwieldy. Sample temperature data are shown in this volume for discussion and are representative of the bulk of the data.

Test Operating Conditions

Nozzle Size (in.)	Water Level (ft)	Pump Flow Rate (gpm)	Stratification Temperature Difference (^{o}F)	Stratification Thickness (ft)
$D_o = 0.625$	$Z = 10$	$V_o = 11.7$	$\Delta T_i = 1.7$	$Z_s = 0.5$
$D_o = 0.875$	$Z = 20$	$V_o = 136.5$	$\Delta T_i = 93.6$	$Z_s = 19.5$

Figure 4 Large-Scale Tank Experimental Operating Conditions

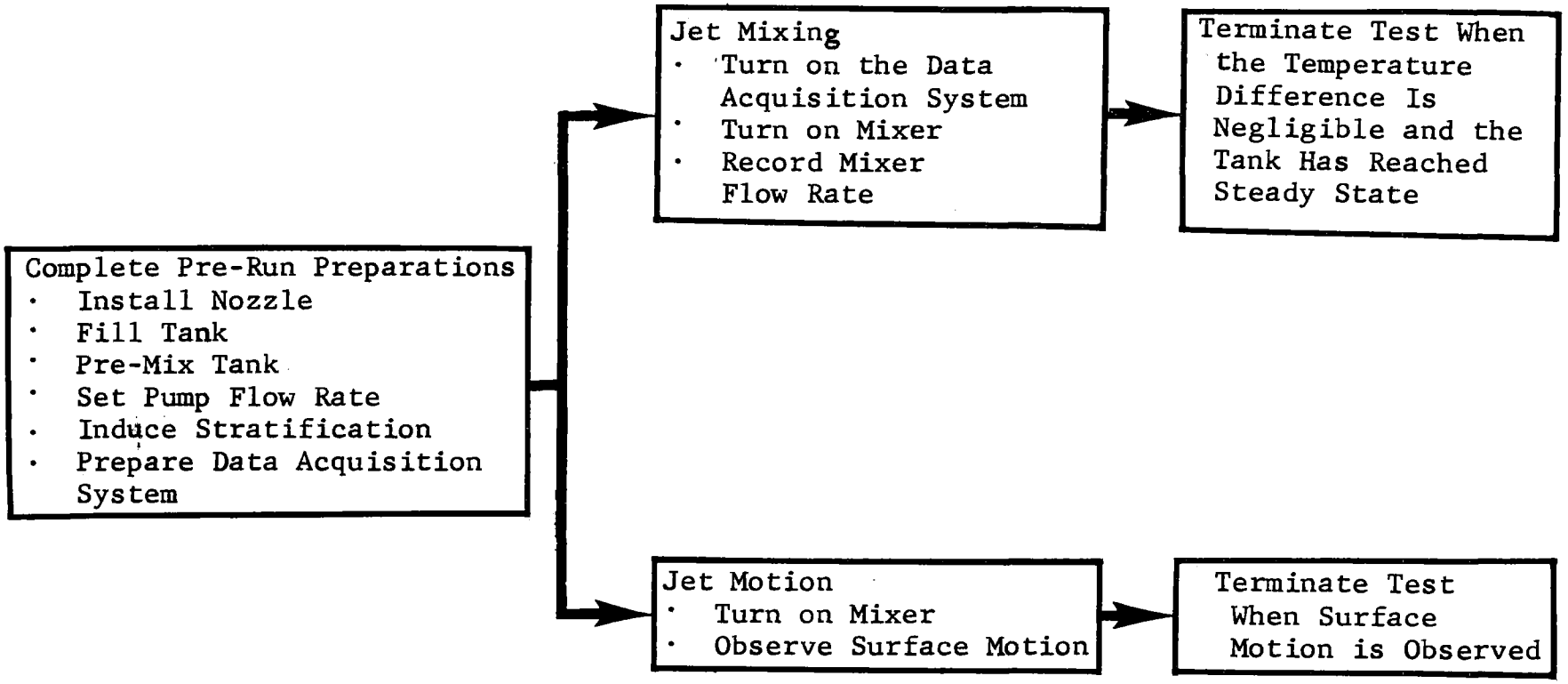

Figure 5 Test Procedure for Large-Scale Tests

2.5.1 Temperature Mixing Data

The temperature data obtained during the mixing of the thermal stratification consist of temperatures as a function of time for various positions in the tank. These positions are detailed in Figure 2 as numbered positions on the thermocouple rake. Although data were obtained throughout the tank, only the temperatures of the liquid surface and bottom are used in the correlations presented in Section 3. The remaining data points are used to determine the stratification depth and the extent of mixing during the test.

The temperature data from the thermocouples immediately below the liquid surface are especially important since, in a closed tank, the ullage pressure is directly related to the surface temperature of the liquid. Consequently, the surface temperature is of major concern in a stratification mixing study. The stratification in the tank is usually considered to be given by

$$T_{strat} = T_s - T_b$$

The surface temperature undergoes some extreme fluctuations almost as soon as the mixing begins. The slight delay is due to the jet transit time and the retardation of the jet penetrating the stratified layer, caused by buoyancy forces. These fluctuations are transient in nature and are due to the

cool jet flowing across the liquid surface and, then, the warm fluid being entrained in the cooler jet as the stratified layer begins to mix. The temperature at any given point on the surface can vary considerably, as shown in Figure 6. In this figure, the temperature at the tank centerline when mixing begins (where the jet impinges first on the surface) is much lower than the surrounding surface because of the cool jet. As mixing progresses, the surrounding surface temperatures also decrease because of the cooler fluid flowing radially across the tank surface toward the wall. The cooler fluid displaces warmer fluid and creates turbulence near the wall. As the warmer fluid is displaced, some of it is intrained into the jet. This raises the temperature of the jet and there is a partial recovery of the surface temperature. After the initial sharp transients, the temperature gradually decays until it reaches the mean temperature in the tank. This is the general mode of mixing in the tank. In a few cases, where the jet momentum is insufficient to immediately penetrate the stratified layer, there is a time period during which the jet slowly erodes away the bottom of the stratified layer as it impinges on it. This action may also result in transient temperature variations at the center of the surface as the jet partially penetrates and then is repulsed by the buoyancy of

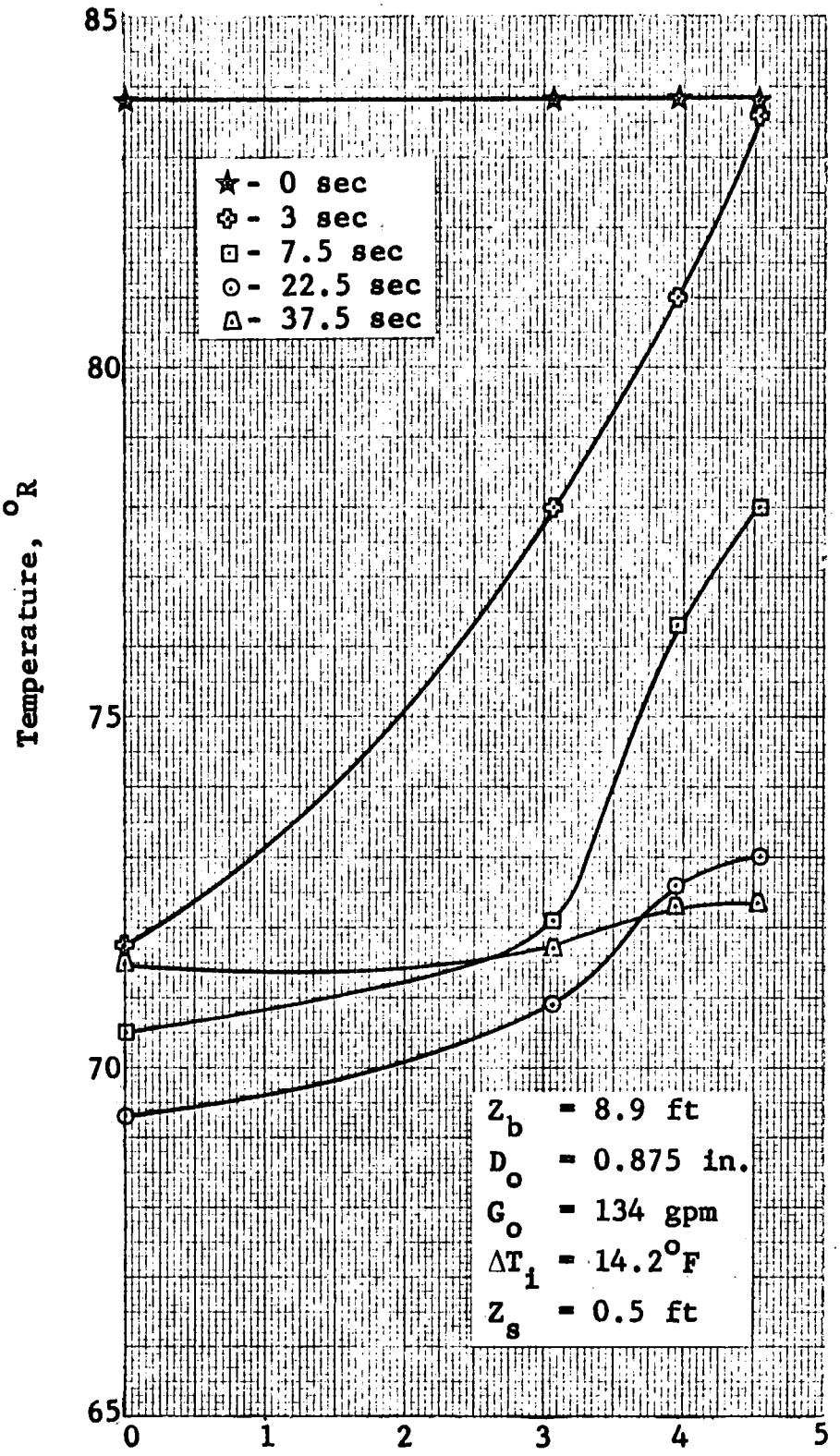

Figure 6 Large-Scale Tank Surface Temperature Variation During Mixing: Run 49

the stratified layer. Once a permanent penetration is obtained the temperature history is much the same as that of the previously described case.

The surface temperature variations can be large, and an average value of the surface temperature is useful to describe the surface mixing since it provides a good indication of the overall condition of the surface. This is especially true when the stratified layer initially begins to mix as a result of the axial jet impinging on the interface, since a large temperature gradient can exist across the liquid surface as cool fluid flows radially outward the wall. An average value was obtained from the temperature data by numerically averaging the output of the four surface thermocouples. This numerical average assumes that each thermocouple represents the temperature of an equal volume of fluid at a uniform temperature. The thermocouples were positioned such that equal-volume annular sections are obtained when boundaries between sections are located halfway between adjacent thermocouples. This also assumes that the flow in the tank is symmetrical about the tank centerline. This average surface temperature is one type of data presented.

A second type of temperature data presented is the surface temperature at the tank centerline, T_{s_1}. This is the point

at which the surface temperature initially begins to decrease; it is subjected to wider variations in temperature than are the other surface locations. Therefore it provides a good indication of when the jet penetrates the stratified layer and tank mixing begins. This temperature also provides an indication of either a sharp and complete penetration or a gradual penetration characterized by the jet slowly eroding away the stratified layer.

The third type of data presented is the fluid temperature at the nozzle exit, T_b. This temperature subtracted from a surface temperature reflects the temperature gradient between the surface and the tank bottom. The bottom temperature remains almost constant until the final phase of mixing. At this time it begins to slowly increase until it reaches equilibrium with the mean temperature of the tank fluid.

The mean temperature of the fluid is the average temperature of the fluid. Since for practical purposes no heat is added to or removed from the tank during mixing, the mean temperature of the fluid is constant during a given mixing test. Therefore the value of the mean temperature was taken as the temperature of the fluid at the end of mixing when the temperature is uniform in the tank. The difference between the surface temperature and the mean temperature reflects the extent to which the surface can be cooled by mixing.

Figure 7 shows a typical set of data obtained during a mixing test. The centerline surface-temperature data points are not connected in order to avoid confusion on the graph when the centerline surface temperature becomes equal to the average surface temperature.

The temperature data reflect the variables of water depth above the nozzle, flow rate, nozzle diameter, stratification temperature difference, and stratification thickness. Because of the number of variables, it is difficult to make comparisons of individual tests. The difference in tank size between the large-and small-tank tests prevent direct comparison of the two types of data. However, a most important observation is that the fluid is always thoroughly mixed, using flow rates which are predicted by scaling-up the small-scale-tank flow rates. This gives a preliminary confirmation of the validity of applying mixing parameters developed from small-scale data to the design of mixer systems for full-scale tanks.

2.5.2 Jet Motion Data

The axial jet motion data obtained during these tests provide data on the transit time of a jet in a large tank. The data were obtained by visually observing the surface of the fluid after turning on the pump and noting the time at which

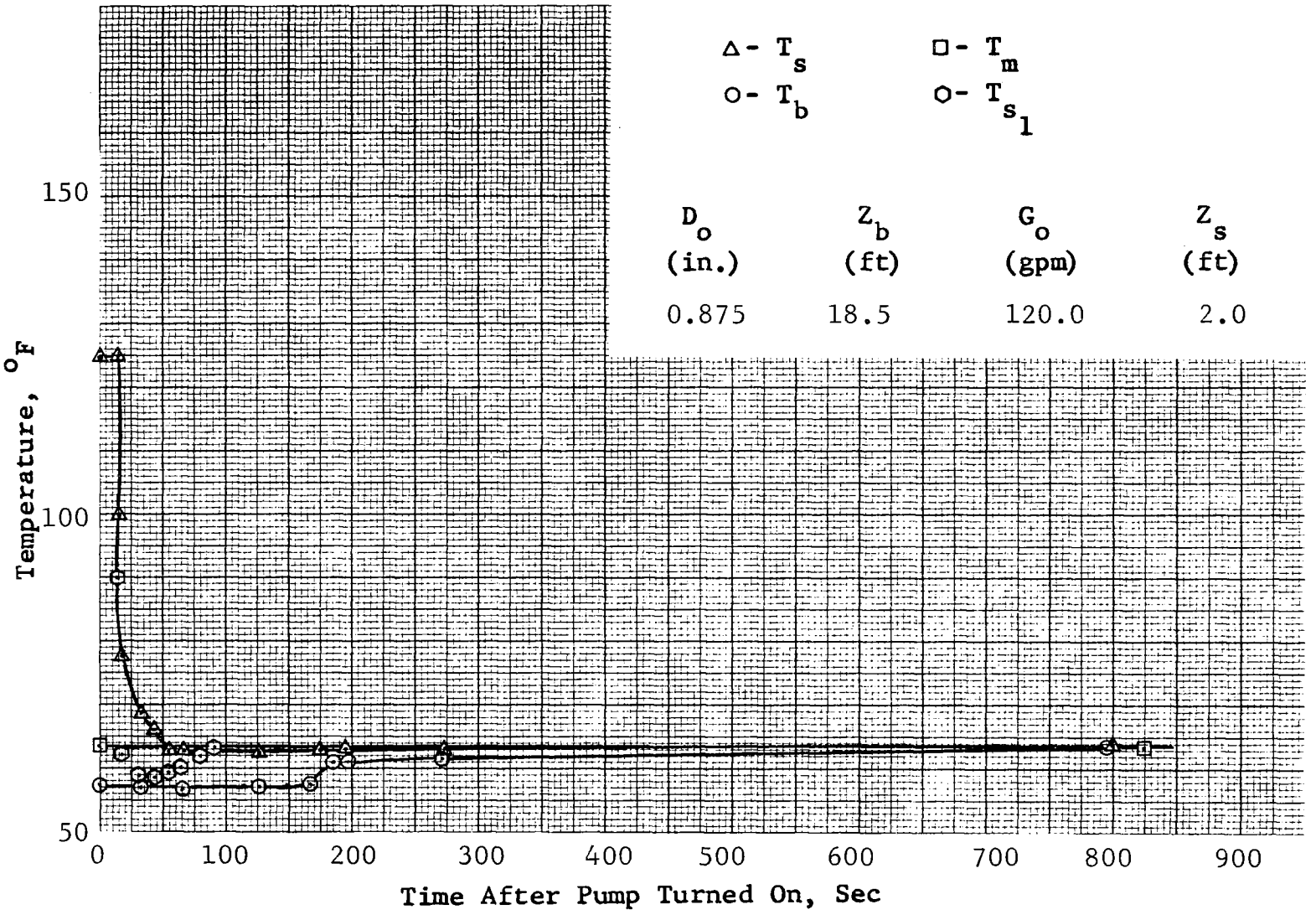

Figure 7 **Transient Temperature Destratification:** Run 3

motion began. The time interval between turning the mixer on and the beginning of surface motion is the jet transit time. Data were taken for both stratified and unstratified cases.

The initial motion of the surface was a slight upwelling of water. The magnitude of the upwelling appeared to be a function of both flow rate and liquid height; however, this was a subjective judgement and was not confirmed by measurements. The initial surface motion was circular in shape, indicating that the jet retained its shape while passing through the stratified layer.

Table 2 contains the jet motion data obtained during the test series. The data without run numbers are from tests conducted without stratification. The tests with the thick stratification of 9.5 feet did not reveal a uniform temperature in the stratified layer. Instead, the temperature gradient across the layer was large in each case.

Table 2

JET MOTION DATA

Run	G_o (gpm)	D_o (in.)	Z_b (ft)	ΔT_i (^oF)	Z_s (ft)	$\Delta\theta_j$ (sec)
20	60.0	0.625	18.2	18.0	9.5	16.0
22	90.55	0.625	18.2	11.7	9.5	10.0
23	89.5	0.625	18.2	7.5	9.5	10.0
25	28.4	0.625	18.2	3.5	9.5	35.0
26	30.0	0.625	18.2	0.0	0.0	33.0
27	30.0	0.625	18.2	1.5	1.5	32.0
28	26.5	0.625	18.2	4.5	5.5	35.0
31	24.6	0.625	18.2	0.0	0.0	40.0
--	20.0	0.625	18.2	0.0	0.0	46.0
--	25.0	0.625	18.2	0.0	0.0	37.0
--	112.0	0.875	18.5	0.0	0.0	13.0
--	100.0	0.875	18.5	0.0	0.0	12.0
--	81.5	0.875	18.5	0.0	0.0	18.0
--	65.0	0.875	18.5	0.0	0.0	20.0
--	40.5	0.875	18.5	0.0	0.0	31.0

SECTION 3

EXPERIMENTAL AND ANALYTICAL DATA CORRELATIONS

Large-scale experimental data correlations and the comparisons of these correlations with analytical predictions are presented in this section. The correlations consist of the transient data correlations for individual tests, the general correlations made from the collective data, and the jet motion correlations.

The transient data correlations consist of the dimensionless temperature decay during mixing and the energy distribution during mixing (energy integral). Only representative transient data are shown in this section because of the large amount of data obtained during these tests. All of the transient data are documented in Volume II.

The general correlations determined from the collective transient data and the jet motion data were used to summarize the following areas of investigation:

1. Transit time of the axial jet from the nozzle exit to the liquid/vapor interface.
2. Effect of buoyancy on mixing.
3. Mixing time of the axial jet mixer.

3.1 TRANSIENT DATA CORRELATIONS

The transient data correlations presented in Volume II consist of three forms of the dimensionless temperature decay and the energy integral as a function of dimensionless time.

3.1.1 Transient Dimensionless Temperature Correlations

In order to make meaningful comparisons between mixing tests with different stratification levels it is convenient to reduce the temperature differences to a dimensionless quantity referenced to the initial stratification when mixing began. This quantity, represented by

$$\frac{\Delta T}{\Delta T_i} = \frac{T_s - T_b}{(T_s - T_b)_i} \quad \text{or} \quad \frac{T_s - T_m}{(T_s - T_m)_i}$$

reflects the stratification remaining in the fluid at any time. Presenting $\Delta T/\Delta T_i$ as a function of a dimensionless time, given by

$$\frac{V_o D_o}{D_t^2}\,\theta$$

enables the other test variables to be considered.

The primary problem in using this type of correlation is establishing the time that the tank fluid begins to mix. In this study, mixing is assumed to begin when the surface temperature begins to drop rather than when the mixer is turned on.

This mixing time is referred to as θ_1. The time interval between these two occurrences consists of the transit time of the jet plus the delay in mixing due to the buoyancy of the stratified layer retarding the penetration of the cool jet to the surface. The following sketch shows the relationship between θ and θ_1

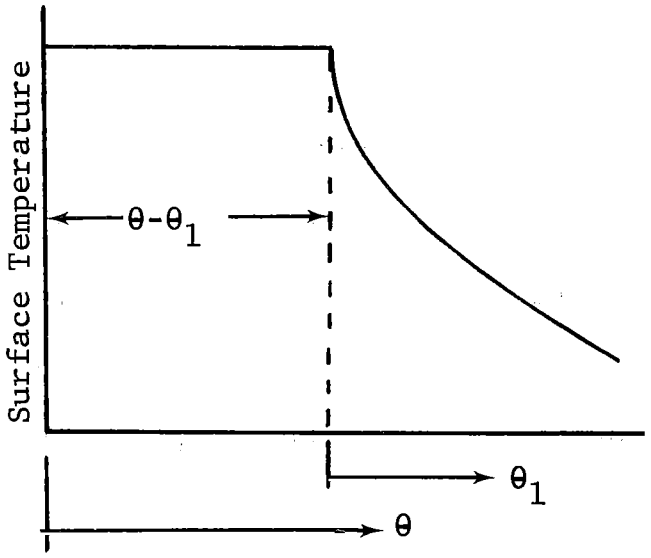

Three forms of the dimensionless temperature are shown in Volume II. These are

$$\frac{T_s - T_b}{(T_s - T_b)_i}$$

$$\frac{T_s - T_m}{(T_s - T_m)_i}$$

and

$$\frac{T_{s_1} - T_b}{(T_{s_1} - T_b)_i}$$

The use of the average surface temperature, T_s, in the correlations provides a good indication of the overall mixing of the surface layer. This form of the correlation tends to moderate the wide variations of temperature that occur at the tank centerline when mixing begins. The use of the centerline surface temperature, T_{s_1}, in the correlations shows this initial variation better. However, this type of correlation indicates that mixing occurs faster than it actually does at the beginning of the test. Therefore the data for the general correlations are based on the average surface temperature. The temperature at the nozzle exit subtracted from the surface temperature reflects the total temperature gradient in the tank and provides an easily determined value of existing stratification. The use of the mean fluid temperature, T_m, in the correlations reflects the extent that the surface temperature has departed from tank equilibrium conditions.

Also shown on the transient temperature decay correlations are the parameters Z_b/D_o, Z_b/D_t, N_{Re}, N_i^*, and $V_oD_o(\theta-\theta_1)/D_t^2$. The terms Z_b/D_o and Z_b/D_t reflect the geometry of the tank and nozzle. N_{Re} is the Reynolds number of the axial jet as it emerges from the nozzle. N_i^* is the ratio of the modified Grashof number to the square of the jet Reynolds number, given by

$$N_i^* = \frac{g\beta(T_s-T_b)_i Z_b^3}{(V_o D_o)^2}$$

where

g = Acceleration

β = Coefficient of thermal expansion

$(T_s-T_b)_i$ = Initial temperature stratification

Z_b = Liquid depth above the nozzle

V_o = Nozzle exit velocity

D_o = Nozzle exit diameter.

$V_o D_o\ (\theta-\theta_1)/D_t^2$ is the dimensionless time interval, consisting of the jet transit time and the buoyancy effect.

In Figure 8 a correlation is shown for a typical mixing test using $(T_s-T_b)/(T_s-T_b)_i$ and $(T_s-T_m)/(T_s-T_m)_i$. In Figure 9 the correlation $(T_{s_1}-T_b)/(T_{s_1}-T_b)_i$ is shown for the same test. An analytical prediction of mixing from Reference 2 is shown for comparison. This analytical prediction, based on dye observations of the bulk fluid motion during the small-scale tests, is given by

$$\frac{Z_b-Z}{Z_b-Z_i} = e^{-C^*\theta} = \frac{Z_d}{Z_{d_i}}$$

where

$$C^* = \frac{0.404}{\rho}\left(\frac{4}{\pi}\right)^{2/3}\frac{\dot{m}_o}{D_t^2 D_o}$$

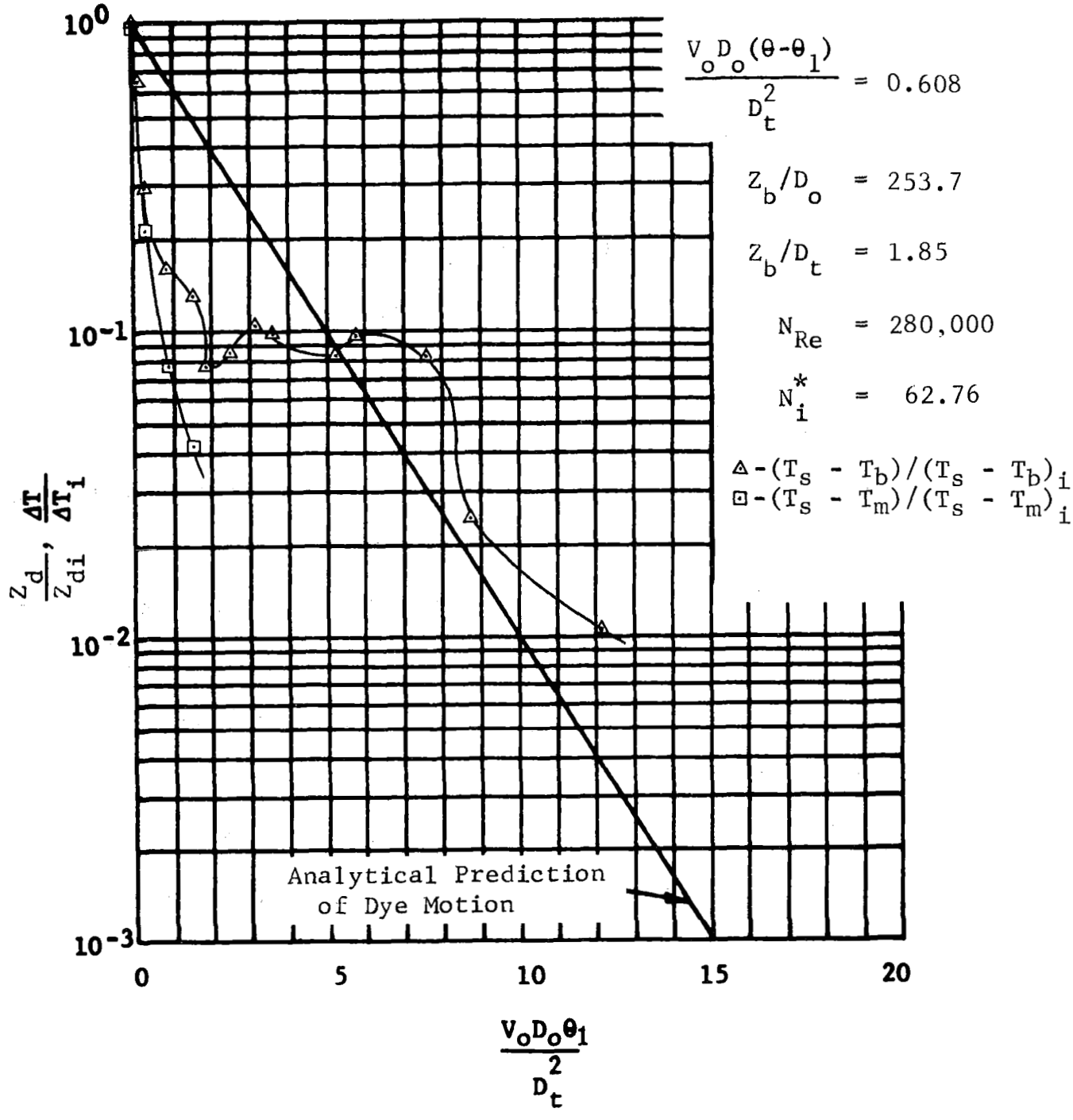

Figure 8 Fraction of Initial Temperature Difference After Surface Temperature Starts to Drop: Pump Starts at θ = 0.0 sec; Average Surface Temperature Drop Starts at θ_1 = 0.0 sec; Run 3

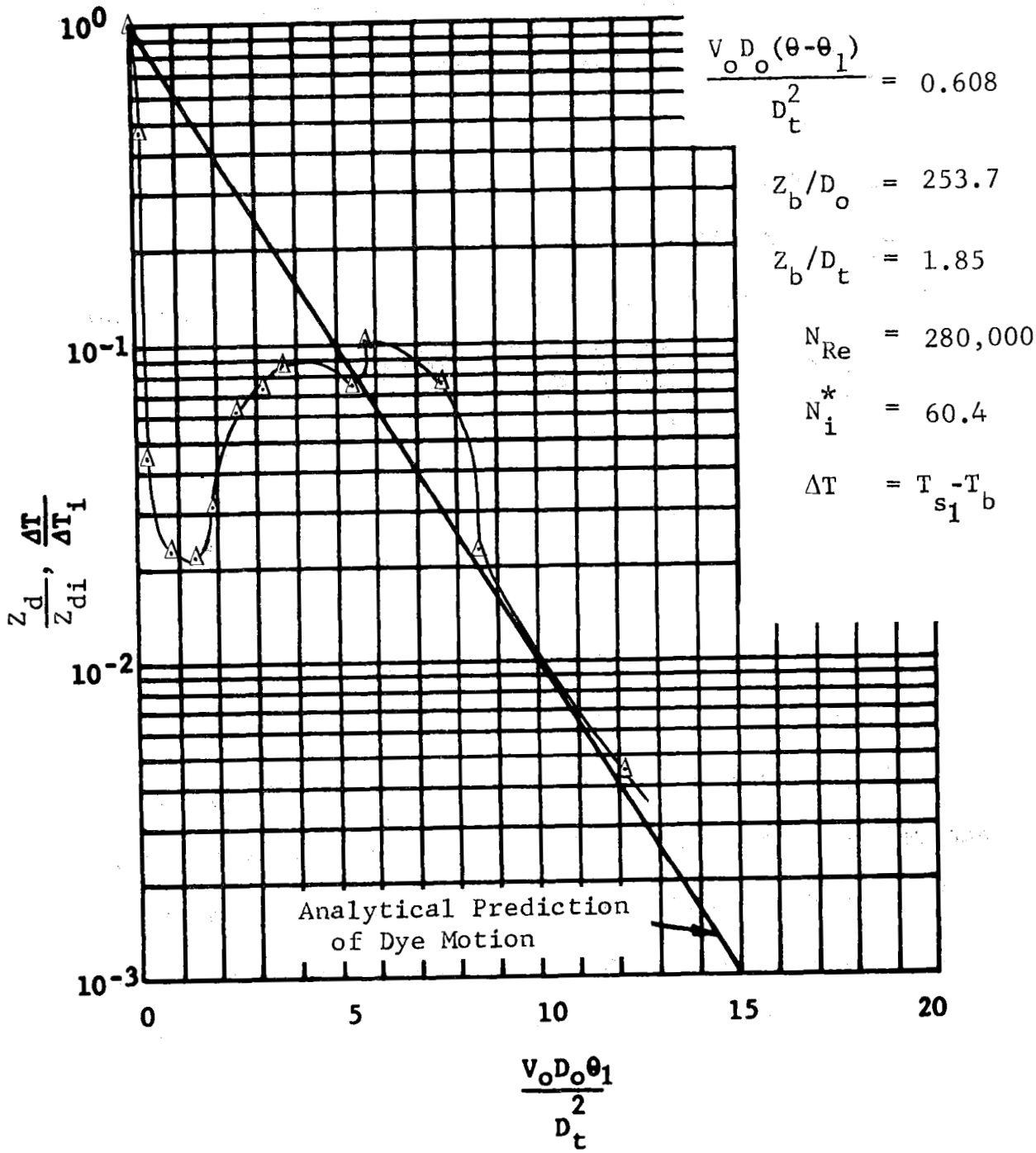

Figure 9 Fraction of Initial Temperature Difference After Surface Temperature Starts to Drop: Pump Starts at θ = 0.0 sec; Centerline Surface Temperature Drop Starts at θ_1 = 0.0 sec; Run 3

and

Z_d = Distance from the nozzle to the dye interface

Z_{d_i} = Initial distance from the nozzle to the dye interface

Z_i = Distance of lower dye interface from the nozzle exit

ρ = Liquid density

$\dot{m}_o$ = Nozzle flow rate

D_t = Tank diameter

These relationships are illustrated in the following sketch:

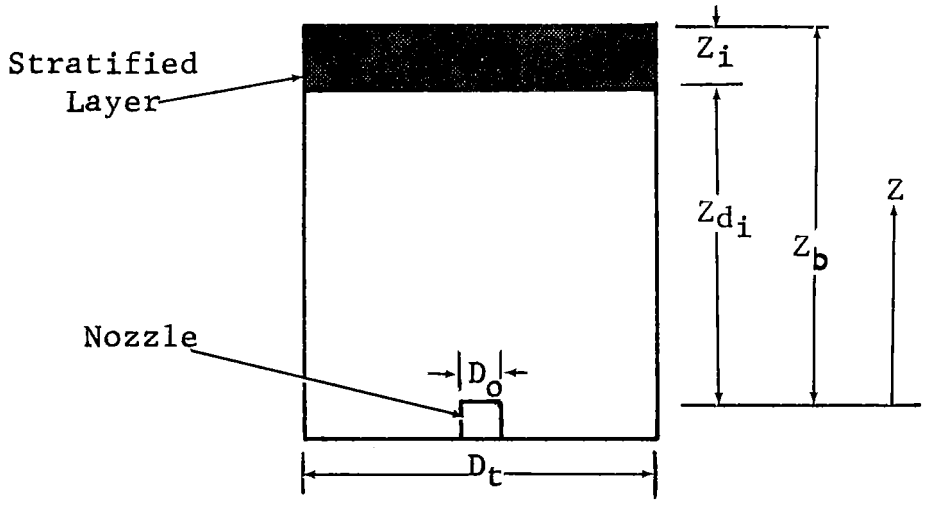

Although the two parameters Z_d/Z_{d_i} and $\Delta T/\Delta T_i$ reflect entirely different quantities, temperature and distance, they both reflect the degree of mixing that has occurred in the fluid. It was found in the Reference 1 study that small-tank transient temperature data indicate faster fluid mixing than predicted analytically when the value of N_i^* is less than approximately 50 (i.e., a plot of the test data as shown in Figures 8 and 9 would show the experimental temperature decay to be to the left or below the analytical prediction). Similar-

ly when N_i^* is greater than approximately 50, the transient temperature decay in the small-scale test tanks will occur slower than predicted analytically. This condition held for many of the large-scale tests, although there were many important exceptions. These included mostly tests with values of N_i^* greater than 50, in which observed mixing was less than or approximately the same as that predicted. There were, however, some tests with values of N_i^* less than 50 in which mixing was slower than predicted.

Since the transition value of $N_i^* = 50$ is an approximate value at best and intended only for use in making initial estimates of mixing, some variations from the norm should be expected. However, checking the data showed that the ratio of stratification thickness to liquid depth above the nozzle, Z_s/Z_b, was often quite different for the various tests. The data shown in Figure 10 illustrate the results of varying stratification depth for constant Z_b/D_o and Z_b/D_t and approximately constant N_i^*. These data show a definite trend toward longer mixing times as the stratified layer thickness is increased. There is also a noticeable decrease in the initial sharp temperature drop when the stratification thickness increases. However, the rate at which the temperature decay initially occurs appears to be the same. The percentage of

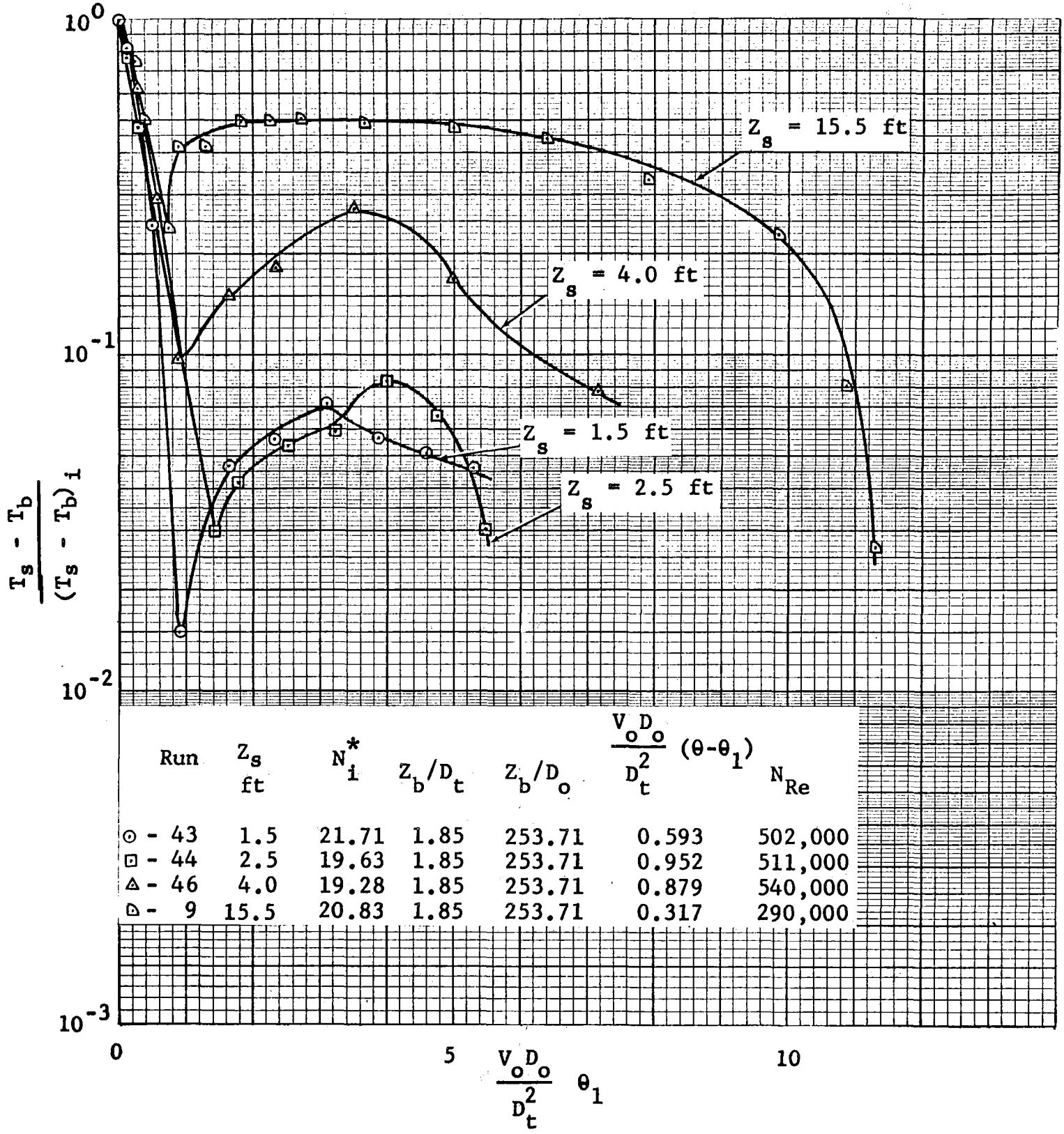

Run	Z_s ft	N_i^*	Z_b/D_t	Z_b/D_o	$\frac{V_o D_o}{D_t^2}(\theta-\theta_1)$	N_{Re}
⊙ - 43	1.5	21.71	1.85	253.71	0.593	502,000
⊡ - 44	2.5	19.63	1.85	253.71	0.952	511,000
△ - 46	4.0	19.28	1.85	253.71	0.879	540,000
⊡ - 9	15.5	20.83	1.85	253.71	0.317	290,000

Figure 10 Effect of Stratification Thickness On Mixing in Large-Scale Tank

temperature recovery is also much smaller for the thin stratified layers than for the thick layers.

In general, experimental mixing occurs faster than predicted for $N_i^* < 50$ and slower than predicted for $N_i^* > 50$. This observation is applicable for ratios of $Z_s/Z_b < 0.3$. The analytical prediction generally agrees with the mixing data for at least part of the mixing time and gives conservative values unless the stratified thickness is large. The common behavior of the dimensionless temperature data is initially to decay sharply, followed by a stratification recovery, and then to decay gradually, which parallels the analytical prediction. There is often a time period in which the stratification remains more or less constant as the temperature of the fluid around the nozzle is slowly increased to the mean fluid temperature.

Since small errors in the data can cause large errors in the correlations, it is valuable to know what the possible error sources are and when they occur in order to reduce their effect. The most significant error sources are due to discrepancies in reading values of data points, linear interpolation between data points to normalize data to a specific time, and the lag in response of the thermocouples to a temperature change. Discrepancies in reading values of data points become significant when the stratified level is small. This

occurs at the end of all runs and during the entire test for runs with small initial temperature differences. In general, when the temperature differences are less than $1^{o}F$ the data become questionable. Errors in the data due to linear interpolation between data points are most severe when large temperature changes are rapidly occuring. This is a characteristic of the time of initial penetration of the stratified layer by the jet. The lag in thermocouple response also creates errors when temperature changes occur rapidly. An analysis is presented in Appendix A for a model of the initial dimensionless temperature decay which approximates many of the results. This model indicates that the maximum error due to the lag in response will occur at the time the fluid begins to mix. This is also the time of the fastest temperature decay in the same area. All of these observations indicate that errors are most likely to occur at the beginning of mixing.

The results of the dimensionless temperature correlations will be used to make more general correlations; however, several points can be made about them now. Probably the most important observation that can be made from a survey of the correlations is that the analytical prediction is not always a good indicator of how mixing takes place. It appears to be a conservative prediction as long as the stratification depth

is moderate or the temperature gradients across the stratified layer are steep. The last case is common in cryogenic tanks with moderate sidewall or ullage heating.

3.1.2 Energy Integral

The energy integral, defined as

$$I_m = 1 - \frac{T_s - T_m}{T_s - T_b}$$

is a measure of the energy distribution in the tank. This term, primarily determined as an intermediate step in the calculation of other parameters, is also a useful indicator of mixing in the tank.

The initial value of the energy integral, I_{m_i}, depends on the type of stratification. When I_{m_i} is 0.0, the mean tank temperature is equal to the bottom temperature, and the thermally stratified layer is either a very thin uniform layer or a thick layer with a sharp temperature gradient. Larger values of I_{m_i} $(0 < I_{m_i} < 1)$ indicate a thicker stratified layer As the tank fluid is mixed, the energy is distributed more evenly and I_m approaches 1. There may be a transient period in which the energy integral becomes greater than 1 as a result of the cool jet penetrating the stratified layer and flowing fluid with a temperature below T_m across the surface. This

is always a very short-lived phenomenon and is associated with the initial sharp temperature drop seen in the dimensionless temperature correlations. The values calculated for I_m during this period are not always dependable, since the temperature differences can be small and slight errors in temperature values result in large changes in I_m. This situation also exists to a lesser extent as the fluid is approaching a mixed condition and I_m approaches 1. When I_m is 1.0, the fluid is completely mixed.

Comparison of the values of I_{m_i} with the transient temperature correlations indicate that runs with values of I_{m_i} that were less than 0.2 tended to undergo faster mixing than predicted analytically.

Figure 11 shows a typical correlation of I_m versus $V_o D_o \theta / D_t^2$. This run had a brief period of inverse stratification.

3.2 LARGE-SCALE DATA CORRELATIONS

The correlations of the large-scale data consist of correlations of jet transit time, correlations demonstrating the effect of buoyancy on mixing, and correlations of the mixing time of the axial jet mixer. With the exception of the jet transient time correlations, the correlations shown are based on the transient dimensionless temperature correlations dis-

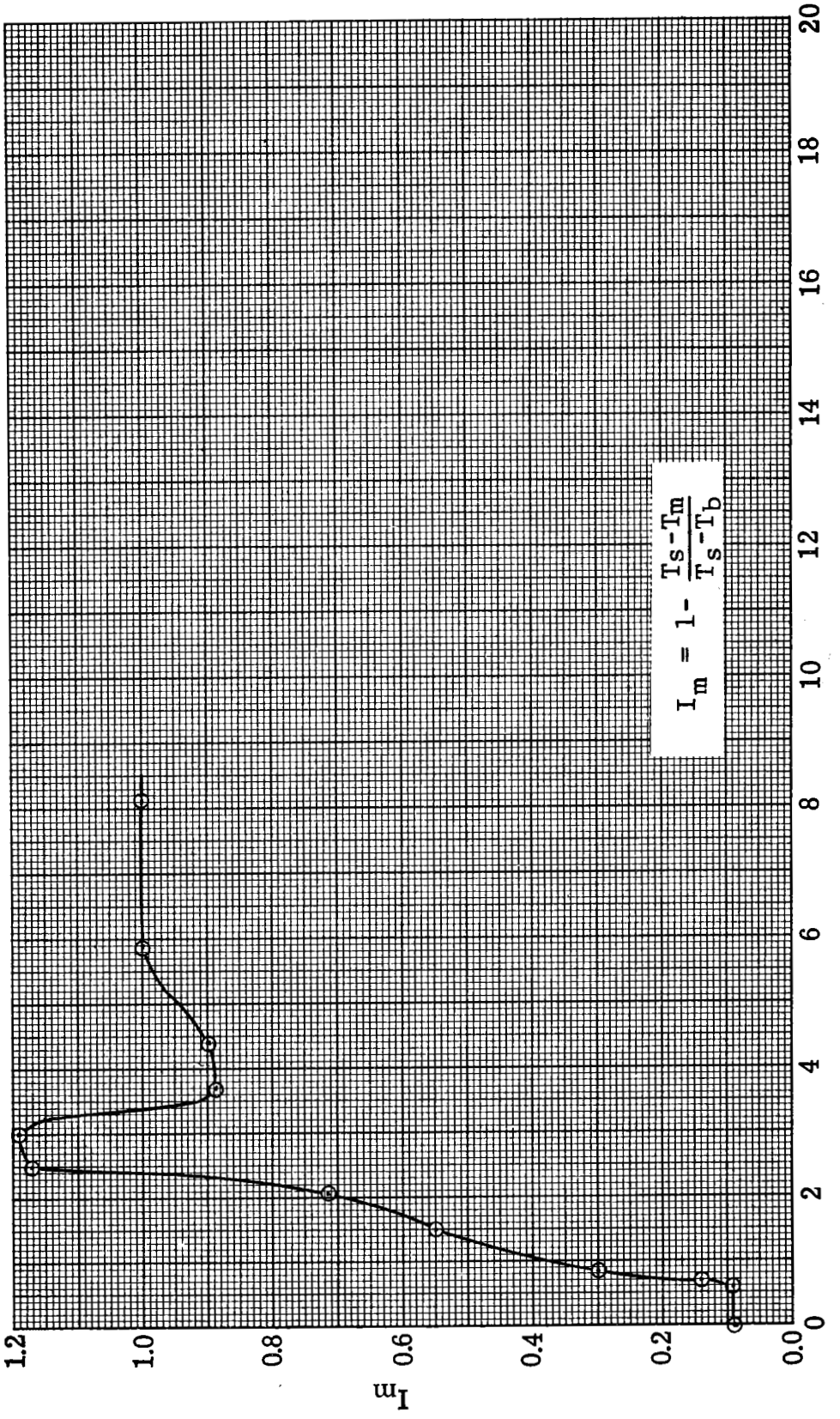

Figure 11 **Transient Energy Integral:** Run 3

cussed in Subsection 3.1 and presented in Volume II. The correlations presented in this section include:

1. A correlation of the dimensionless time for the axial jet to reach the liquid surface ($V_o D_o \Delta\theta_j / D_t^2$ versus Z_b/D_t).

2. A correlation of the dimensionless time interval between turning the pump on and the initial drop in surface temperature minus the dimensionless jet transit time $V_o D_o(\theta-\theta_1-\theta_j)/D_t^2$ as a function of a parameter N, where

$$N = 4b^2 N_i^* \frac{\left(I_{m_i} - I_{m_i}^2\right)}{1 + 2 I_{m_i}}$$

3. Correlations of the dimensionless time after the temperature starts to drop to the point where the temperature difference between T_s and T_b reaches a desired percentage of its initial value as a function of N_i^*.

3.2.1 Jet Transit Time Correlation

The time required for the jet to reach the surface is shown in Figure 12 as a function of the nozzle exit flow rate. The data display a distinct trend for each nozzle diameter. Also shown are predictions made from the analytical equation (developed in Reference 3 but using a corrected coefficient shown in Reference 1)

$$\frac{V_o D_o}{D_t^2} \Delta\theta_j = 0.152\left(\frac{Z_b}{D_t}\right)^2$$

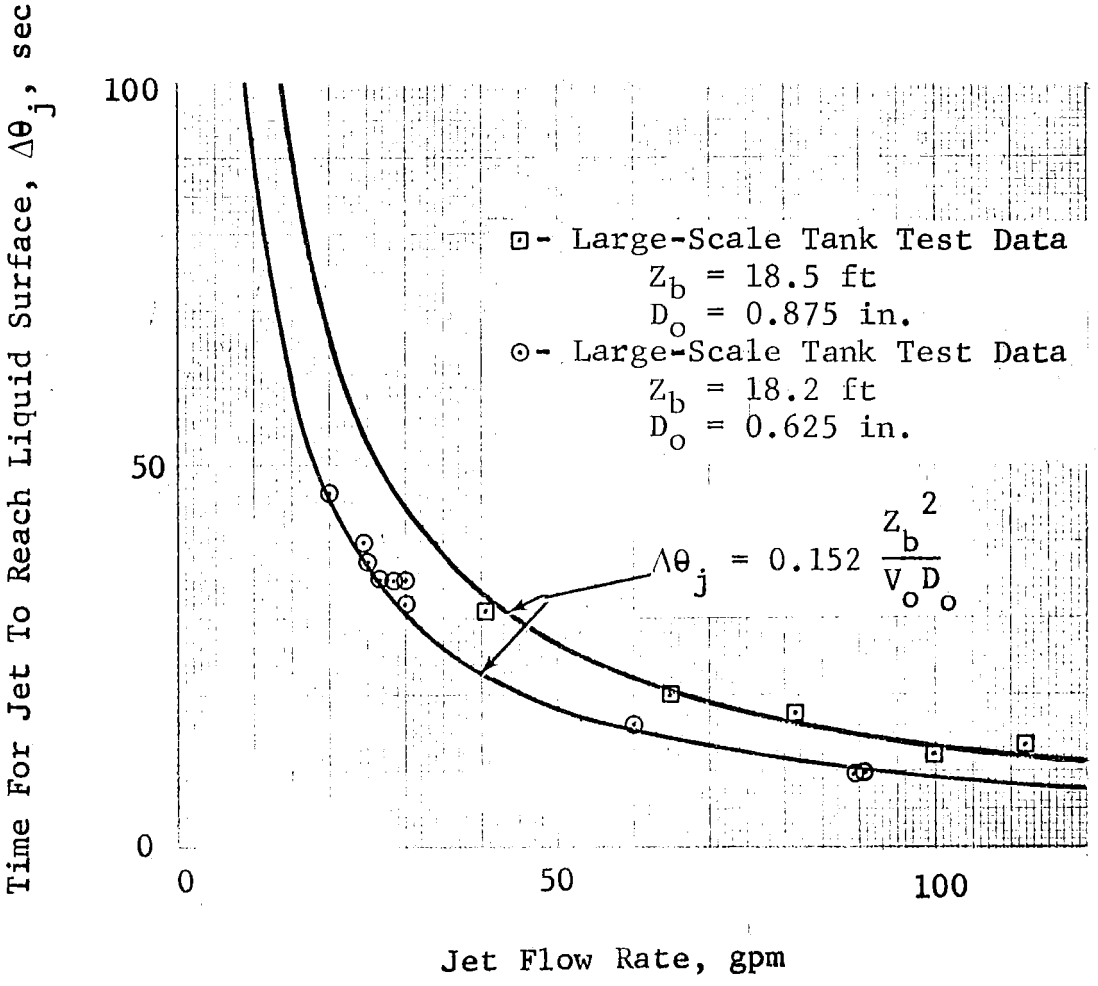

Figure 12 Large Scale Tank Experimental Axial Jet Motion Compared with Prediction From Small Scale Tank Correlations

The agreement between the experimental data and the prediction is excellent. This equation predicts twice the transit time as the equation developed in Reference 3.

Figure 13 shows the jet transit time as a function of Z_b/D_t. The plot of the analytical prediction and the test data again demonstrate the good agreement between the two.

3.2.2 Correlation of Buoyancy Effects

The difference between the jet transit time and the time interval between mixer activation and the initial surface temperature drop is due to the buoyancy of the stratified layer retarding the jet. This time interval in dimensionless form is given by

$$\frac{V_o D_o}{D_t^2} \quad (\theta - \theta_1 - \theta_j)$$

and is shown in Figure 14 as a function of the parameter N, given by

$$N = 4b^2 N_i^* \frac{\left(I_{m_i} - I_{m_i}^2\right)}{1+2I_{m_i}}$$

where the constant b is 0.25.

Figure 14 shows a decline in the buoyancy effect as N decreases, and then a more or less constant value of the buoyancy effect. The value of N at which the buoyancy effect becomes

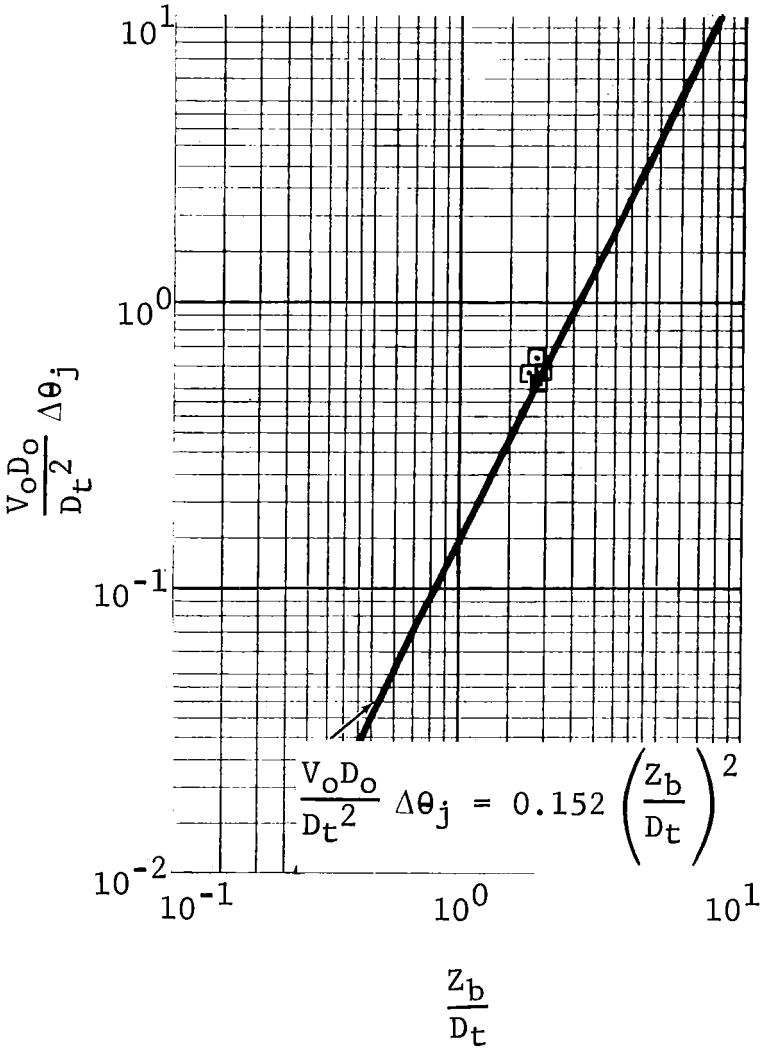

Figure 13 Correlation of Axial Jet Transit Time for Large-Scale Tank Tests

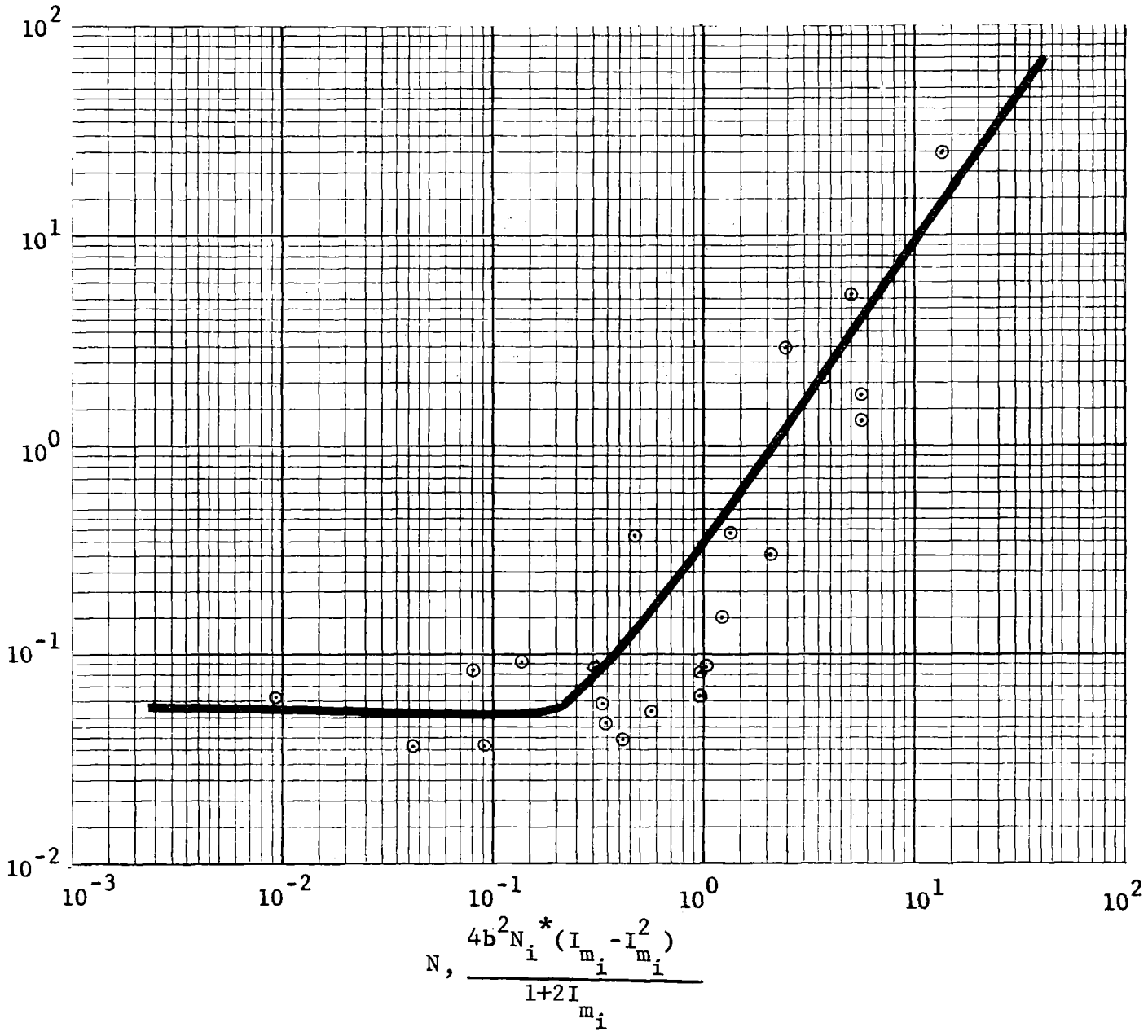

Figure 14 Effect of Buoyancy On Mixing: Large Scale Water Tests

approximately constant is about 0.5. The value of $V_o D_o(\theta-\theta_1-\theta_j)/D_t^2$ at this point is about 0.08. This is a relatively small value and indicates that the buoyancy effects can be ignored at values of N less than 0.5. Since N is a function of N_i^*, which is a function of the local acceleration, the effect of buoyancy may be ignored in the prediction of mixing time for low-g situations.

3.2.3 Correlation of Mixing Times

The time required for the dimensionless transient temperature to be reduced to some desired percentage of its initial value is by definition, the mixing time required to obtain the desired condition. The time can be obtained from the plots of the dimensionless mixing time given in Volume II. The dimensionless temperature considered is

$$\frac{T_s-T_b}{(T_s-T_b)_i}$$

The times required for this term to reach 20%, 10%, and 5% of its initial value were selected from each test. It was assumed that the temperature stratification is reduced to its desired value when there is no stratification recovery to a point above this value. This is demonstrated in the following sketch,

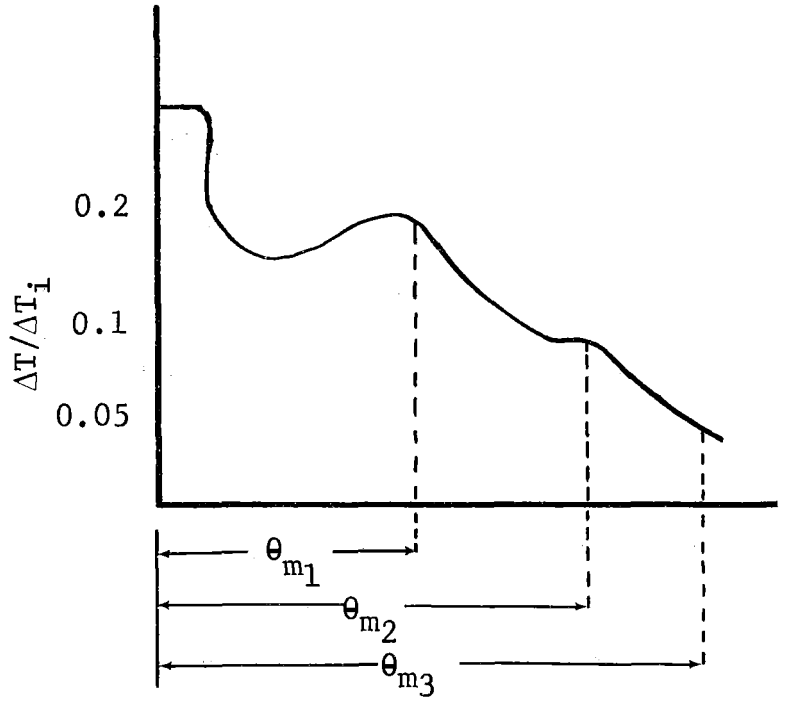

where θ_{m_1}, θ_{m_2}, and θ_{m_3} are the mixing times for reducing the stratification to 20%, 10% and 5%, respectively.

Figures 15, 16, and 17 show the data points from the transient data as a function of N_i^* for the three mixed conditions. These figures show the data falling into two separate groups. Examination of the individual test data show that the data points in the two data groups correspond to tests with stratification depths that can be described as "thick" and "thin". In the so called "thin" layer tests, mixing is much faster than in the "thick" layer tests for otherwise equivalent mixing conditions. However, as N_i^* increases, the mixing times

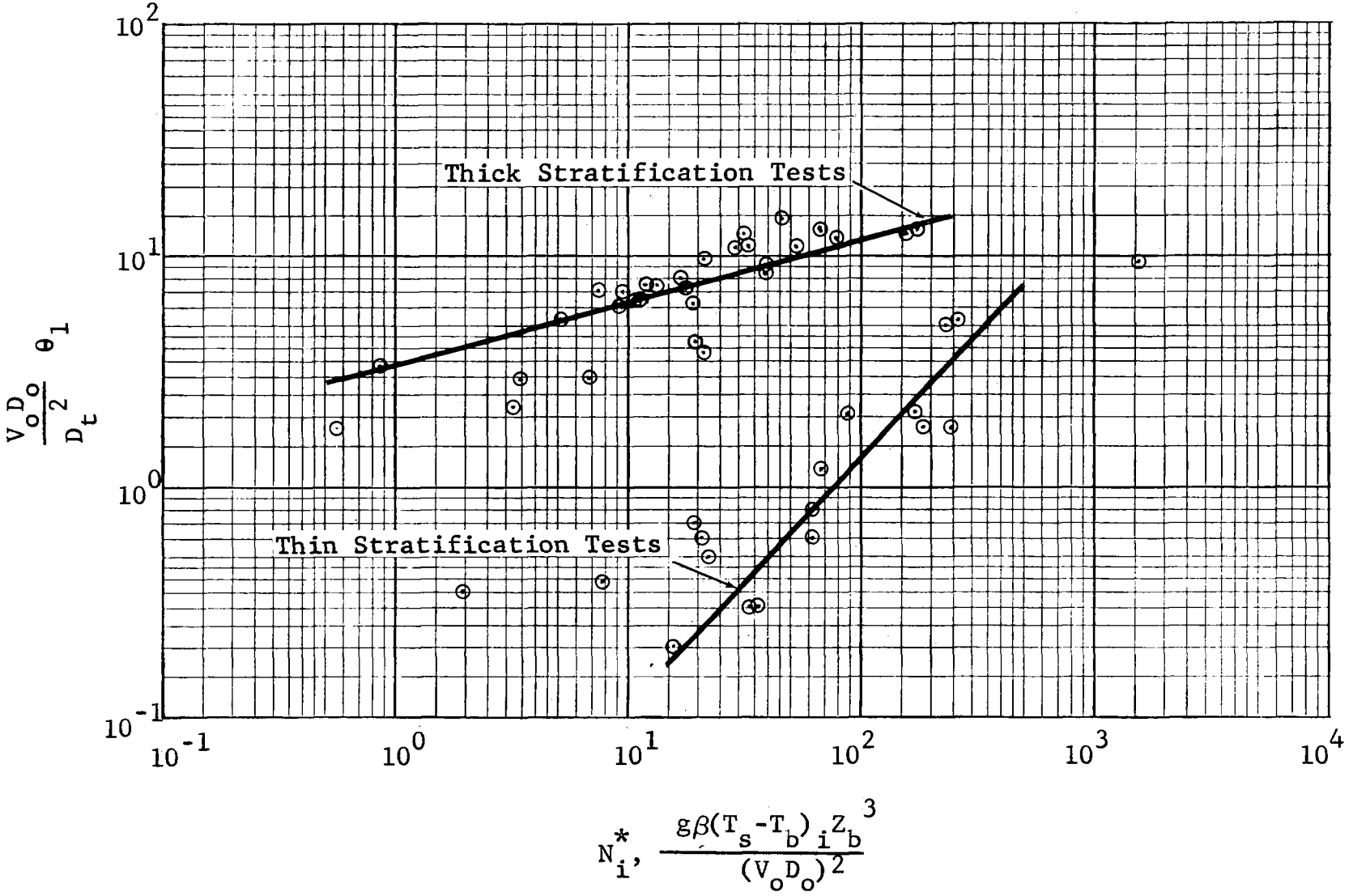

Figure 15 Correlation of Dimensionless Time Required for Temperature Stratification to Reach 20% of Its Initial Value Versus N_i^*: Large-Scale Tank Tests

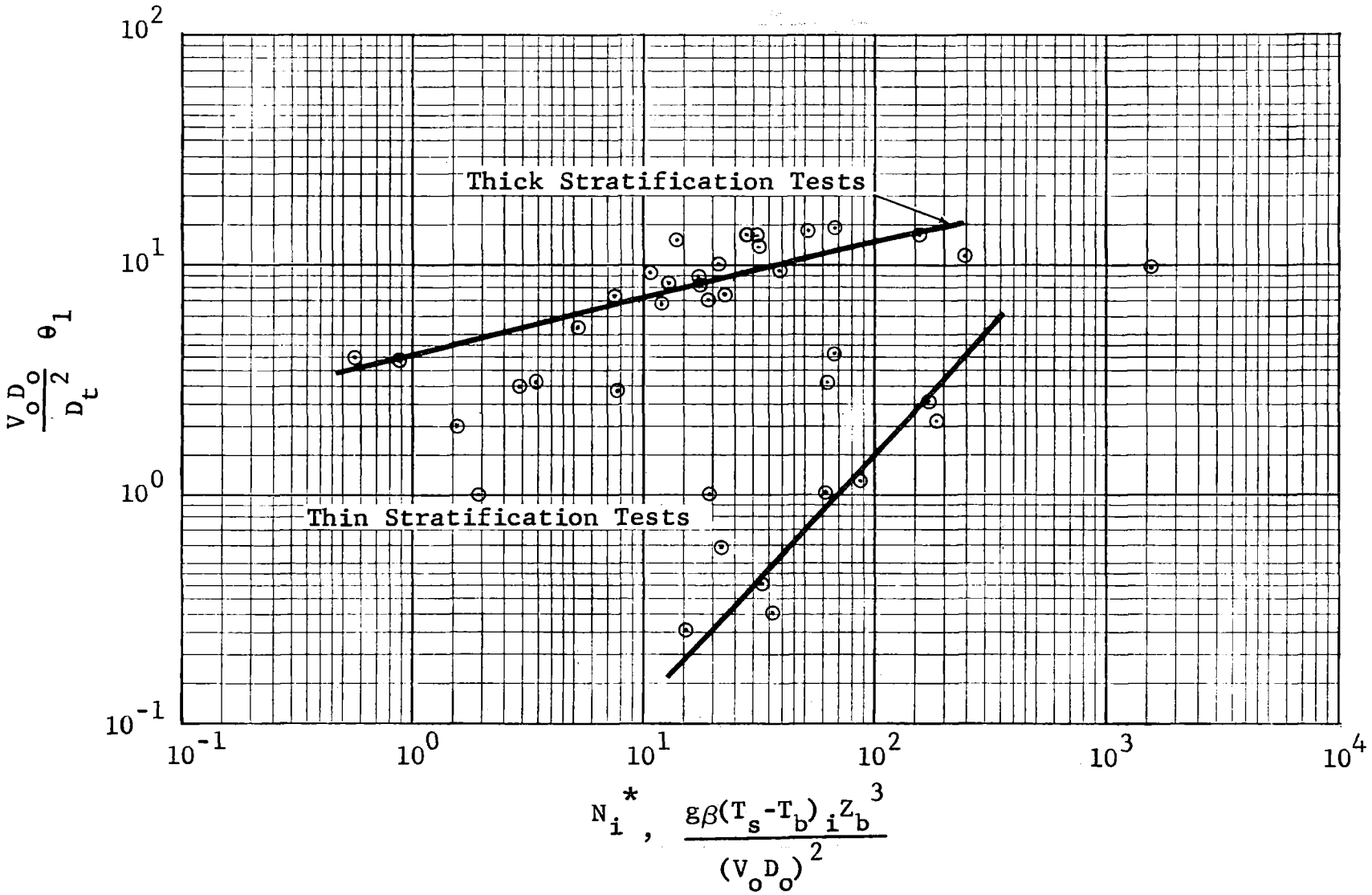

Figure 16 Correlation of Dimensionless Time Required for Temperature Stratification to Reach 10% of Its Initial Value Versus N_i^*: Large-Scale Tank Tests

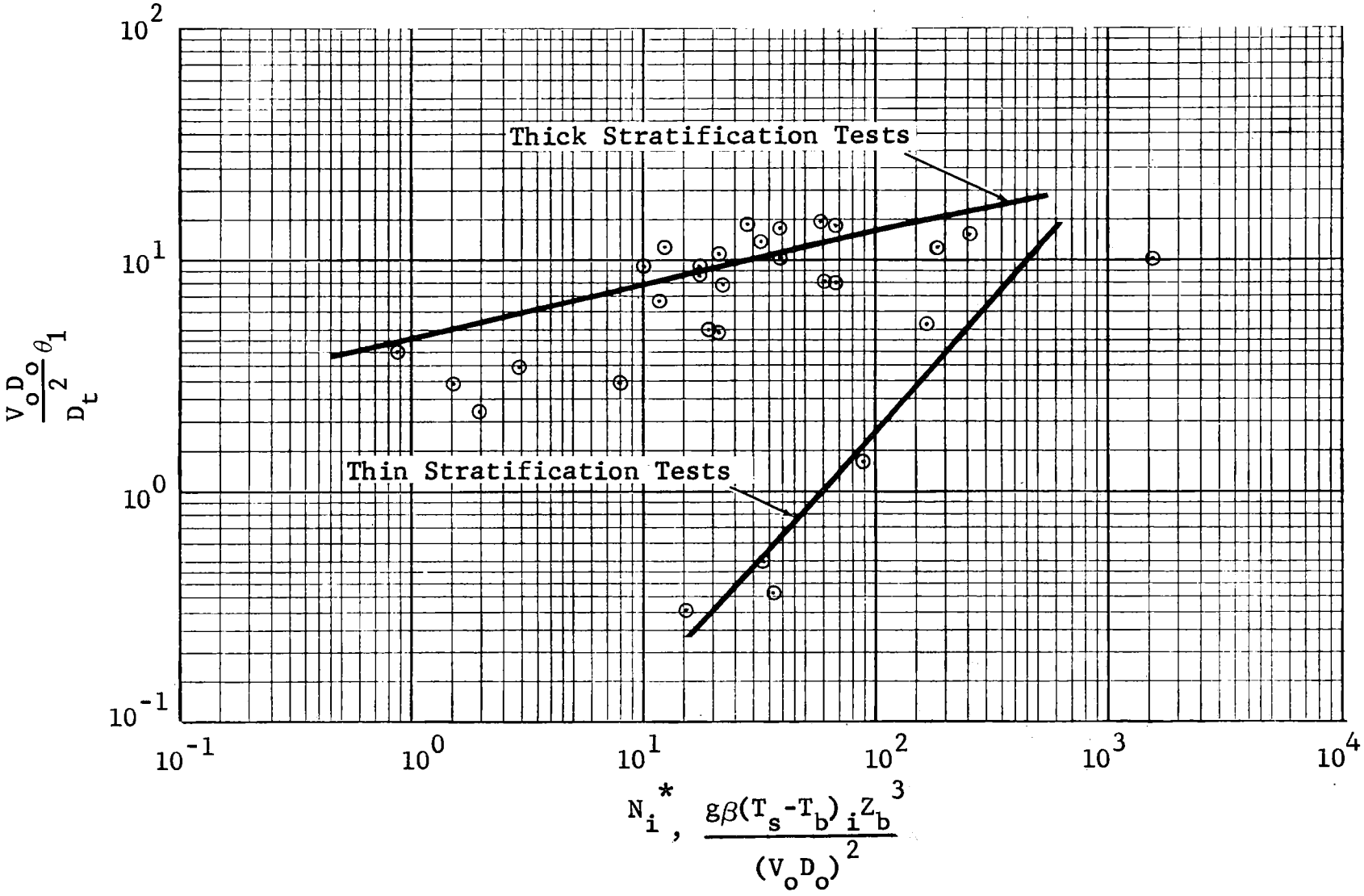

Figure 17 Correlation of Dimensionless Time Required for Temperature Stratification to Reach 5% of Its Initial Value Versus N_i^*: Large-Scale Tank Tests

for both sets of tests approach each other. This is as expected since buoyancy forces increase with increasing N_i^*.

An effort was made to obtain correlations that would reflect the stratification thickness or the energy distribution. The most successful correlation was the mixing time versus N. Figures 18, 19, and 20 show this correlation. The data show the mixing time to increase with N. The data scatter for these correlations decreases with increased mixing time.

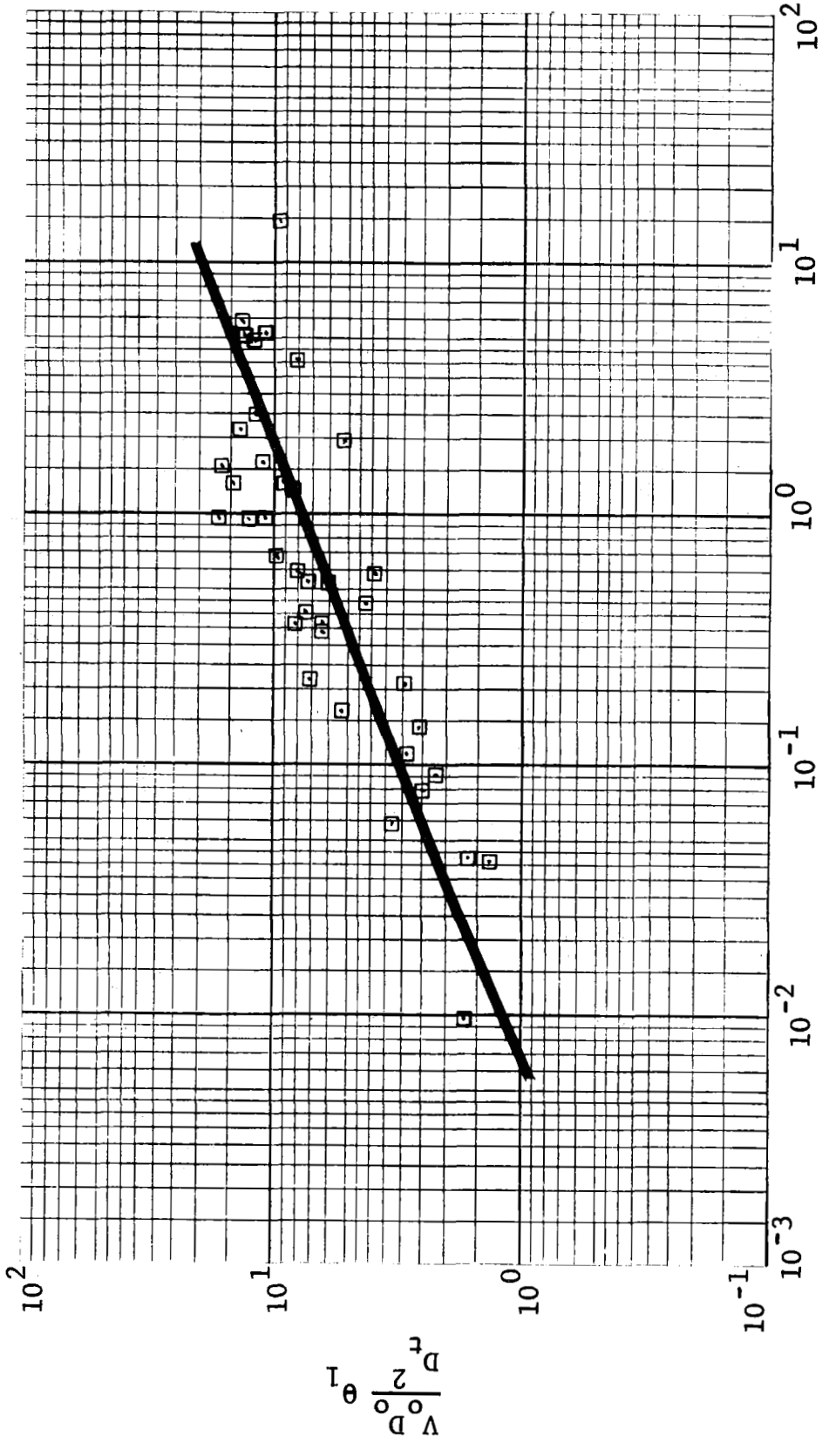

Figure 18 Correlation of Dimensionless Time Required for Temperature Stratification to Reach 20% of Its Initial Value Versus N: Large-Scale Tests

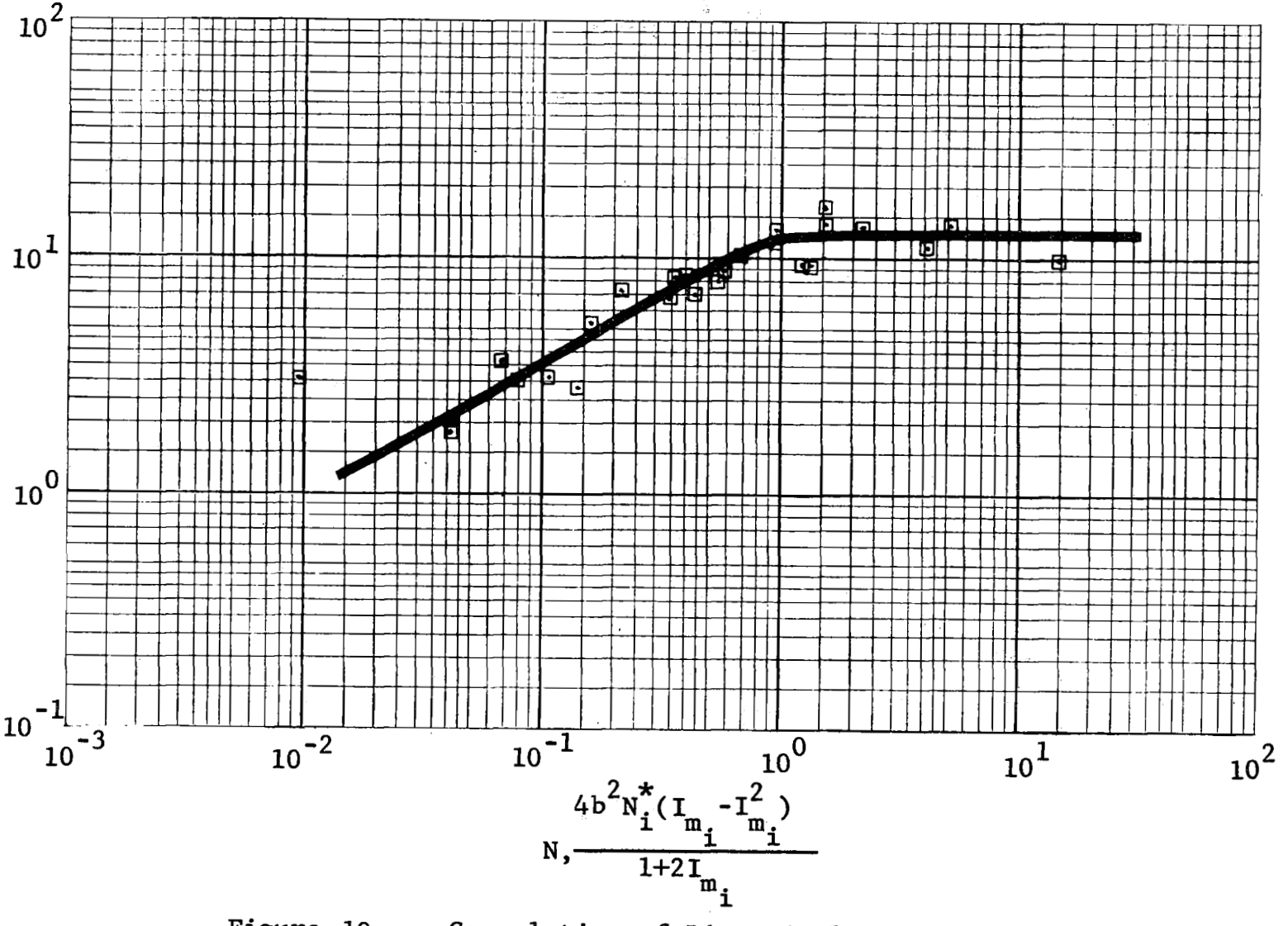

Figure 19 Correlation of Dimensionless Time Required for Temperature Stratification to Reach 10% of Its Initial Value Versus N: Large-Scale Tests

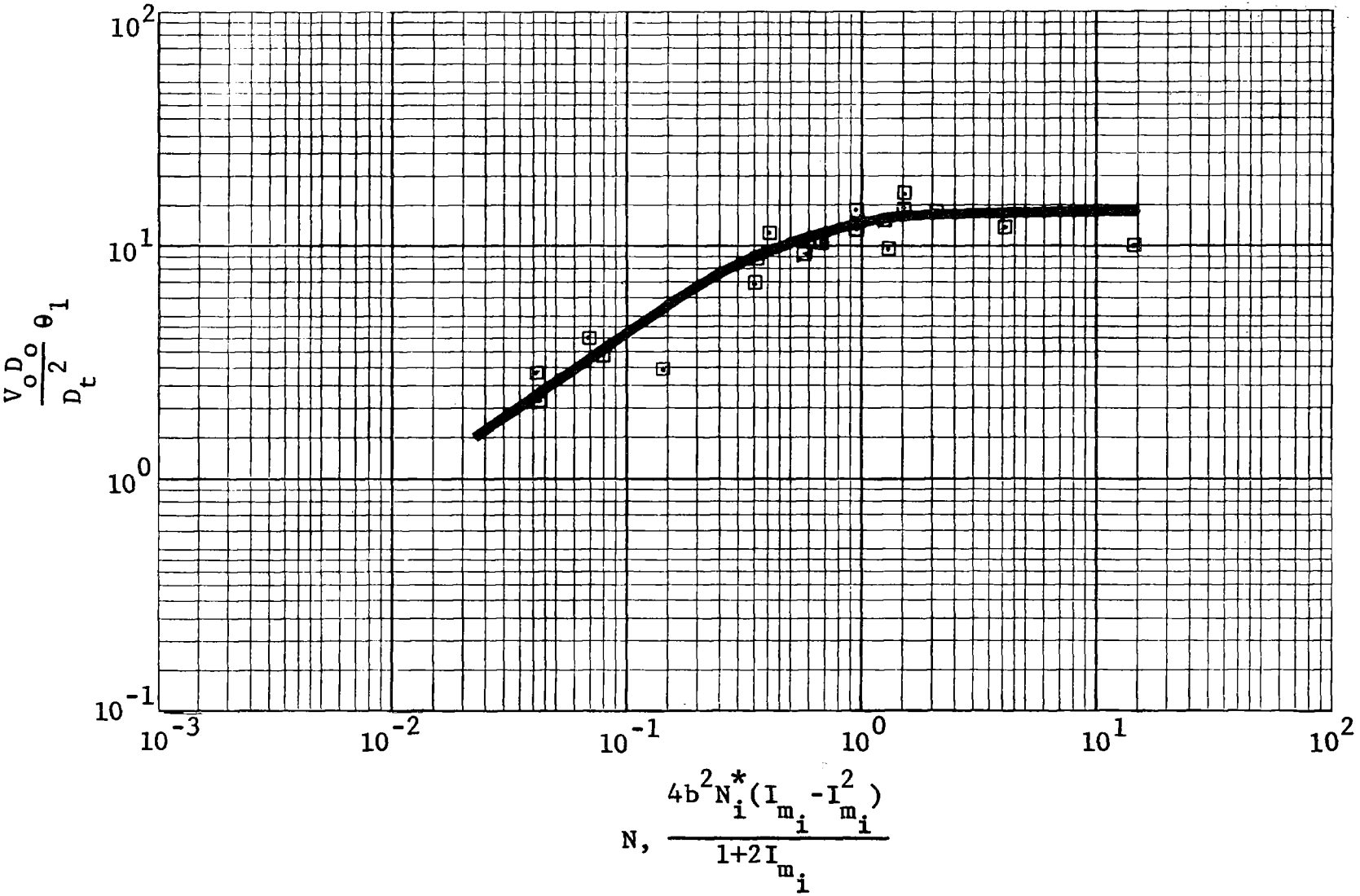

Figure 20 Correlation of Dimensionless Time Required for Temperature Stratification to Reach 5% of Its Initial Value Versus N: Large-Scale Tests

SECTION 4
COMPARISON OF LARGE- AND SMALL-SCALE CORRELATIONS

The purpose of the experimental investigation was to confirm the validity of using small-scale test data to develop parameters and methods for the design of mixer systems for use in full-scale tanks. This was to be accomplished by determining if the small-scale data correlations from Reference 1 agree with the values of the same parameters obtained from large-scale tests conducted under similar conditions. This is done by direct comparison of the two types of data.

4.1 COMPARISON OF LARGE- AND SMALL-SCALE JET TRANSIT TIME CORRELATIONS

The large- and small-scale data for the transit time of the axial jet to travel from the nozzle exit to the liquid surface are shown in Figure 21 as a function of Z_b/D_t. The analytical prediction given by

$$\frac{V_o D_o}{D_t^2} \Delta\theta_j = 0.152 \left(\frac{Z_b}{D_t}\right)^2$$

is also shown in this figure. This coefficient for this equation was developed from small-scale test data. The excellent

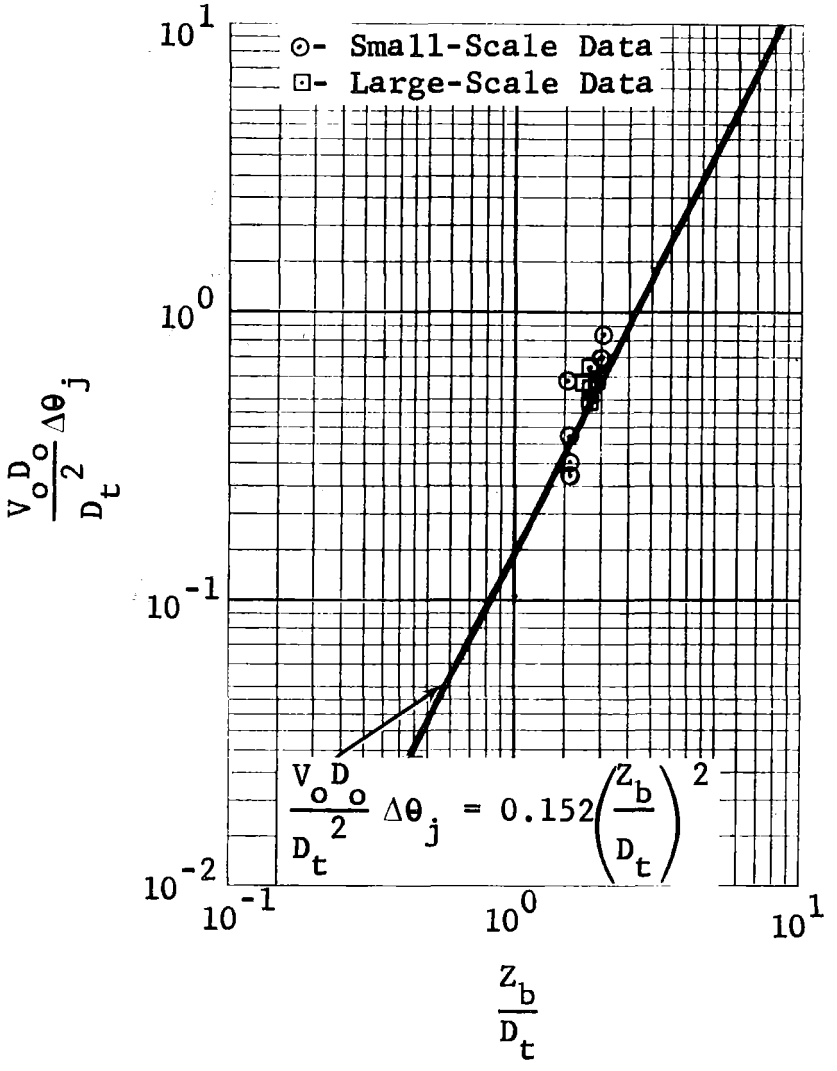

Figure 21 Correlation of Axial Jet Transit Time for Large and Small-Scale Tests

agreement of the large- and small-scale data is apparent from this comparison. Therefore, the previous finding that the jet transit time is approximately twice that given in the prediction of Reference 3 still holds.

4.2 COMPARISON OF LARGE- AND SMALL-SCALE TANK BUOYANCY EFFECTS

A major conclusion from the previous study was that buoyancy effects in the tests simulating low-g mixing could be neglected when determining the mixing time. Figure 22 shows the combined data from the large- and small-scale tanks. The two data sets overlap each other and the data points are closely associated to give good agreement. Both sets of data indicate a decrease in the buoyancy effect with decreasing N until a value of $N = 0.5$ is reached. For values of $N < 0.5$, the buoyancy effect is approximately constant with a value of about 0.1. The previous conclusion that buoyancy effects can be neglected when predicting low-g mixing times is valid.

4.3 COMPARISON OF LARGE- AND SMALL-SCALE TANK MIXING TIMES

In the large-scale tests, stratification thickness was found to be an important variable affecting mixing time, and

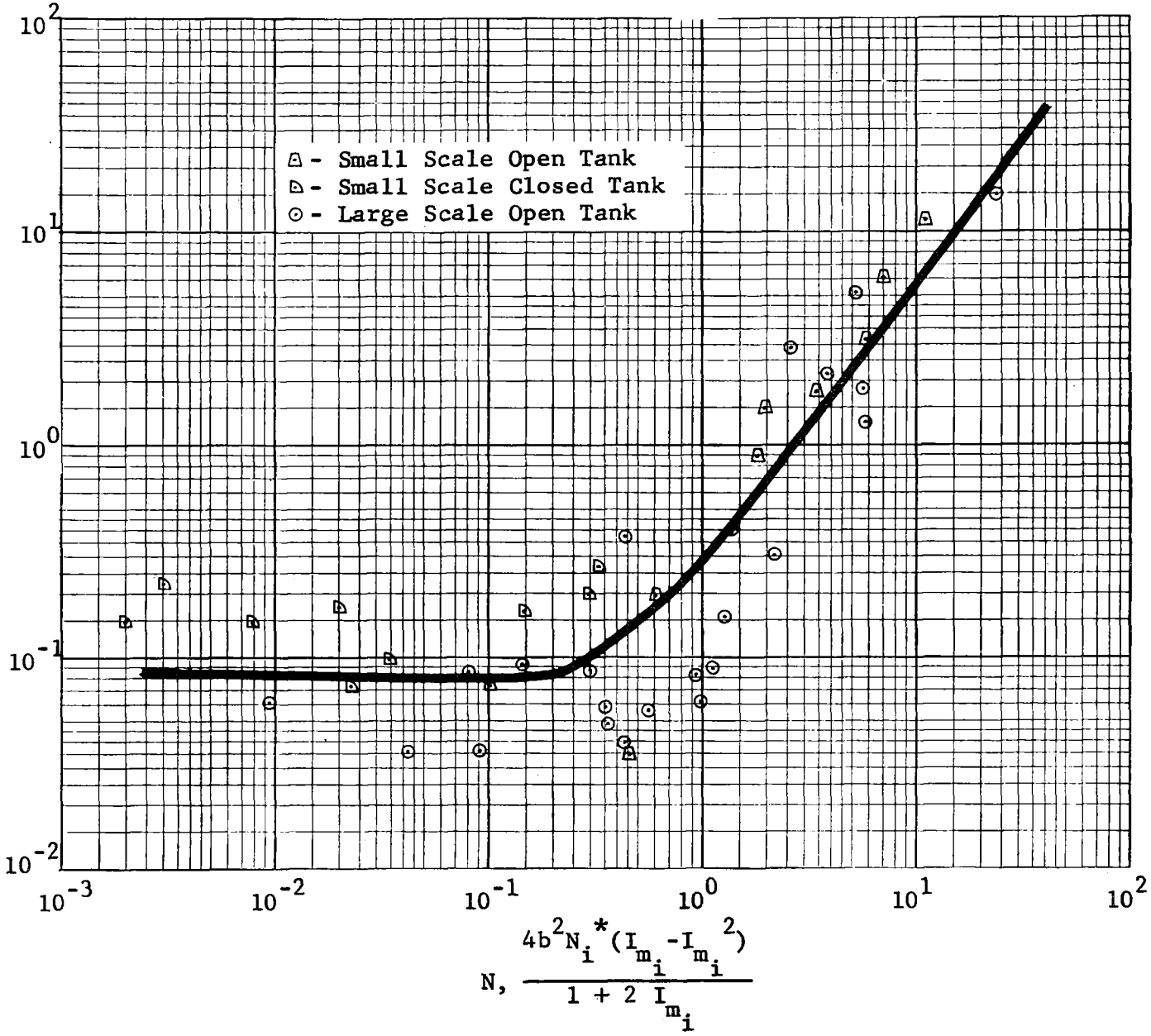

Figure 22 Effect of Buoyancy On Mixing; Large and Small Scale Water Tests

a different correlation was necessary to produce a good data grouping. The small-scale tests do not have as wide a variation in stratification thickness as did the large-scale tests, and the correlation of N_i^* versus mixing time does not show the distinct bands as did the large-scale tests, but there is considerable data scatter. Combining both sets of data in the correlation of N_i^* versus $V_o D_o \theta_1 / D_t^2$ indicates that much of the small-scale data agrees with the large-scale data correlations. This is especially true as the mixing progresses. Figures 23, 24, and 25 show these correlations.

A comparison of large- and small-scale data based on the correlation of N versus $V_o D_o \theta_1 / D_t^2$ shows excellent agreement. These correlations, presented in Figures 26, 27, and 28, show the small-scale data overlapping the entire range of the large-scale data with good agreement. Mixing times increase slightly with increasing N. These correlations indicate that mixing-time predictions based on small-scale data are valid in large-scale tanks.

The analytical prediction of mixing time from Reference 1 tends to give conservative values of the mixing time for cases in which the stratification is not thick ($Z_s/Z_b < 0.3$). The previous finding that a stratified fluid will mix faster than predicted analytically when N_i^* is less than 50 appears to hold

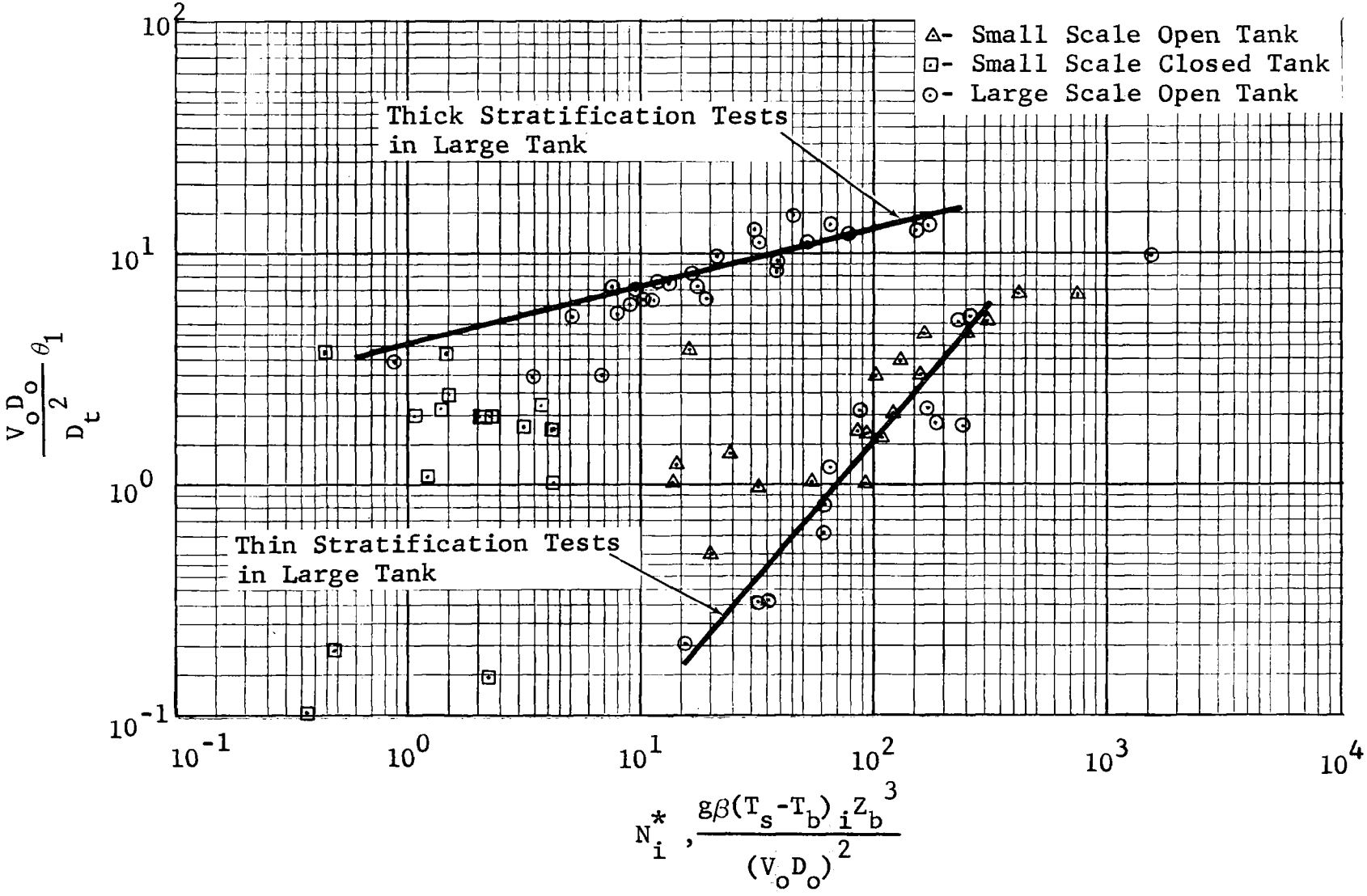

Figure 23 Correlation of Dimensionless Time Required for Temperature Stratification or Ullage Pressure To Reach 20% of Its Initial Value Versus N_i^*: Large and Small-Tank Tests

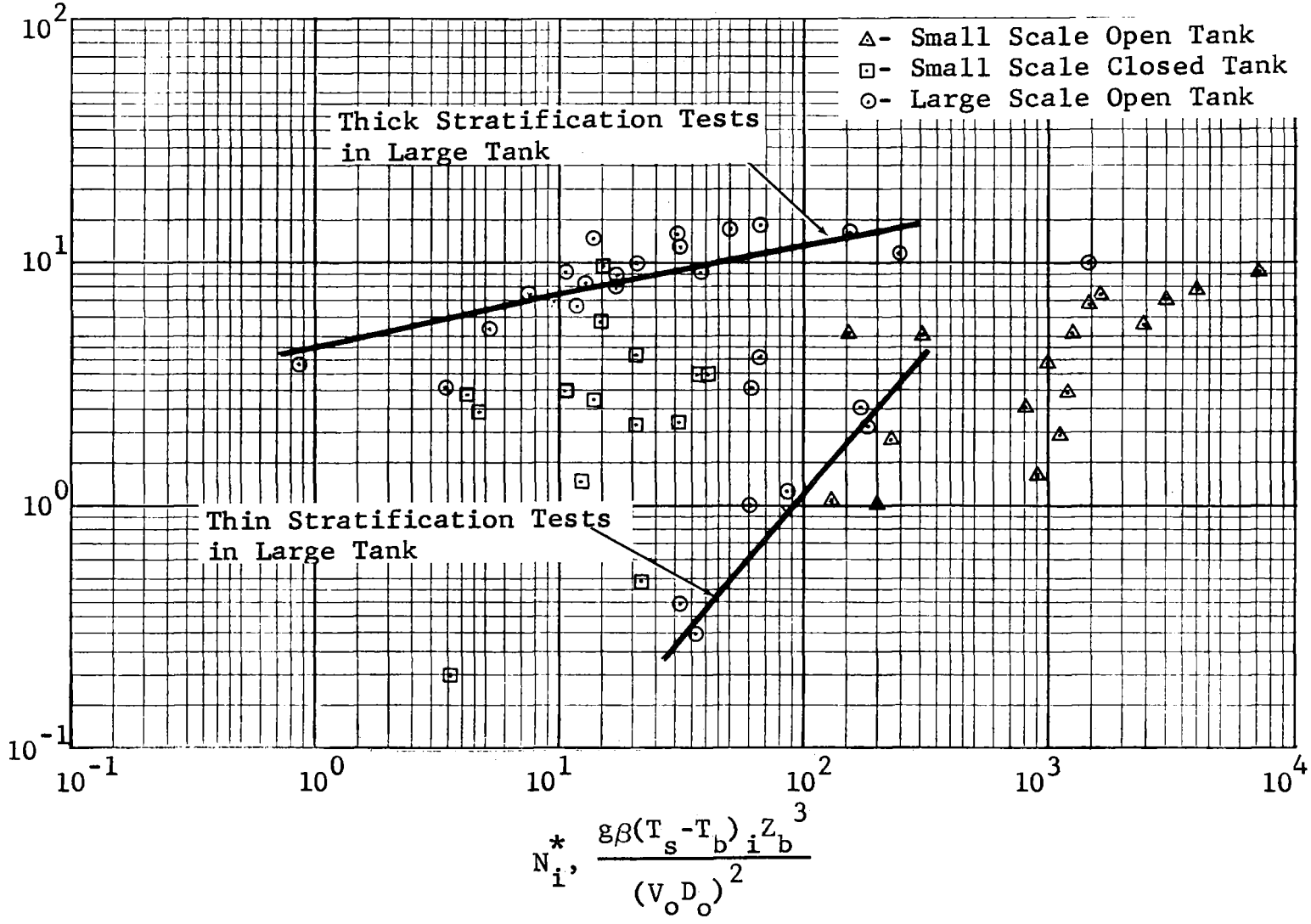

Figure 24 Correlation of Dimensionless Time Required for Temperature Stratification or Ullage Pressure To Reach 10% of Its Initial Value Versus N_i^*: Large and Small-Tank Tests

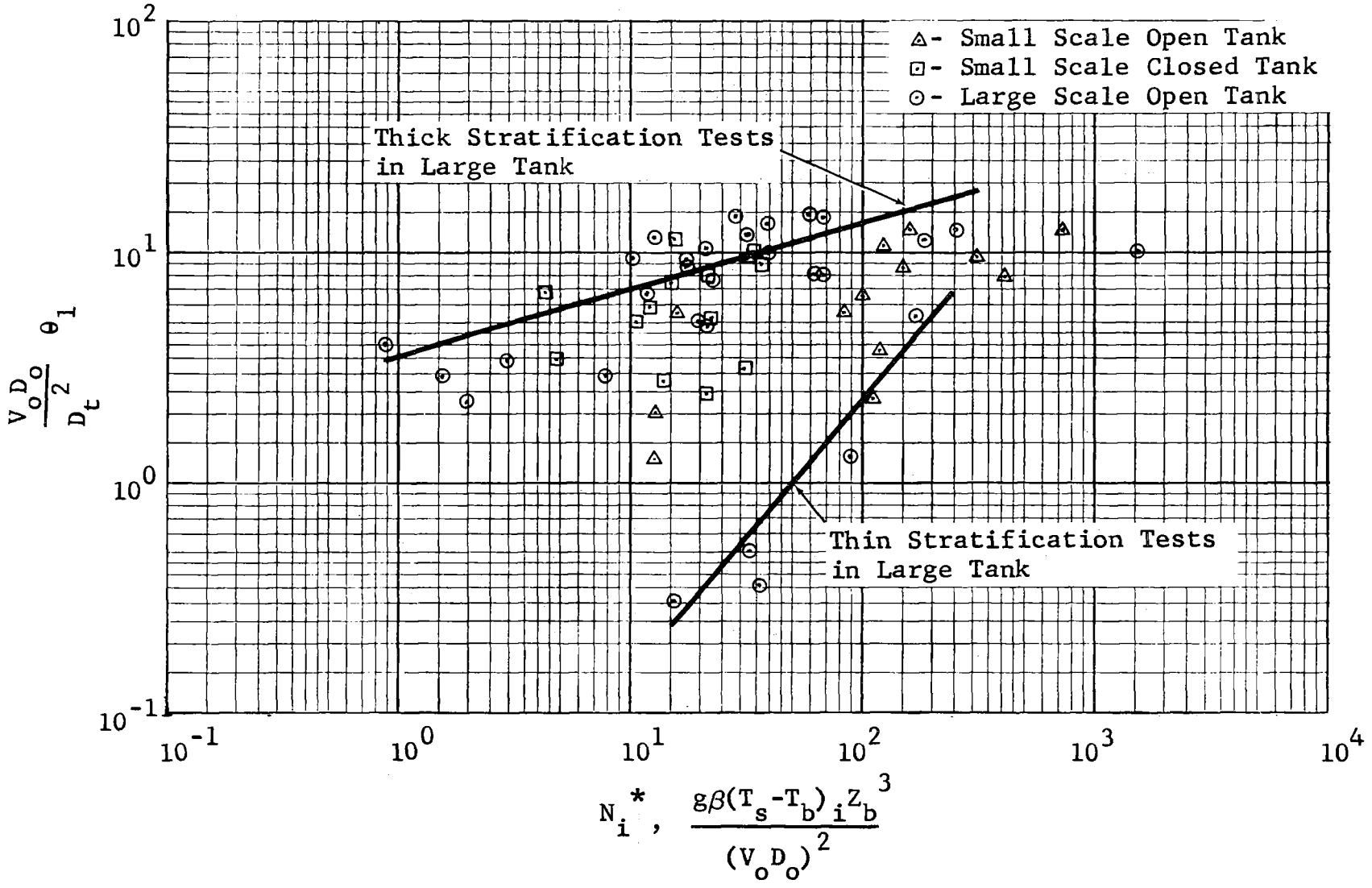

Figure 25 Correlation of Dimensionless Time Required for Temperature Stratification or Ullage Pressure To Reach 5% of Its Initial Value Versus N_i^*: Large and Small-Tank Tests

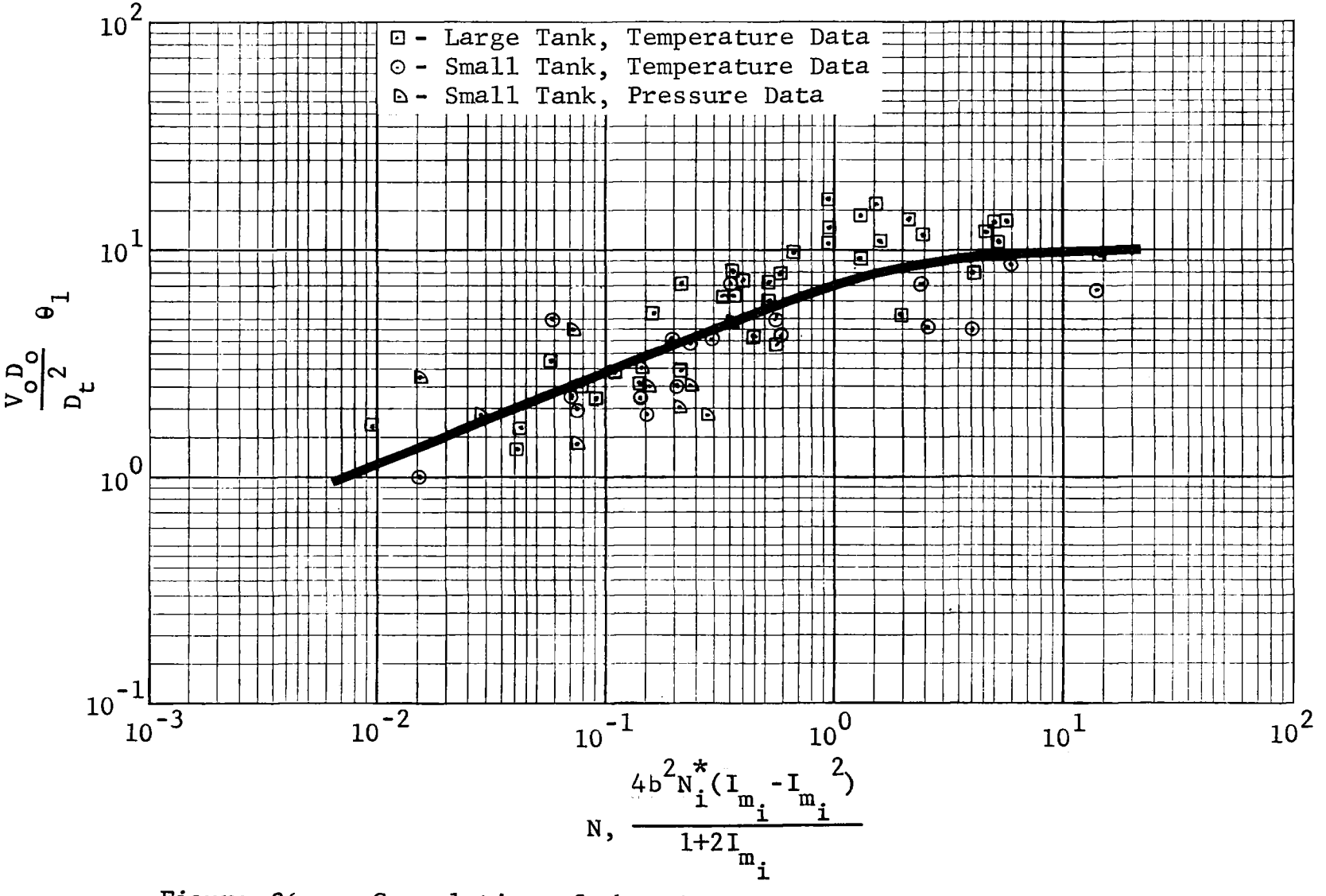

Figure 26 Correlation of the Dimensionless Time Required for Temperature Stratification or Ullage Pressure to Reach 20% of Its Initial Value Versus N: Large and Small Tank Tests

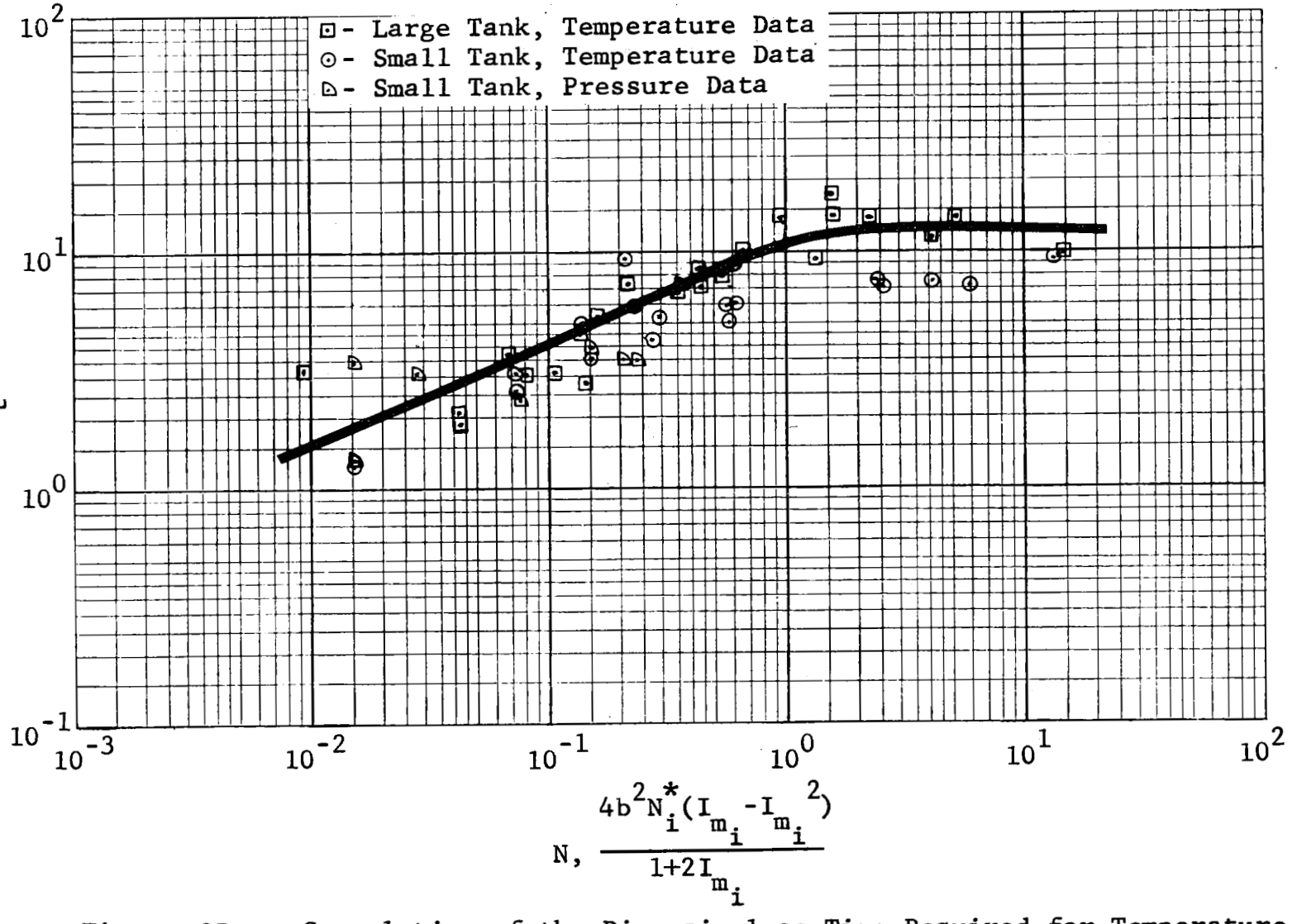

Figure 27 Correlation of the Dimensionless Time Required for Temperature Stratification or Ullage Pressure To Reach 10% of Its Initial Value Versus N: Large and Small Tank Tests

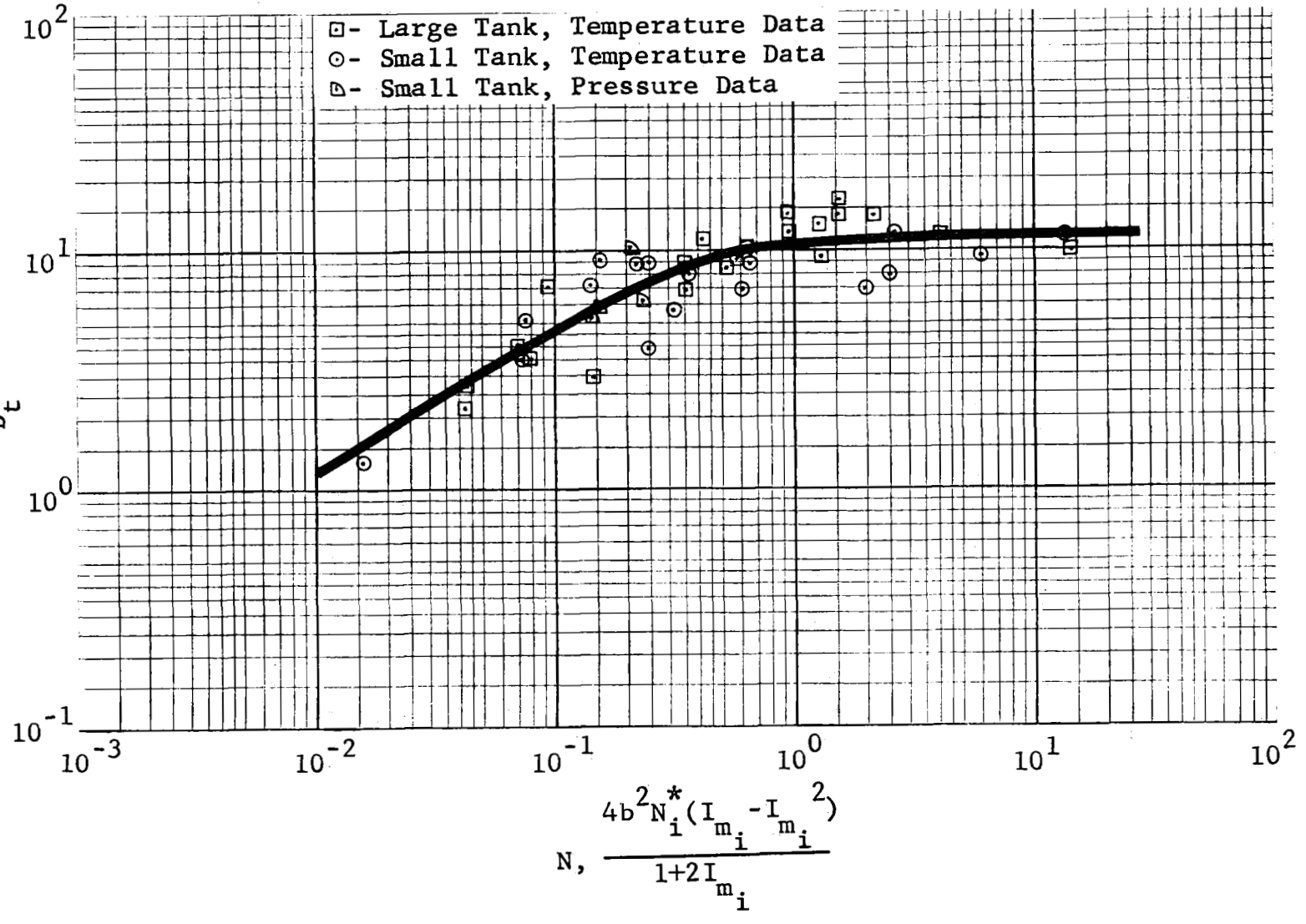

Figure 28 Correlation of the Dimensionless Time Required for Temperature Stratification or Ullage Pressure To Reach 5% of Its Initial Value Versus N: Large and Small Tank Tests

true for moderate levels of stratification. However, the initial energy integral, I_{mi}, appears to be a better indicator. When I_{mi} is greater than 0.2 mixing takes place slower than predicted analytically.

4.4 EFFECT OF LARGE-SCALE DATA ON PREVIOUS LIQUID HYDROGEN MIXER SYSTEM ESTIMATES

One of the objectives of this study was to determine if the large-scale test results indicated that changes were required in previous sizing estimates of the liquid-hydrogen mixer systems described in Reference 1. These estimates were partly based on mixing parameters developed from small-scale mixing tests. Any departure of the large-scale data correlations from the previous small-scale correlations would signal a possible need to re-evaluate the previous mixer analysis.

Comparison of large- and small-scale jet motion and buoyancy effect correlations reveals excellent agreement. Since previous conclusions concerning jet motion and buoyancy effects remain valid, there is no effect on any of the mixing estimates due to variations in these conditions.

There are variations between large- and small-scale correlations of dimensionless mixing times versus N_i^* due to variations

in the ratio Z_s/Z_b. New correlations of the dimensionless mixing times versus N for large- and small-scale data give excellent agreement, indicating that dimensionless mixing times are approximately the same for both tank sizes under equivalent conditions. The expression for mixing time given in previous studies (References 1 and 2) is found to be generally conservative, and previous results based on it are valid.

The net result of the large- and small-scale data correlation comparisons is that no significant disagreement is found and, therefore, no changes are necessary in previous estimates of liquid-hydrogen mixing systems. This is confirmed not only by comparison of correlations but by the fact that the large-scale-tank experimental flow rates which give good mixing results can be obtained by scaling small-scale data.

SECTION 5

OXYGEN STORAGE MIXER DESIGN STUDIES

The stratification prediction methods and mixer design criteria which were developed in previous studies for liquid-hydrogen systems were applied in this study to two types of oxygen storage systems. These systems are an S-IIB Orbital Tanker configuration and a small supercritical tank.

A basic guideline of the studies was that any system design would consist of conventional pumps and power supplies Only systems which are compatible with expected tank modifications were considered, and no radical vehicle changes are required.

5.1 REFERENCE SYSTEMS AND MISSIONS

The two oxygen storage systems considered in this study are vastly different; however, the same basic parameters establish the mixer design requirements for both. Some of the significant parameters are

1. Cryogenic storage mode
2. Propellant heating rate
3. Mission time

4. Tank acceleration

5. Tank size and geometry

Typical examples of these parameters were determined for the S-IIB LOX orbital tanker and the small supercritical oxygen storage tank.

5.1.1 S-IIB LOX Tanker Design Conditions

Several configurations of an orbital tanker based on S-IIB or S-II vehicles have been proposed. The vehicle selected for investigation during the study was a design requiring no major structural changes to the LOX tank. This configuration, the S-IIB/TK is described in Reference 4. The LOX tank in this vehicle consists of the basic S-IIB LOX tank (an oblate spheroid) with minor modification to the internal systems. The J-2S engines are considered to be insulated, since the study reported in Reference 4 determined that this was required to make the S-IIB/TK system acceptable. The basic vehicle mission parameters for the S-IIB/TK are shown in Table 3.

A significant difference between this LOX system and previously considered liquid-hydrogen systems is the physical properties of the LOX. The increase in saturation pressure with temperature for oxygen is not as severe as for hydrogen; however, the heat capacity of liquid oxygen is much less than that of hydrogen. Therefore, for equal masses of oxygen and

Table 3

VEHICLE MISSION PARAMETERS

Parameter	S-IIB/TK LOX	Supercritical Oxygen
Tank Diameter, ft	33.0	3.25
Tank Length, ft	22.0	3.25
Tank Volume, ft^3	12,553	17.97
Tank Area, ft^2	2692	33.18
Initial Oxygen Mass, lb_m	182,000	988
Initial Temperature, ^oR	162.3	247.6
Initial Pressure, psia	14.7	870.0
Initial Density, lb_m/ft^3	71.27	55.0
Initial Void Fraction	0.797	0
Storage Time, days	163.0	---
Final Temperature, ^oR	179.4	---
Final Pressure, psia	37.0	---
Orbital Heating, Btu/hr	673	0
Acceleration, a/g	5×10^{-6}	0
Orbital Altitude, n.mi	263	---
Use Rate, lb_m/hr	0	1
Internal Heating, W	0	400

hydrogen being heated at the same rate, the oxygen will undergo a much larger increase in temperature. In addition, the heat of vaporization of liquid oxygen is less than half that of liquid hydrogen.

5.1.2 Supercritical Oxygen Storage Tank

The second oxygen tank considered in this study was a supercritical storage tank such as is used in life-support systems. This storage mode, which had not been considered in previous studies, is in many respects unique in both purpose and operation. The purpose of using high-pressure supercritical storage is to avoid the low-gravity separation problems encountered when a two-phase fluid is utilized. Since there is no ullage, many problems with mixer design are eliminated, although several additional problems in the stratification analysis of the system are encountered because of the mode of operation. This type oxygen tank is used to supply oxygen continuously to the life-support system and to the fuel cells of current spacecraft. This requires a more or less constant withdrawal of small amounts of oxygen from the tank, and it is necessary to heat the oxygen in order to maintain the tank pressure during the withdrawals. The simultaneous processes of withdrawal and heating compound the problem of stratification prediction. However, the recent Apollo 13

accident and past Gemini incidents point out the importance of a good analysis of this problem, even though neither the Apollo nor the two Gemini problems were the result of natural stratification development (Reference 5).

The tank selected for analysis in this study is a typical example of a supercritical oxygen system. It is a small sphere with a low environmental heat leak, similar to the tank proposed in Reference 6. The major parameters are listed in Table 3 and are for a so-called "thin wall" tank with high performance superinsulation.

5.2 APPLICATION OF LIQUID-HYDROGEN MIXER TECHNOLOGY TO LIQUID-OXYGEN SYSTEMS

The technology developed to design liquid-hydrogen mixer systems is directly applicable to liquid-oxygen mixer systems. The differences in the thermal properties of the two fluids will affect the final results but not the design methods. The only problem in using previously developed mixing methods is the occasional inclusion of liquid-hydrogen properties in equation constants. This requires a check of the original derivations.

In the analysis of stratification development in the S-IIB LOX tank by the use of computer procedure U94 (Reference 7),

no serious difficulty was encountered as long as the problems conformed to the originally intended usage of the program. All logic in the program is independent of the type of fluid being analyzed.

However, the application of U94 to the analysis of stratification development in the supercritical storage tank was found to be impractical. The modifications which would have been required were of such a major nature that a new program was developed. This program, SW6, is described in Volume III of this report.

5.3 S-IIB LOX TANKER MIXER DESIGN STUDY

A thermal stratification mixer system was sized for an S-IIB/TK orbital LOX tanker configuration in which conventional components and power supplies were used. This approach was used rather than selection of an optimum system since it was felt that a mixer system would be required before the advanced technology components required in the more sophisticated system would be available.

In general, the mixer design was accomplished by using the same methods as presented in References 1 and 2. The major difference in the design of this system and that of previously considered systems (other than fluid properties) was due to

the large ullage volume (initial ullage void fraction is 0.797). This large ullage volume presented two problems:

1. Ullage heating is very large and is the dominant cause of the pressure increase.

2. If the axial jet disrupts the stored oxygen and disperses it throughout the tank, thermal control becomes difficult.

Consideration of these two problems was a major factor in the mixer design.

The number of mixer duty cycles was estimated on the basis of the time required for the tank pressure to rise from an initial mixed condition to a value slightly less than the tank design pressure. Tank pressure rise due to the ullage heating was found to be dominant over the pressure increase caused by stratification induced from strictly liquid heating and the duty cycles are based on ullage heating.

The mixer requirements are based on the considerations that (1) it would be undesirable to cause the liquid/vapor interface to be disrupted and the liquid distributed throughout the tank, and (2) the pump must be a conventional model. The requirement of no interface disruption resulted in low flow rates. Mixing times were calculated based on correlations of jet motion, bulk fluid motion, and temperature decay obtained by previous experimental and analytical methods.

The additional weights attributed to mixing were obtained as a function of total operating time. The power penalty assumed a fuel-cell power supply.

5.3.1 Stratification

Stratification development and the associated pressure increase in the S-IIB/TK were evaluated both numerically and analytically for various heating conditions. The numerical method of prediction, General Dynamics Computer Procedure U94 (Reference 7), was used mainly to check the effect on stratification development of various locations of liquid heating. The liquid heating conditions were also studied by use of an analytical conduction model.

Numerical analysis of a model in which uniform tank heating was assumed indicated that ullage heating caused a much faster pressure increase than that obtained in the previous liquid heating models. A more exact analysis, based on an ullage heating model originally presented in Reference 2, was then made for this heating case. This model predicts a rate of tank pressure increase by the equation

$$\frac{dP}{d\theta} = \frac{Z\ R\ Q_V}{V_V\ c_V}$$

This equation had been previously shown to have good agreement with data from the S-IVB 203 flight. The resulting S-IIB/TK pressure rise predicted by this model is shown in Figure 29 along with the predictions from some of the other models. Although these models all consider the same heat input to the tank, the location of the heat inputs vary and, consequently, direct comparison between models is difficult since the stratified conditions are different. These different models were used in order to determine the heating mode which produced the most severe stratification and pressure buildup. Most of the tank is occupied by vapor, and the engines are considered to be insulated; therefore, most of the heat conducted into the tank will be transferred to the vapor. The ullage heating model assumes that the fraction of the total heat that is transferred to the vapor is proportional to the ratio of the ullage wall surface area and the total tank surface area. The heat shorts to the ullage are included in the total ullage heating.

5.3.2 Duty-Cycle Evaluation for Nonvented Storage

The ullage heating pressure rise model was used to evaluate the number of duty cycles for the characteristic pressure rise during nonvented storage. The duty cycle was considered to

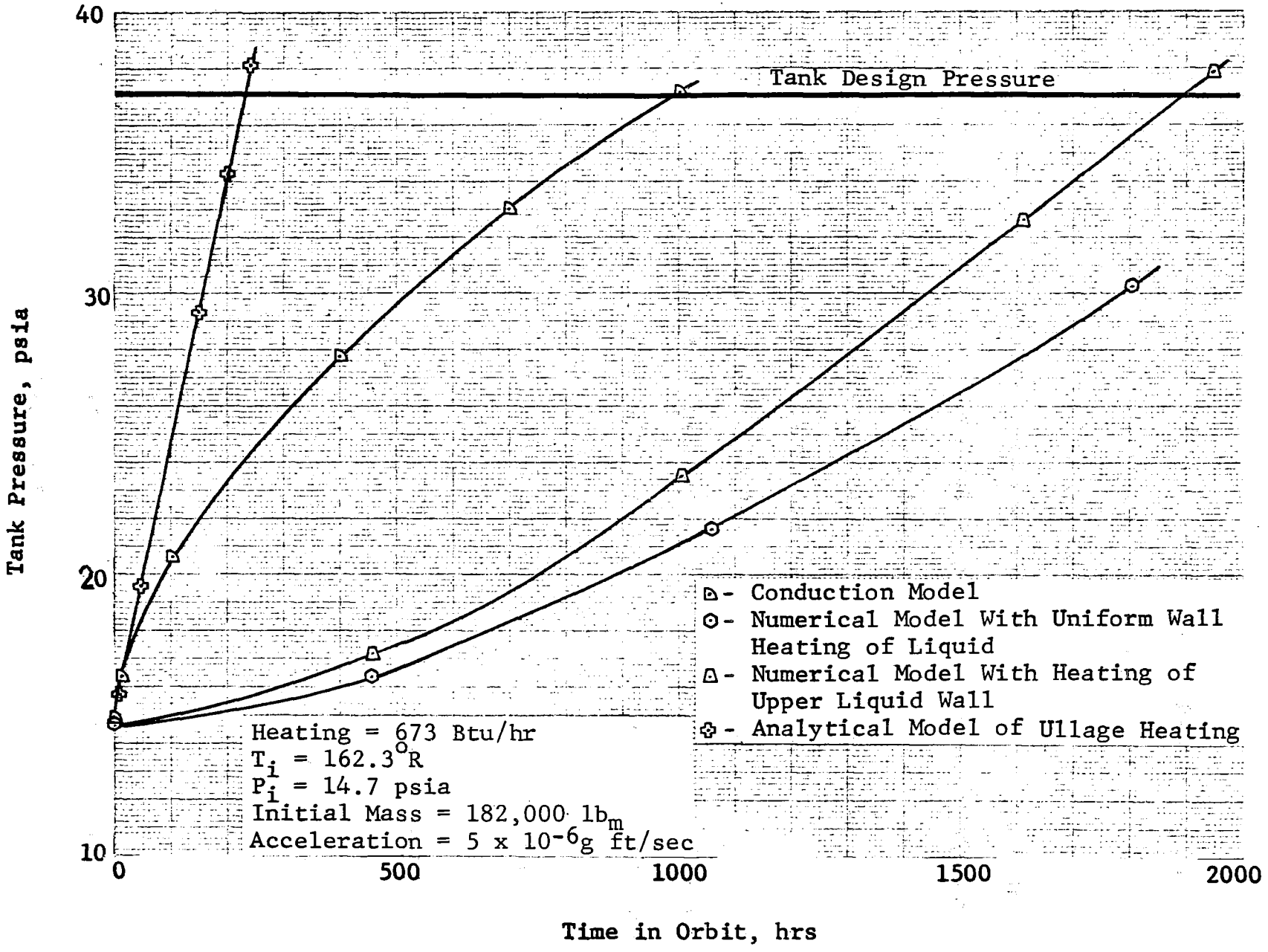

Figure 29 S-IIB/TK LOX Pressure Rise in Orbit for Various Heating Locations and Models

begin when the ullage pressure reached 36 psia, which is 1 psia below the tank design pressure.

An analysis was conducted to determine the ullage pressure decay that could be expected when mixing began. This was done as a check to see if the ullage pressure could actually be reduced in reasonable time periods. The analysis, which is presented in Appendix C, resulted in an expression for the pressure decay as follows:

$$\frac{P-P_b}{P_i-P_b} = 1 - \frac{C_2\theta}{2(P_i-P_b)^{1/2}}$$

where

P is the ullage pressure at time θ

P_b is the saturation pressure of the fluid at the bulk temperature

P_i is the initial ullage pressure

C_2 is a constant.

Small-scale pressurized mixing data given in Reference 8 indicate a rapid pressure decay during mixing when the ullage volume is small compared to the liquid volume; however, no test data are available for large ullages.

The predicted duty-cycle sequence is presented in Figure 30. The results of the duty-cycle evaluation are presented in Table 4 along with the results of the mixing time and mixer sizing analyses discussed below.

5.3.3 Mixing Time

The mixing time required to completely mix the liquid oxygen was found from the equation

$$\theta_m = \frac{6D_t^2}{0.456\ V_o D_o}$$

The term $V_o D_o$ was selected (using the ullage breakup criterion) to be a value that would not cause disruption of the liquid/vapor interface. The value of θ_m is a maximum value and represents a conservative value of the time to mix the fluid completely. The results of this analysis are also presented in Table 4.

5.3.4 Mixer Sizing and Location

The selection of the nozzle and mixer size was accomplished under the criteria of no liquid/vapor interface breakup and use of state-of-the-art equipment. The pump was located on the centerline at the tank bottom. No heat-short problem is expected at this location since the engines must be insulated.

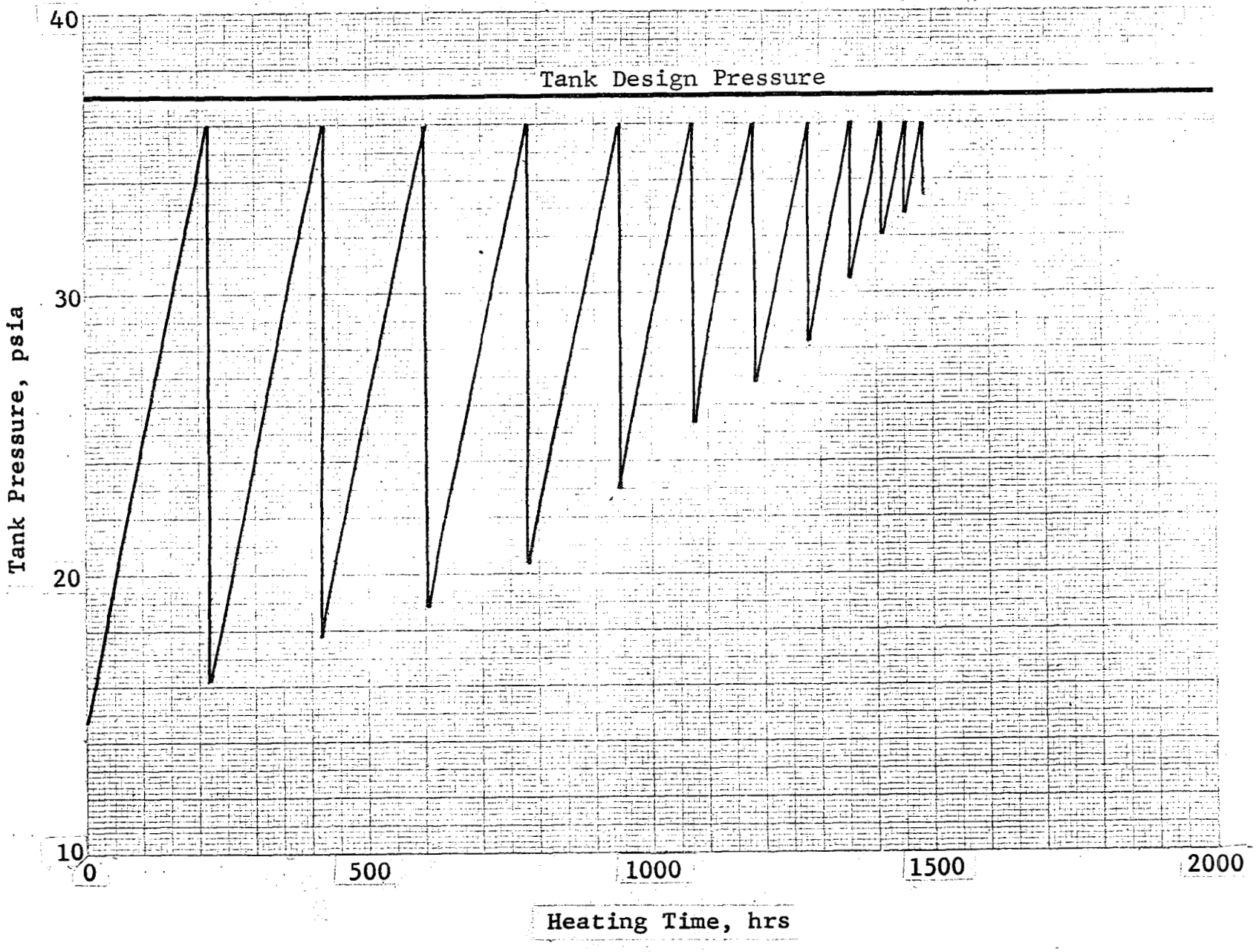

Figure 30 S-IIB/TK LOX Stratification Mixer Duty Cycles

Table 4

S-IIB/TK LOX TANK PUMP/MOTOR DESIGN DATA

First Stratification Development Time, hr	217.5
Last Stratification Development Time, hr	33.1
Number of Duty Cycles	12
Mixing Times, hr	33.1
Fluid Power, W	.0026
Outlet Velocity, ft/sec	0.9271
Pump Head, feet of LOX	0.01335
Flow Rate, gpm	0.9087
Specific Speed	10,000
Head Coefficient	0.1
Pump Blade Diameter, in.	1.187
Outlet Diameter, in.	0.633
Fluid Power X Outlet Diameter, W-ft	0.000138
Pump Speed, rpm	400
Hydraulic Efficiency, %	60
Torque, in.-oz	0.015
Overall Pump-Motor Efficiency, %	0.19
Power Input, W	0.9
Inverter Weight, lb_m	0.004
Power Supply Output, W	1.8
Power Supply Fixed Weight, lb_m	0.27

Table 4 (Cont'd)

Number of Mixers	1
Mixer Weight (Excluding Support Structure) lb_m	0.6

Only one mixer location is utilized since the acceleration conditions are sufficient to maintain a settled liquid if the mixer does not disrupt the interface. Figure 31 shows the selected mixer location.

The restriction of the axial jet flow rate to a value given by the ullage breakup criterion

$$V_o D_o \leq (1.055\sigma Z_b g_c/\rho)^{\frac{1}{2}}$$

results in a small value of the axial jet flow rate. No currently available or anticipated pump can efficiently produce the small values of fluid power required; therefore, a much larger pump must be utilized, resulting in a very low efficiency. The pump selected was similar to that described in Reference 9, although the blade diameter and rotational speed were derated in order to match it to a nozzle. The pump specific speed and head coefficient were maintained at their original values. A rotational speed was selected and the blade and nozzle determined on the basis of the ullage breakup criterion and the equations shown in Appendix D. The pump utilizes an a.c. motor system, and the pump motor has a very low overall efficiency since most of the input power is absorbed by system losses.

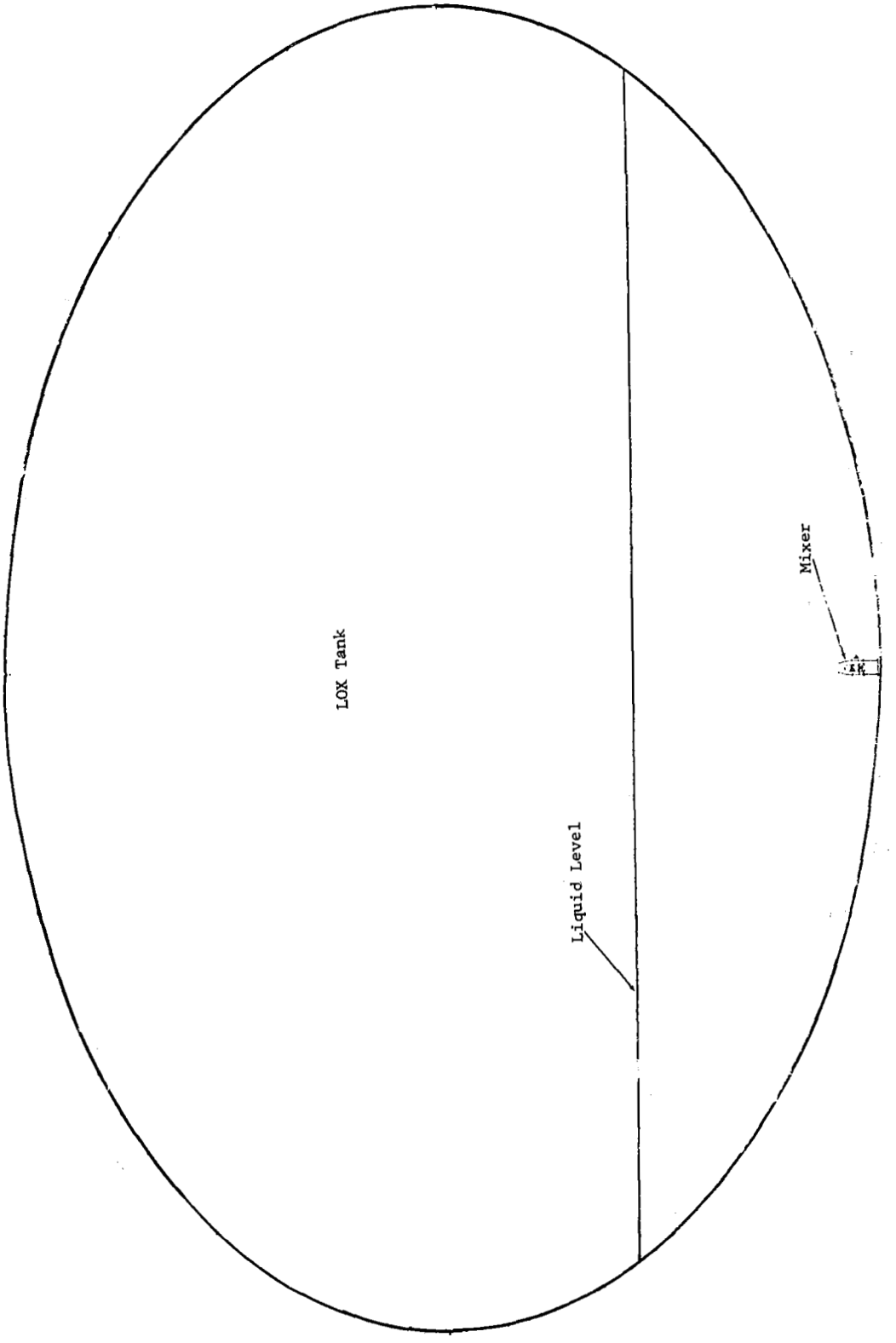

Figure 31 Mixer Installation in S-IIB/TK LOX Tank

The pertinent parameters required to define the mixer design are also presented in Table 4. This includes information on both the nozzle and the pump.

5.3.5 Mixer Weight Summary

The weight summaries of the mixer system (excluding wiring, supports, etc.) are given in Table 5. The weights listed include those for the mixer, fuel cell power supply, and boiloff. The boiloff penalty consists of the total mass that would be evaporated if all the pump input power was used to evaporate fluid. All weights listed in Table 5 are based on data given in Table 6, which are based on data from Reference 1.

5.3.6 Mixer Operational Sequence

The mixer operational sequence and associated controls are simple. The system operates during the non-vent portion of the earth orbit, and mixing is initiated when the tank pressure reaches a desired value below the tank design pressure and continues until the tank pressure decays to a pre-programmed tank pressure. This cycle is repeated until the mixed saturation pressure of the oxygen is equal to the mixer initiation pressure. The tank pressure is then allowed to increase until

Table 5

S-IIB/TK LOX MIXER WEIGHT SUMMARY

Fuel Cell Weight, lb_m	1.235
Boiloff Weight, lb_m	13.316
Inverter Weight, lb_m	0.043
Pump Weight*, lb_m	0.600
Total Weight, lb_m	15.194

*Excluding Structural Supports and Other Fixed Weight.

the vent system is automatically operated when the ullage pressure reaches the vent pressure. Venting continues until the pressure drops an amount specified by a practical vent band.

The controls assumed to operate the mixer system consist only of a pre-programmed thermal-equilibrium pressure history and appropriate pressure sensors. The system is automatic and functions with or without override switches.

5.4 SUPERCRITICAL OXYGEN TANK MIXER DESIGN

The analysis of the storage of supercritical oxygen was conducted to assess the effects of thermal stratification on the tank pressure. Stratification is developed by environmental heating and by the use of heaters to maintain the tank pressure during fluid withdrawal. However the extent of the stratification and its effect on tank equilibrium conditions were not large for the conditions and storage times studied.

The heater and drain locations may be important criteria in deciding if a mixer is required. Heater installations that disperse the heat input throughout the tank are clearly more desirable than a "point source" or restricted local heating. This was shown in Reference 11. Location of the drain is also important, since flow in the tank tends to mix the contents and reduce stratification.

Table 6

POWER SUPPLY WEIGHT COEFFICIENTS

	Power Level Operating Time Coefficient (lb_m/w)	Power Level Coefficient (lb_m/w)
Fuel Cell	0.00135	0.15
Boiloff	0.03725	---
Silver Zinc Battery	0.014	---
Inverter (50% efficient)	---	0.024

The actual design of a mixer for a supercritical system is not as complicated a task as for a two-phase system. There is no ullage to contend with since the fluid is stored as a single phase. Also the tanks are generally small and feasible pump designs produce more fluid power than is required for mixing. Therefore a conventional pump-motor design must be used that is too large for the system. The Apollo system is a typical example.

The data used to make the analysis is presented in Table 3. The computer procedure developed to predict stratification is presented in Volume III.

5.4.1 Stratification Prediction

Previously developed methods of predicting stratification development are not valid for use in an analysis of the supercritical tank. The system is unique since during normal operation there is almost constant fluid withdrawal, which causes flow to develop in the tank. Coupling fluid withdrawal with internal heat generation to maintain tank pressure results in a more complex situation to analyze for stratification. In addition, the extreme range of operating conditions requires that variable fluid properties be considered.

The purpose of predicting stratification in this type of tank is primarily to determine the difference between the stratified and the mixed tank pressures. The mixed pressure is more important since the stratification pressure can be controlled largely by regulation of the internal heating and fluid withdrawal. Consequently there is little danger of too high a pressure unless the heater controls fail. However, mixing of the stratified fluid might possibly result in an equilibrium pressure which is less than the minimum pressure at which the system can function properly.

The computer procedure developed, General Dynamics Computer Procedure SW6, considers stratification developing radially in a spherical tank. Internal heat generation is considered to be from heaters located on the tank wall. Fluid is withdrawn from the tank center.

The results of the analysis of the supercritical tank described in Table 3 are presented in Figures 32 through 34. The data shown in Figure 32 represent the stratified and mixed tank pressures. Fluid withdrawal begins at time zero. Tank heating begins when withdrawal reduces the pressure below 840 psia (the lower limit of the operating band). The difference between the stratified and mixed pressure is very small and at no point does the tank pressure drop below the critical

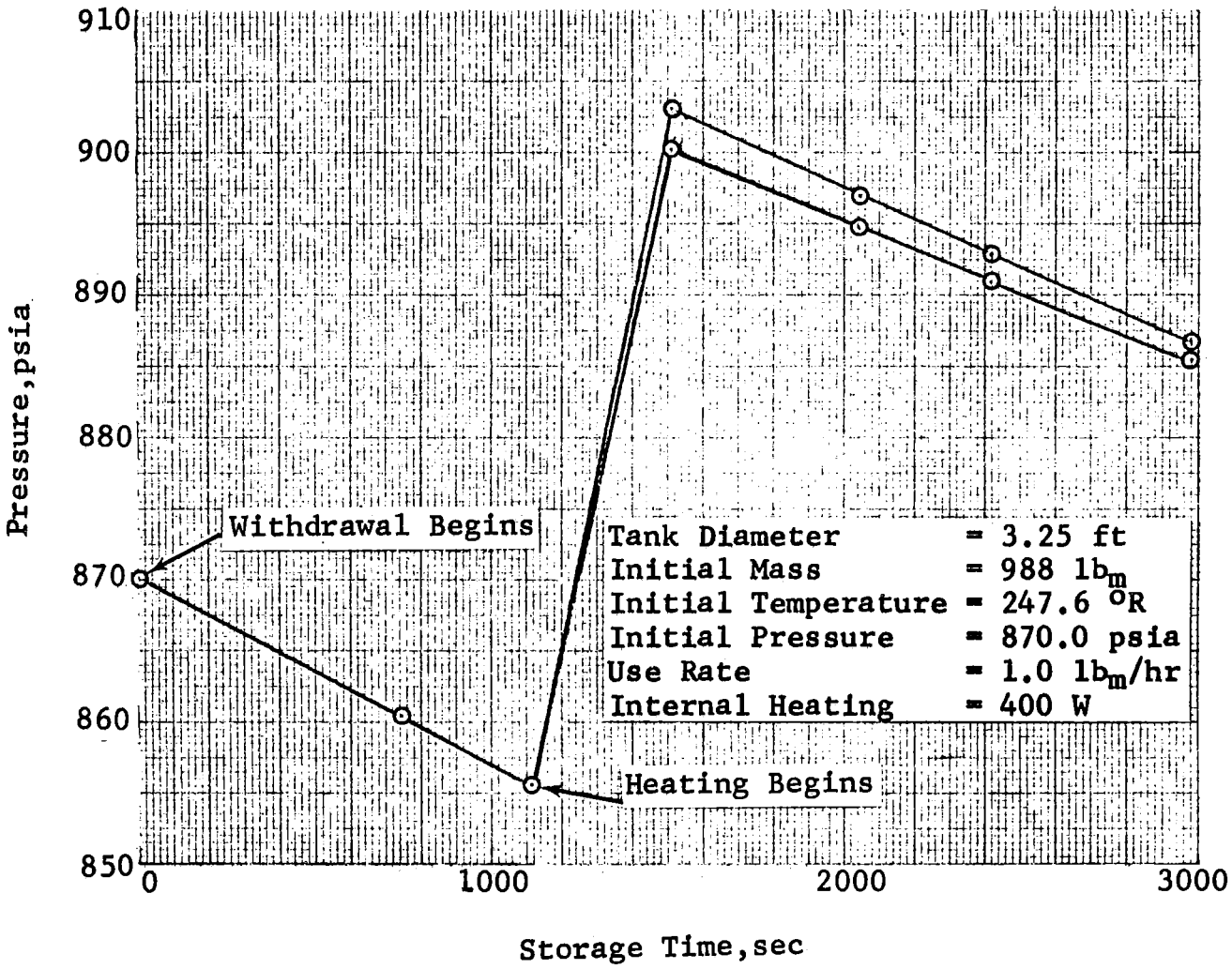

Figure 32 Stratified and Mixed Pressure in Supercritical Oxygen; Tank Diameter = 3.25 Ft

pressure. Figure 33 contains the temperature history of the tank. Figure 34 presents the fluid density variation in the tank.

The results indicate that no mixer operation is required during this peroid of time. It was noted during the analysis that in many regions the thermodynamic properties of oxygen had large variations with small changes in the tank conditions. Therefore it is possible that there are operating conditions which could lead to pressure collapse when the analysis is performed for a long period of time. It has been noted that the heater location and the heat flux affect the severity of the stratification. In addition, the oxygen property data used, in some instances, produced apparent property data slope discontinuties between interpolation regions.

5.4.2 Mixer Requirements

A cursory examination was made of the requirements for supercritical oxygen mixer systems. Supercritical tanks are normally much smaller than the liquid hydrogen tanks considered in previous studies. Consequently the fluid power requirements to mix the fluid are small. The pump-motor need not be sized to optimize the system since (1) the mixer power can be greater than required without creating problems and (2) heating of the fluid does not result in a penalty since the fluid is heated deliber-

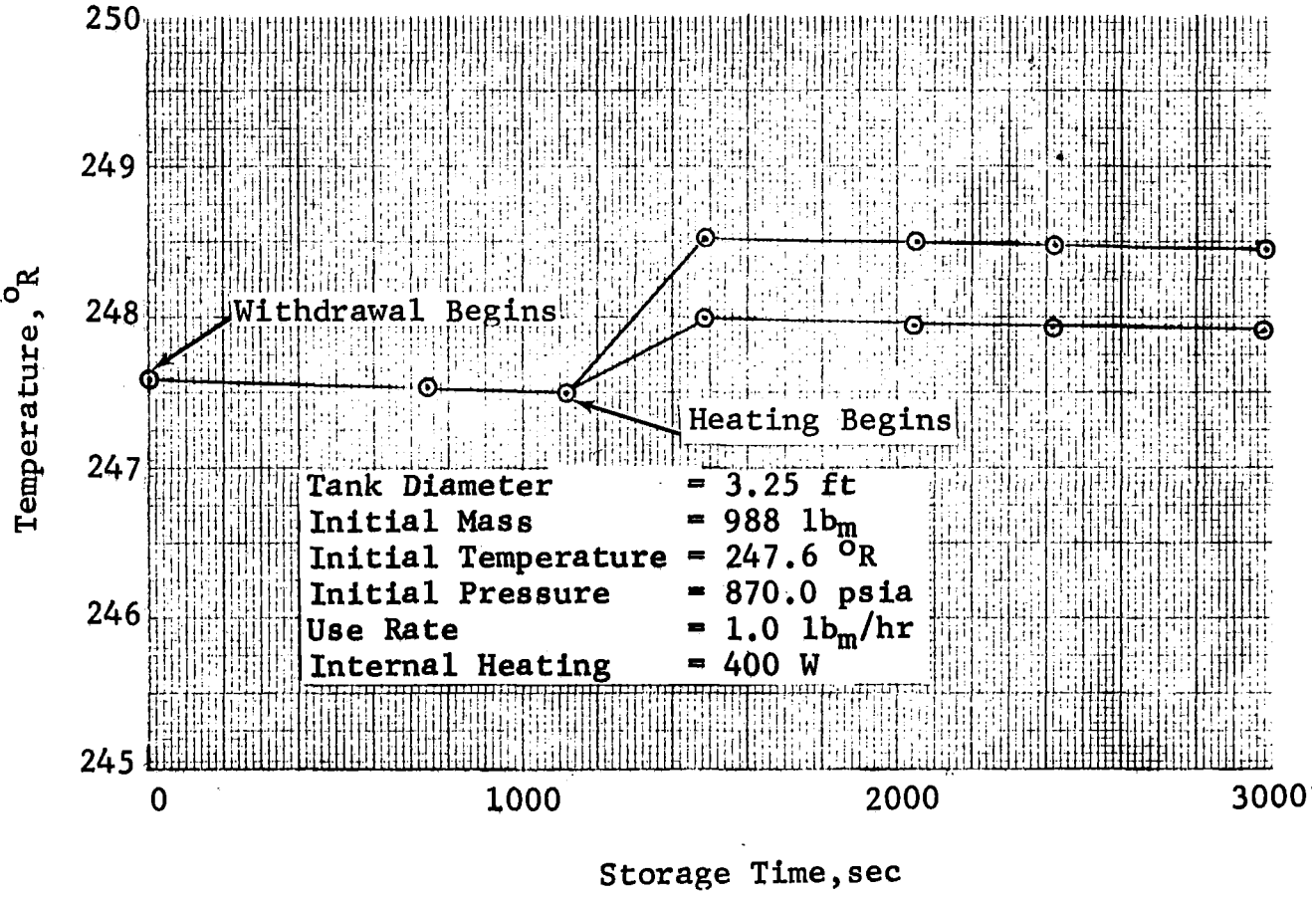

Figure 33 Stratified Temperature in Supercritical Oxygen; Tank Diameter = 3.25 Ft

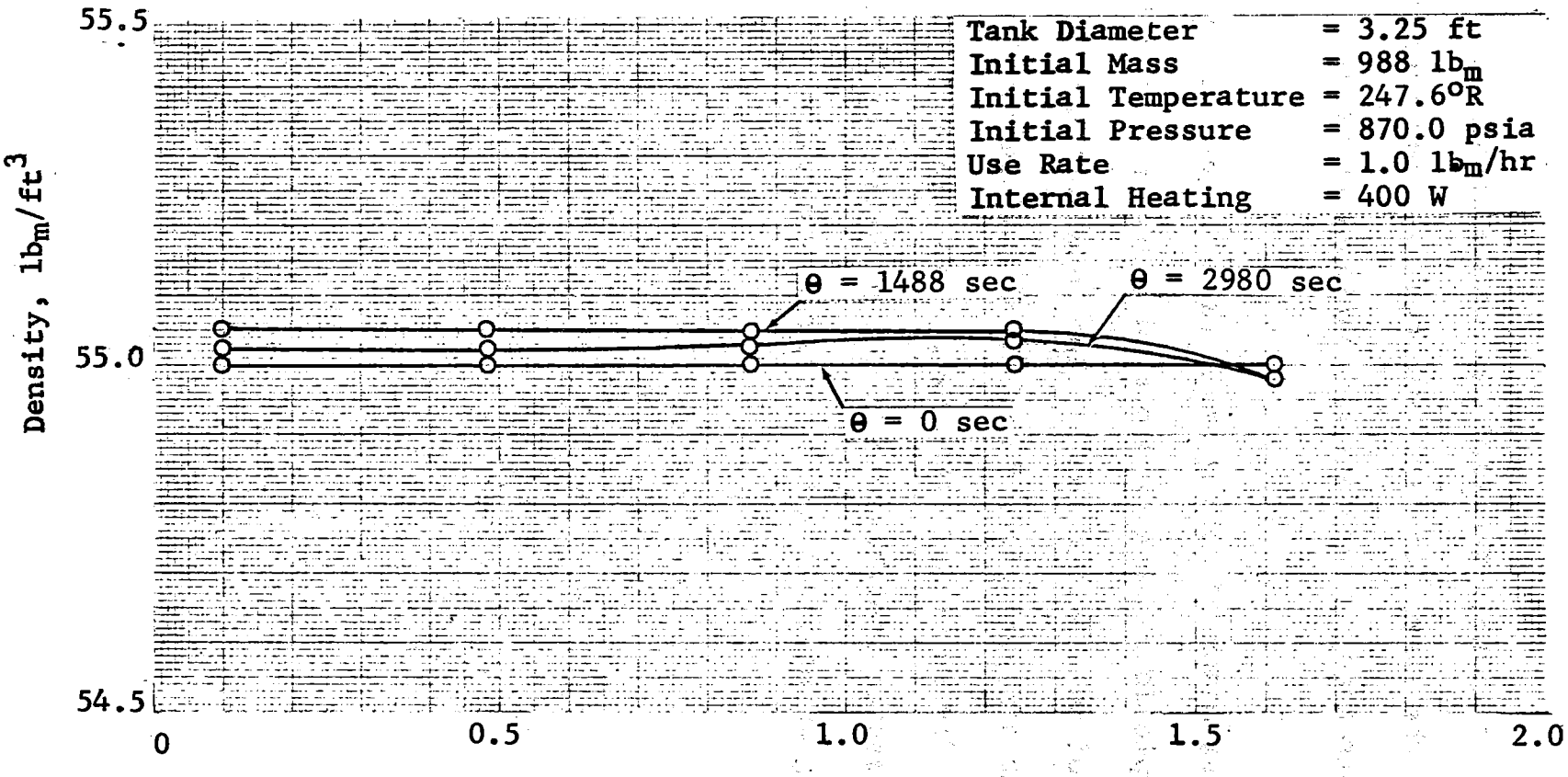

Figure 34 Density Variations in Supercritical Oxygen; Tank Diameter =3.25 Ft

ately in any case. The fluid is always present as a single phase in the tank, and mixer designs need not consider two-phase operation. Therefore conventional pumps are recommended for use.

Other means of mixing small tanks should be investigated. One example is the use of a pressure driven hydraulic motor instead of an electric motor. The tank contents would be stored at a higher pressure (e.g. 50 psi higher) than usual and expanded to provide the energy to operate the fan. This type of system would eliminate the problems resulting from operating an electric motor in liquid oxygen.

SECTION 6

CONCLUSIONS

Principal conclusions derived from the experimental and mixer design investigations during this study are as follows:

1. Small-scale tests provide an excellent means of investigating mixing in large-scale tanks.

2. The effect of buoyancy on jet-mixing may be neglected in mixer designs for low-gravity conditions.

3. Dimensionless mixing times in large-scale tanks are approximately the same as for small-scale tanks with the same parametric conditions.

4. The jet-transit-time prediction coefficient given in Reference 1 should be used rather than that given in Reference 3.

5. Stratification depth is an important parameter to consider in mixing.

6. Mixing, as demonstrated by the test results, was adequately achieved with a ratio of tank diameter to mixer diameter as high as 192.

7. Mixer flow rates scaled up from small-scale mixing data were adequate to mix the large tank.

8. Mixer design parameters developed from small-scale test data are adequate for use in designing mixer systems for large-scale tanks.

9. Mixer design methods developed for liquid-hydrogen tanks are applicable to liquid-oxygen systems.

10. Ullage pressure decay in tanks with large void fractions will occur within reasonable mixing times for axial jet mixing that does not disrupt the liquid/vapor interface.

11. Ullage disruption in a tank with a large void fraction is not necessary nor desirable from the standpoint of fluid control.

12. No evidence of a serious pressure collapse was found in the analysis of the supercritical oxygen tank.

SECTION 7

RECOMMENDATIONS

The recommendations of this study concerning analytical and experimental investigations and mixer design are given below.

In the case of analytical investigations, the following analyses are recommended:

1. Develop a more comprehensive supercritical storage computer program in order to include two-dimensional stratification effects in spherical or other axisymmetric tank geometries. This will improve predictions and increase the tank configurations that can be analyzed. Additional options should be added to allow more flexibility in heater and drain locations, initial conditions, and variable transport properties. This type of program would be a powerful tool for use in the analysis of supercritical systems.
2. Perform a parametric analysis of stratification development and pressure collapse in supercritical tanks, with tank size, heater position, and drain location used as study variables. This study would

provide information as to whether or not a mixer is required in various tanks for a wide range of conditions. In addition, the analysis would also show the effect of heater and drain location on the systems performance and provide valuable design information regarding these requirements.

3. Modify Computer Procedure U94 to improve liquid/ullage coupling and to reduce data preparation. An improved liquid/ullage coupling would produce a significant improvement in the program's solution to problems having ullage heating. This becomes especially important when problems with large ullages are solved. The reduction of the amount of data which must be prepared and loaded into the program can be accomplished by program modifications to make the program perform the calculation of the many nodal coefficients.

4. Perform a detailed analysis of the effect on the ullage pressure decay of an initial pressure spike caused by the cool jet striking a hot bulkhead. The delay in pressure decay due to this effect should be added to the mixing time.

5. Perform an analysis to determine the desirability of ullage breakup mixing in a large-ullage tank and subsequent fluid settling by engine burn as opposed to non-disruptive mixing. The ullage breakup mixing technique has an advantage of a faster mixing time than non-disruptive mixing, however, fluid resettling requirements may be unacceptable.

In the case of mixer design studies, the following efforts are recommended:

1. Investigate the possibility of heating the fluid externally to pressurize supercritical tanks. An external fan would be used to mix the tank contents. This would be an alternative to more hazardous internal controls.
2. Produce a mixer design handbook, summarizing in one convenient source all previous work.

Experimental recommendations are:

1. Evaluate experimentally the condensing heat transfer coefficients for axial jet impingement on the liquid/vapor interface in order to support and confirm analytical predictions of the ullage pressure decay during mixing.
2. Conduct an investigation to determine the pressure

decay time for various ullage volumes in order to include this effect in mixing time estimates.

3. Perform cryogenic mixing tests to determine the effect of heat shorts on mixing.
4. Conduct an experimental investigation on the pressure collapse in supercritical cryogenic tanks to support and verify analytical predictions.
5. Conduct an investigation to define orbital experiments on stratification and mixing.
6. Investigate, in small-scale tests, the effect of stratification depth on mixing and develop correlations of its effect on mixing time.

REFERENCES

1. Poth, L. J., et al, A Study of Cryogenic Propellant Mixing Techniques, Volume I, Mixer Design and Experimental Investigations, Final Report, General Dynamics Fort Worth Division Report FZA-439-1, 1 November 1968.

2. Poth, L. J., et al, A Study of Cryogenic Propellant Stratification Reduction Techniques, Volume I, Analytical and Experimental Investigations, Annual Report, General Dynamics Fort Worth Division Report FZA-419-1, 15 September 1967.

3. Schlichting, Herman, Boundary Layer Theory, McGraw-Hill Book Company, Inc., New York, 1960.

4. Denison, D. E., et al, Feasibility of Modifying the S-II Stage As An Injection Stage For Manned Planetary Fly-By Missions, Final Report, North American Aviation, Inc., Space and Information Systems Division Report SID67-275-3, March 1967.

5. Personal Communication from Jerry Smithson, NASA/MSC, to L. J. Poth, General Dynamics Fort Worth Division, 1970.

6. McDonnell Douglas Single Wall Cryogen Storage Systems, McDonnell Douglas Corporation Report CR-CSS-02.

7. Van Hook, J. R., et al, Study of Cryogenic Propellant Stratification Reduction Techniques, Volume II, Computer Programs, Annual Report, General Dynamics Fort Worth Division Report FZA-419-1, 15 September 1967.

8. Poth, L. J., Van Hook, J. R., et al, A Study of Cryogenic Propellant Mixing Techniques, Volume II, Experimental Data, Final Report, General Dynamics Fort Worth Division Report FZA-439-2, 1 November 1968.

9. Bradshaw, R. D., et al, Thermodynamic Studies of Cryogenic Propellant Management, General Dynamics Convair Division Report GDC-ERR-AN-1144, December 1967.

10. Strickland, Z., "Many Tests Reveal Mishap Cause", Aviation Week and Space Technology, Vol. 92, No. 23, June 1970.

R E F E R E N C E S (Cont'd)

11. Kamat, D.A., Control Design For A Cryogenic Fluid Storage and Supply System, Iowa State University of Science and Technology, Ames, Iowa, 1966.

A P P E N D I X E S

A P P E N D I X A

T H E R M O C O U P L E R E S P O N S E E R R O R

The error of a thermocouple reading due to the thermal response lag can be found from the experimental data and a thermocouple energy balance. The following sketch defines the thermocouple bead and its surroundings.

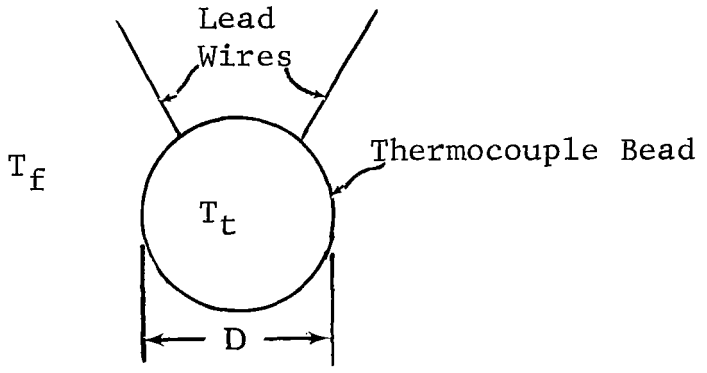

Considering the thermocouple bead to be a sphere with diameter D, the thermocouple energy balance is

Rate of Energy Leaving = Change in Energy Stored

$$hA\Delta T = m\, c_p \frac{dT_t}{d\theta}$$

$$h(\pi D^2)(T_f - T_t) = c_p \rho \pi \frac{D^3}{6} \frac{dT_t}{d\theta}$$

Solving this equation for the rate of change in the thermocouples temperature yields

$$\frac{dT_t}{d\theta} = \frac{6h}{D\rho c_p}(T_f - T_t). \qquad (1)$$

The temperature data from the experimental tests represents the thermocouple temperature, T_t, and $dT_t/d\theta$. The difference between the surrounding fluid temperature, T_f, and T_t is the error.

The prediction of the mixing time given in Reference 2 is

$$C^*\theta = 0.456 \frac{V_o D_o}{D_t^2} \theta .$$

However the experimental data often displayed an initial period of faster mixing. This is shown in the following sketch

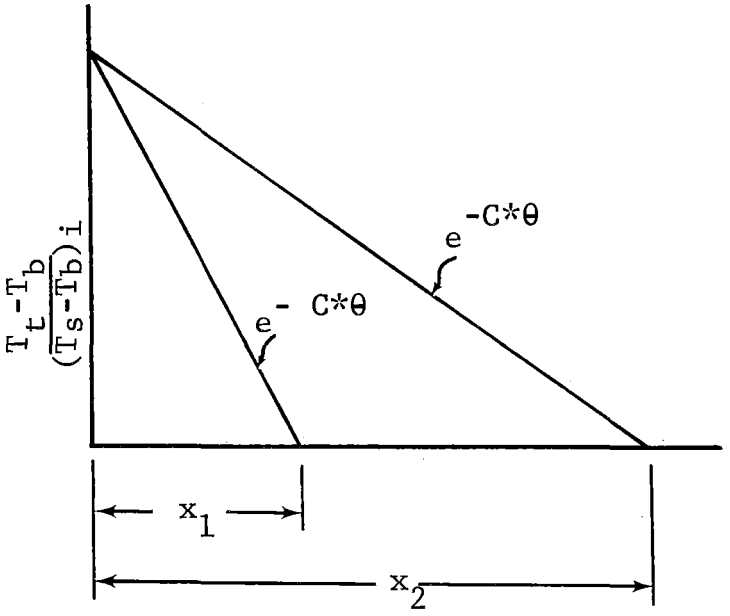

$$\frac{V_o D_o}{D_t^2} \theta$$

The experimental data initially followed a path described by

$$\frac{T_t-T_b}{(T_s-T_b)_i} = e^{-\frac{x_2}{x_1} C^*\theta}$$

Then

$$T_t - T_b = (T_s - T_b)_i \, e^{-0.456\alpha V_o D_o \theta / D_t^2}$$

and

$$\frac{dT_t}{d\theta} = -(T_s - T_b)_i \, \frac{0.456\alpha V_o D_o}{D_t^2} e^{-0.456\alpha V_o D_o \theta / D_t^2} \qquad (2)$$

Substituting Equation 2 into Equation 1 yields

$$\frac{T_t - T_f}{(T_s - T_b)_i} = \frac{0.456 D \rho c_p \alpha V_o D_o}{6 h D_t^2} e^{-0.456\alpha V_o D_o \theta / D_t^2}$$

The error is a maximum when $\theta = 0$ and is

$$\frac{T_t - T_f}{(T_s - T_b)_i} = \frac{0.456 D \rho c_p \alpha V_o D_o}{6 h D_t^2}$$

SYMBOLS AND ABBREVIATIONS

A Thermocouple bead surface area, ft^2

C* $0.456 V_o D_o / D_t^2$, 1/sec

c_p Thermocouple bead specific heat, $Btu/lb_m \, {}^oR$

D Thermocouple bead diameter, ft

D_o Nozzle Diameter, ft

D_t Tank diameter, ft

h Heat transfer coefficient between thermocouple and surrounding fluid, $Btu/hr \, ft^2 \, {}^oF$

m Mass of thermocouple bead, lbm

T_b Fluid temperature at the nozzle, ${}^oF$

T_f Fluid temperature, ^oF

T_s Fluid surface temperature, ^oF

T_t Thermocouple bead temperature, ^oF

V_o Nozzle exit velocity of jet, ft/sec

X_1 $V_o D_o \theta / D_t^2$ required for rapid temperature decay prediction to reach some percentage of its initial value.

X_2 $V_o D_o \theta / D_t^2$ required for slow temperature decay prediction to reach same $\Delta T / \Delta T_i$ as fast prediction.

α X_2 / X_1

θ Time

ρ Thermocouple bead density

SUBSCRIPTS

i Initial

APPENDIX B

PRESSURE DECAY HEAT TRANSFER COEFFICIENT

The expression for the heat transfer coefficient from the ullage to the liquid during non-disruptive mixing is necessary to predict the pressure decay. The following sketch illustrates the environment

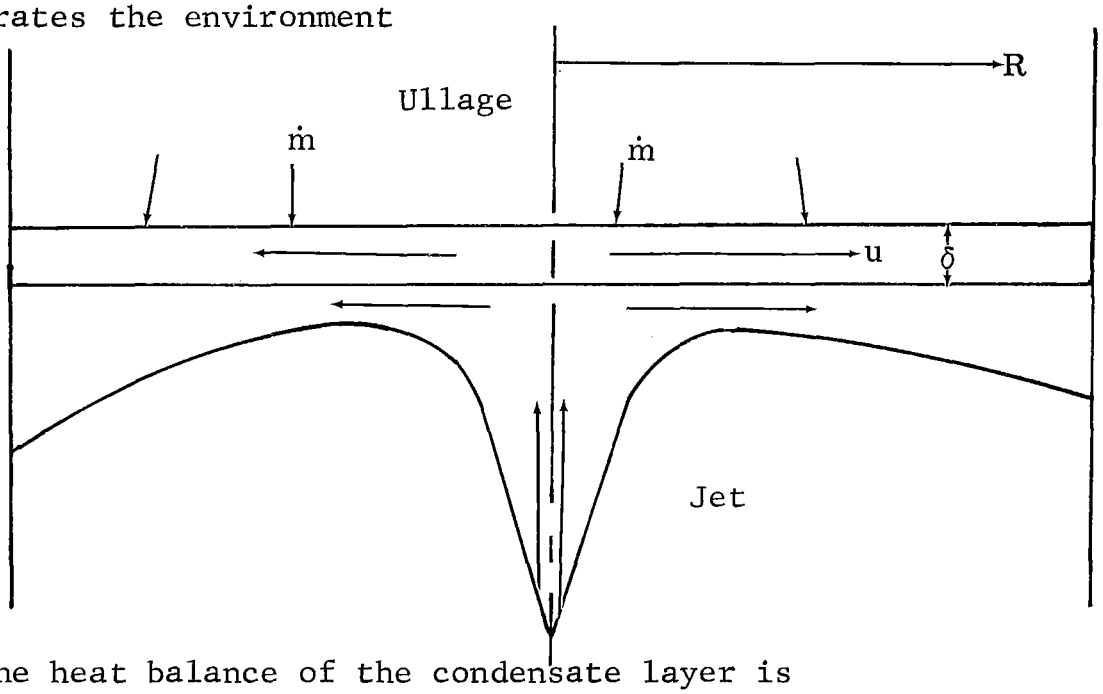

The heat balance of the condensate layer is

$$h_{fg} \frac{d}{dR} (\delta \rho 2\pi Ru) = \frac{2\pi Rk(T_s - T_b)}{\delta}$$

Assume the condensate thickness has a form

$$\delta = C_2 R^n$$

and substituting yields

$$h_{fg} \frac{d}{dR} (C_2 R^n \rho C_1 R^2) = \frac{Rk(T_s - T_b)}{C_2 R^n}$$

where from Reference 1

$$u = C_1 R$$

and

$$C_1 = 0.912 V_o D_o / Z_m Z_1$$

then

$$h_{fg} C_2 \rho C_1 \frac{d}{dR} (R^{2+n}) = \frac{k(T_s - T_b)}{C_2} R^{1-n}$$

and

$$h_{fg} C_2 \rho C_1 (2+n) R^{n+1} = \frac{k(T_s - T_b) R^{1-n}}{C_2}$$

By comparison of the exponents of R on both sides of the equation, it can be seen that n=0. Hence, the condensate thickness is constant and is given by $\delta = C_2$

and

$$h_{fg} \rho C_1 \delta (2R) = \frac{k}{\delta} (T_s - T_b) R.$$

Solving for δ

$$\delta = \left[\frac{k(T_s - T_b)}{2 h_{fg} \rho C_1} \right]^{1/2}$$

but

$$h = \frac{k}{\delta}$$

Therefore

$$h = \left[\frac{2k\ h_{fg}\ \rho\ C_1}{(T_s - T_b)} \right]^{1/2}$$

SYMBOLS AND ABBREVIATIONS

D_o Nozzle exit diameter, ft

h Heat transfer coefficient between ullage and liquid, Btu/hr ft^2 ^oR

h_{fg} Heat of vaporization, Btu/lb_m ^oR

k Thermal conductivity, Btu/ft ^oR hr

R Radial distance, ft

T_s Surface temperature, ^oR

T_b Bulk or bottom temperature, ^oR

u Radial velocity, ft/sec

V_o Nozzle exit velocity, ft/sec

Z_m Mixing region thickness, ft

Z_1 Distance from bottom of mixing region to nozzle top, ft

δ Thickness of condensate layer, ft

ρ Density of condensate, lb_m/ft^3

APPENDIX C

ULLAGE PRESSURE DECAY

The mixing of a settled fluid without a disruption of the liquid/vapor interface causes an ullage pressure decay due to condensation of vapor from the ullage. Considering the ullage to be described by

$$PV = mRT \tag{1}$$

and the heat removed from the ullage to be

$$\dot{m}h_v = -\frac{d}{d\theta}(mc_vT) \tag{2}$$

an expression can be obtained for the ullage pressure decay. Substituting the term T from Equation 1 into Equation 2 yields

$$\dot{m}h_v = -\frac{c_v}{R}\frac{d}{d\theta}(PV).$$

If the ullage volume is constant

$$\dot{m}h_v = -\frac{c_vV}{R}\frac{dP}{d\theta}$$

and

$$\frac{dP}{d\theta} = -\frac{R\dot{m}h_v}{c_vV} \tag{3}$$

The condensation rate, $\dot{m}$, can be found by considering that the rate heat is removed from the ullage is given by

$$Ah(T_s-T_b) = \dot{m}h_{fg}\ .$$

The term is T_s-T_b is related to the saturation pressure by a relationship

$$P-P_b = B(T_s-T_b)$$

where B is the slope of the variation of pressure with temperature (between T_s and T_b), thus

$$\dot{m} = \frac{Ah(P-P_b)}{Bh_{fg}} . \qquad (4)$$

The expression for h is given in Appendix B by

$$h = \left[\frac{2kh_{fg}\rho C_1}{(T_s-T_b)}\right]^{1/2} .$$

Substituting the value of h into Equation 4 yields

$$\dot{m} = \left[\left(\frac{P-P_b}{B}\right) \frac{2k\rho C_1 A}{h_{fg}}\right]^{1/2} \qquad (5)$$

$$= C(P-P_b)^{1/2}$$

where

$$C = \left[\frac{2k\rho C_1 A^2}{Bh_{fg}}\right]^{1/2}$$

and

$$C_1 = 0.456Z_1V_oD_o/8Z_mR_1^2 .$$

Substitution of the value of $\dot{m}$ into Equation 3 yields

$$\frac{dP}{d\theta} = -\frac{Rh_v}{c_vV} C(P-P_b)^{1/2}$$

$$= -C_2(P-P_b)^{1/2}$$

where

$$C_2 = \frac{Rh_vC}{c_vV}$$

Collecting variables and integrating from the initial ullage pressure when the mixer is turned on yields

$$2\left[(P-P_b)^{1/2} - (P_i-P_b)^{1/2}\right] = -C_2\theta$$

This can be reduced to

$$\frac{P-P_b}{P_i-P_b} = \left[1-\frac{C_2\theta}{2(P_i-P_b)^{1/2}}\right]^2$$

SYMBOLS AND ABBREVIATIONS

A Liquid/vapor interface area, ft^2

B Slope of saturation pressure versus temperature, $lbf/ft^{2o}R$

C Constant, $C = (2k\rho C_1 A^2/Bh_{fg})^{1/2}$, $lb_m ft/hr\ lb_f^{1/2}$

C_1 Constant, $C_1 = 0.456Z_1V_oD_o/8Z_mR_1^2$, 1/sec

C_2 Constant, $C_2 = Rh_vC/c_vV$, $lbf^{1/2}/ft\ hr$

c_v Constant volume specific heat of ullage, $Btu/lb_m{}^oR$

D_o Nozzle exit diameter, ft

h Heat transfer coefficient between ullage and liquid, $Btu/hr\ ft^2\ {}^oR$

h_{fg} Heat of vaporization, Btu/lb_m

h_v Ullage enthalpy, Btu/lb_m

k Thermal conductivity of condensate, $Btu/hr\ ft\ {}^oR$

m Ullage mass, lb_m

$\dot{m}$ Condensation rate, lb_m/hr

P Ullage pressure, lb_f/ft^2

R Gas constant, $ft\text{-}lb_f/lb_m\text{-}^oR$

R_1 Jet radius at bottom of mixing region, ft

T Temperature, ^oR

V Ullage volume, ft^3

V_o Nozzle exit velocity, ft/sec

Z_m Mixing region thickness, ft

Z_1 Distance from bottom of mixing region to nozzle, ft

θ Time, sec

ρ Condensate density, lb_m/ft^3

SUBSCRIPTS

b Bottom or bulk

i Initial

APPENDIX D

PUMP AND NOZZLE OPERATING CHARACTERISTICS

The selection of the pump and matching nozzle are based on three equations. The ullage breakup criterion given by

$$V_o D_o \leq (1.055 Z_b g_c \sigma/\rho)^{\frac{1}{2}} \qquad (1)$$

determines the limiting value of the nozzle exit diameter, D_o. The relationship between D_o and the blade diameter, D_B, is given by

$$D_o = 1.6853 \times 10^{-4} K^{\frac{1}{4}} \psi^{\frac{1}{2}} N_s D_B \ . \qquad (2)$$

Finally the pump speed is determined from

$$n = \frac{3.144 \times 10^5}{\psi N_s D_B^{\ 2} K^{\frac{1}{2}}} \left(\frac{P_o D_o}{\rho}\right)^{1/3}, \text{ rpm.} \qquad (3)$$

Choosing a conventional pump and retaining its head coefficient, ψ, and specific speed, N_s, and assuming $K = 1.0$ permits a value of the blade diameter as a function of D_o to be obtained.

The fluid power is given by

$$P_o = \Delta P \ \dot{V}_o$$

but

$$\Delta P = \frac{k \rho V_o^{\ 2}}{2 g_c}$$

and

$$\dot{V}_o = V_o \frac{\pi D_o^2}{4}$$

Therefore

$$P_o = \frac{k\rho V_o^3 \pi D_o^2}{8 g_c}$$

The nozzle exit velocity can be obtained from the ullage breakup criterion in terms of D_o. Substituting into Equation 3 yields

$$n = \frac{3.144 \times 10^2}{4\ N_s D_B^2}\ C. \qquad (4)$$

Substituting values of N_s and ψ into Equations 1, 2, and 4 and assuming a value of n, D_B, or D_o determines the relationship between D_B, D_o, and n. The electric motor output torque is then given by

$$T = \frac{25.5\ \psi^{\frac{1}{2}}}{\eta_p}\ D_B\ \rho^{1/3} (P_o D_o)^{2/3},\ \text{in.-oz.}$$

SYMBOLS AND ABBREVIATIONS

D_B Blade diameter, ft

D_o Nozzle exit diameter, ft

g_c Dimensional conversion factor, g_c = 32.2 ft-lbm/lbf-sec^2

K Loss coefficient

N_s Specific speed

n Pump speed, rpm

P_o Fluid power, watts

T Motor output torque, in-oz

V_o Nozzle exit velocity, ft/sec

$\dot{V}_o$ Nozzle exit volume flow rate, ft^3/sec

Z_b Liquid height above nozzle, ft

ΔP Nozzle pressure drop, psf

η_p Pump hydraulic efficiency

ρ Density, lbm/ft^3

σ Surface tension, lbf/ft

ψ Head coefficient

A P P E N D I X E

D I S T R I B U T I O N L I S T

COPIES	RECIPIENT	DESIGNEE
	NASA Headquarters, Washington, D.C. 20546	
1	Contracting Officer	
1	Patent Office	
	NASA Lewis Research Center 2100 Brookpark Rd., Clevelend, Ohio 44135	
1	Office of Technical Information	
1	Contracting Officer	
1	Patent Office	
	NASA Manned Spacecraft Center Houston, Texas 77001	
1	Office of Technical Information	
1	Contracting Officer	
1	Patent Office	
	NASA Marshall Space Flight Center Marshall Space Flight Center, Alabama 35812	
2	Office of Technical Information, A&TS-MS-I	(X)[1]
1	Technical Library, A&TS-MS-IPL	(X)[1]
1	Purchasing Office, A&TS-PR-M	(X)[1]
1	Patent Office, A&TS-PAT	(X)[1]
1	D. Burrows, S&E-ASTN-PP	(X)[1]
1	Technology Utilization Office, A&TS-TU	(X)[1]
1	B. Birdwell, S&E-ASTN-RRI	(X)[1]
	NASA Pasadena Office 4800 Oak Grove Drive, Pasadena, Calif. 91103	
1	Patents and Contracts Management	
5	Thomas W. Winstead S&E-ASTN-PFC Marshall Space Flight Center Marshall Space Flight Center, Alabama 35812	(X)[1]

[1]Copies sent directly to "Recipient" marked with an "X" under the column headed "Designee".

COPIES	RECIPIENT	DESIGNEE
3	Chief, Liquid Propulsion Technology, RPL Office of Advanced Research and Technology NASA Headquarters Washington, D. C. 20546	(X)[1]
1	Director, Technology Utilization Division Office of Technology Utilization NASA Headquarters Washington, D. C. 20546	(X)[1]
25	NASA Scientific and Technical Information Facility P. O. Box 33 College Park, Maryland 20740	(X)[1]
1	Director, Launch Vehicles and Propulsion, SV Office of Space Science and Applications NASA Headquarters, Washington, D.C. 20546	(X)[1]
1	Director, Advanced Manned Missions, MT Office of Manned Space Flight NASA Headquarters, Washington, D. C. 20546	(X)[1]
1	Mission Analysis Division NASA Ames Research Center Moffett Field, California 24035	(X)

NASA FIELD CENTERS

2	Ames Research Center Moffett Field, California 94035	Hans M. Mark
2	Goddard Space Flight Center Greenbelt, Maryland 20771	Merland L. Moseson
2	Langley Research Center Langley Station Hampton, Virginia 23365	Ed Cortwright Director

[1]Copies sent directly to "Recipient" marked with an "X" under the column headed "Designee".

NASA FIELD CENTERS

COPIES	RECIPIENT	DESIGNEE
2	Lewis Research Center 21000 Brookpark Road Cleveland, Ohio 44135	Gordon Smith
2	John F. Kennedy Space Center, NASA Cocoa Beach, Florida 32931	Dr. Kurt H. Debus

GOVERNMENT INSTALLATIONS

1	Aeronautical Systems Division Air Force Systems Command Wright-Patterson Air Force Base Dayton, Ohio 45433	D. L. Schmidt Code ASRCNC-2
1	Air Force Missile Development Center Holloman Air Force Base, New Mexico 88330	Maj. R. E. Bracken
1	Air Force Missile Test Center Patrick Air Force Base, Florida	L. H. Ullian
1	Space and Missile Systems Organization Air Force Unit Post Office Los Angeles, California 90045	Col. Clark Technical Data
1	Bureau of Naval Weapons Department of the Navy Washington, D. C. 20546	J. Kay RTMS-41
1	Defense Documentation Center Headquarters Cameron Station, Building 5 5010 Duke Street Alexandria, Virginia 22314 Attn: TISIA	
1	U. S. Army Missile Command Redstone Arsenal Alabama 35809	Mr. Walter Wharton
1	U. S. Naval Weapons Center China Lake California 93557	Code 4562 Chief, Missile Propulsion Div.

NASA FIELD CENTERS

COPIES	RECIPIENT	DESIGNEE
2	Jet Propulsion Laboratory California Institute of Technology 4800 Oak Grove Drive Pasadena, California 91103	Henry Burlage, Jr. Propulsion Div., 38
2	Manned Spacecraft Center Houston, Texas 77001	Joseph G. Thibodaux, Jr. Chief, Propulsion & Power Division

GOVERNMENT INSTALLATIONS

1	Arnold Engineering Development Center Arnold Air Force Station Tullahoma, Tennessee 37388	Dr. H. K. Doetsch
1	Headquarters, U.S. Air Force Washington, D. C. 20546	Col. C. K. Stambaugh
1	Picatinny Arsenal Dover, New Jersey 07801	I. Forsten, Chief Liquid Propulsion Laboratory
1	Air Force Rocket Propulsion Laboratory Research and Technology Division Air Force Systems Command Edwards, California 93523	RPRR/Mr. H. Main

INDUSTRY CONTRACTORS

1	Hughes Aircraft Co. Aerospace Group Centinela and Teale Streets Culver City, California 90230	E. H. Meier V. P. and Div. Mgr. Research and Dev. Div.
1	Walter Kidde and Company, Inc. Aerospace Operations 567 Bellville, New Jersey	R. J. Hanville Dir. of Research Engr.
1	Baltimore Division Martin Marietta Corporation Baltimore, Maryland 21203	John Calathes (3214)
1	Denver Division Martin Marietta Corporation P. O. Box 179 Denver, Colorado 80201	Dr. Morganthaler

C P I A

COPIES	RECIPIENT	DESIGNEE
1	Chemical Propulsion Information Agency Applied Physics 8621 Georgia Avenue Silver Spring, Maryland 20910	Tom Reedy

INDUSTRY CONTRACTORS

1	Aerojet-General Corporation P. O. Box 296 Azusa, California 91703	W. L. Rogers
1	Aerojet-General Corporation P. O. Box 1947 Technical Library Bldg. 2015, Dept. 2410 Sacramento, California 95803	R. Stiff
1	Space Division Aerojet-General Corporation 9200 East Flair Dr. El Monte, California 91734	S. Machlawski
1	Aerospace Corporation 2400 East El Segundo Boulevard P. O. Box 95085 Los Angeles, California 90045	John G. Wilder MS-2293
1	Atlantic Research Corporation Edsall Road and Shirley Highway Alexandria, Virginia 22314	Dr. Ray Friedman
1	Avco Systems Division Wilmington, Massachusetts	Howard B. Winkler
1	Beech Aircraft Corporation Boulder Division Box 631 Boulder, Colorado	J. H. Rodgers

INDUSTRY CONTRACTORS

COPIES	RECIPIENT	DESIGNEE
1	Bell Aerosystems Company P. O. Box 1 Buffalo, New York 14240	W. M. Smith
1	Bellcomm 955 L'Enfant Plaza, S.W. Washington, D. C.	H.S. London
1	Bendix Systems Division Bendix Corporation 3300 Plymouth Street Ann Arbor, Michigan	John M. Brueger
1	Boeing Company P. O. Box 3707 Seattle, Washington 98124	J.D. Alexander
1	Boeing Company 1625 K Street, N. W. Washington, D. C. 20006	Library
1	Boeing Company P. O. Box 1680 Huntsville, Alabama 35801	Ted Snow
1	Missile Division Chrysler Corporation P. O. Box 2628 Detroit, Michigan 48231	John Gates
1	Wright Aeronautical Division Curtiss-Wright Corporation Wood-Ridge, New Jersey 07075	G. Kelley
1	Research Center Fairchild Hiller Corporation Germantown, Maryland	Ralph Hall
1	Republic Aviation Corporation Fairchild Hiller Corporation Farmingdale, Long Island, New York	Library

INDUSTRY CONTRACTORS

COPIES	RECIPIENT	DESIGNEE
1	General Dynamics, Convair Division Library & Information Services (128-00) P. O. Box 1128 San Diego, California 92112	Frank Dore
1	Missile and Space Systems Center General Electric Company Valley Forge Space Technology Center P. O. Box 8555 Philadelphia, Pa.	F. Mezger F. E. Schultz
1	Grumman Aircraft Engineering Corp. Bethpage, Long Island, New York	Joseph Gavin
1	Honeywell, Inc. Aerospace Division 2600 Ridgway Road Minneapolis, Minnesota	Gordon Harms
1	Arthur D. Little, Inc. 20 Acorn Park Cambridge, Massachusetts 02140	Library
1	Lockheed Missiles and Space Co. Attn: Technical Information Center P. O. Box 504 Sunnyvale, California 94088	J. Guill
1	Lockheed Propulsion Company P. O. Box 111 Redlands, California 92374	H.L. Thackwell
1	The Marquardt Corporation 16555 Saticoy Street Van Nuys, California 91409	Howard McFarland
1	Orlando Division Martin Marietta Corp. Box 5837 Orlando, Florida	J. Ferm

INDUSTRY CONTRACTORS

COPIES	RECIPIENT	DESIGNEE
1	McDonnell Douglas Aircraft Corp. P. O. Box 516 Municipal Airport St. Louis, Missouri 63166	R.A. Herzmark
1	Space & Information Systems Division North American Rockwell 12214 Lakewood Boulevard Downey, California 90241	Library
1	Northrop Space Laboratories 3401 West Broadway Hawthorne, California	Dr. William Howard
1	Aeronutronic Division Philco Corporation Ford Road Newport Beach, California 92663	D.A. Garrison
1	Astro-Electronics Division Radio Corporation of America Princeton, New Jersey 08540	Y. Brill
1	Sunstrand Aviation 2421 11th Street Rockford, Illinois 61101	R.W. Reynolds
1	TRW Systems Group TRW Incorporated One Space Park Redondo Beach, California 90278	G.W. Elverum
1	TAPCO Division TRW, Incorporated 23555 Euclid Avenue Cleveland, Ohio 44117	P.T. Angell
1	Reaction Motors Division Thiokol Chemical Corporation Denville, New Jersey 07832	Dwight S. Smith

INDUSTRY CONTRACTORS

COPIES	RECIPIENT	DESIGNEE
1	Research Laboratories United Aircraft Corporation 400 Main Street East Hartford, Connecticut 06108	Erle Martin
1	Hamilton Standard Division United Aircraft Corporation Windsor Locks, Connecticut 06096	R. Hatch
1	United Technology Center 587 Methilda Avenue P. O. Box 358 Sunnyvale, California 94088	Dr. David Altman
1	Florida Research and Development Pratt and Whitney Aircraft United Aircraft Corporation P. O. Box 2691 West Palm Beach, Florida 33402	R. J. Coar
1	Vickers, Inc. Box 302 Troy, Michigan	
1	Missile and Space System Division McDonnell-Douglas Aircraft Company 3000 Ocean Park Boulevard Santa Monica, California 90406	R. W. Hallet Chief Engineer Adv. Space Tech.
1	Rocketdyne (Library 586-306) 6633 Canoga Avenue Canoga Park, California 91304	Dr. R. J. Thompson S. F. Iacobellis
1	Rocket Research Corporation 520 South Portland Street Seattle, Washington 98108	Foy McCullough, Jr.
1	Stanford Research Institute 333 Ravenswood Avenue Menlo Park, California 94025	Dr. Gerald Marksman

GENERAL DYNAMICS

Fort Worth Division

P. O. Box 748

Fort Worth, Texas 76101